Technische Universität Wien
Vienna University of Technology

Diplomarbeit

Wetting and infiltration behavior of copper and copper alloys on carbon nanofibers

ausgeführt am
Institut für Festkörperphysik
der
Technischen Universität Wien

unter der Anleitung von
Ao. Univ. Prof. Dr. Christoph Eisenmenger-Sittner

durch
Michael Kitzmantel
Haslingergasse 34/8
1170 Wien

Wien, 1. Februar 2008 Michael Kitzmantel

Abstract

In electronic devices materials with a high thermal conductivity and a coefficient of thermal expansion matching to the ones of Si, GaAs or alumina are used as heat sinks, heat spreaders and substrates. Besides the high thermal conductivity a low coefficient of thermal expansion (CTE) is a crucial property for the long-term stability and reliability of the products. Today commonly used materials such as Mo-Cu, W-Cu, Kovar, Al/SiC, AlN or diamond exhibit several limitations in respect to limited thermal conductivity (Kovar), high density (Mo-Cu, W-Cu), bad machinability (Al/SiC, AlN) or high price (diamond).

Within this feasibility study the wetting and infiltration behavior of copper and some copper alloys containing carbide forming elements such as Ti, Mo, Cr or B on carbon nanofibers were investigated. These additives promote wetting on the carbon surface. It is shown how carbon nanofibers (i.e. nanofilaments and nanotubes) can be used to reinforce a copper matrix. Several ways of producing metal matrix composites (MMC) with carbon nanoparticles as building blocks were investigated, including infiltrating carbon preforms with the metal matrix, powder metallurgical approaches and chemical coating of the nanofibers.

Characterisation of the accomplished samples was done by measuring thermal properties and studying the microstructure of the interface zone using scanning electron microscopy and EDX analysis. Hotpressing, conventional heating and microwave heating was carried out for fabricating the samples. The different producing routes show various problems addressed in this work.

Kurzfassung

In elektronischen Bauteilen werden Materialien mit hoher thermischer Leitfähigkeit als Wärmesenken verwendet, deren thermische Ausdehnungskoeffizienten jenen von Silizium, GaAs oder Aluminium ähnlich sind. Für Langzeitstabilität und Verlässlichkeit des Produkts sind diese beiden thermischen Eigenschaften von großer Bedeutung. Heutzutage werden Materialien wie Mo-Cu, W-Cu, Kovar, Al/SiC, AlN und Diamanten eingesetzt, bei denen diverse Einschränkungen in Bezug auf limitierte thermische Leitfähigkeit (Kovar), hohe Dichte (Mo-Cu, W-Cu), schlechte Bearbeitbarkeit (Al/SiC, AlN) oder hoher Preis (Diamant) in Kauf genommen werden müssen.

Diese Arbeit ist eine Studie über unterschiedliche Varianten zur Herstellung von Metall Matrix Verbundwerkstoffen mit Kohlenstoff Nanofasern (d.h. Nanofilamente und Nanotubes) als Verstärkungsphase, wobei primär die Machbarkeit und das Benetzungs- bzw. Infiltrationsverhalten von Kohlenstoff Nanofasern durch Kupfer und Kupferlegierungen sowie der Einfluss von Karbid bildenden Additiven wie Ti, Mo, Cr oder Bor auf die Benetzungseigenschaften der Kohlenstoffoberfläche untersucht wurde. Dazu wurden Techniken wie Infiltration durch flüssiges Metall, pulvermetallurgische Verfahren und chemische Beschichtung von Nanofasern verwendet.

Die hergestellten Proben wurden durch Bestimmung der thermischen Eigenschaften sowie durch Untersuchung der Faser-Matrix Verteilung unter dem Elektronenmikroskop charakterisiert. Mittels unterschiedlicher Sinter- und Schmelzmethoden wie Heißpressen, Induktives Heizen und Erhitzen durch Mikrowellen hergestellte Materialien wurden in dieser Arbeit sowohl anhand ihrer thermischen Eigenschaften wie auch ihrer Mikrostruktur miteinander verglichen.

Acronyms

ABA	Active Brazing Alloy (by Wesgo GmbH)
Ag	Silver
Al	Aluminum
α	Thermal Diffusivity
α_c	Thermal Diffusivity of the Composite
α_i	Thermal Diffusivity of Material i
ANSYS	Computer Programm for Finite Element Analysis
Ar	Argon
ARC	Austrian Reserch Centers Seibersdorf GmbH
at%	Atom Percent
Au	Gold
B	Boron
Be	Beryllium
BET	Brunauer Emmet and Teller (Value for Surface Area)
Bi	Bismuth
BJH	Barrett, Joyner and Halenda (Pore Volume)
BSD	Backscattered Image
C	Carbon
CCVD	Catalytic Chemical Vapor Deposition
χ	Infiltration Quantity
CISP	Center for Innovative Sintered Products
Cl	Chlorine
C_{mg}	Pseudomonocrystalline Graphite
CNF	Carbon Nanofilament
CNF-HB	Carbon Nanofilaments with Herringbone Structure
CNFiber	Carbon Nanofiber
CNF-PL	Carbon Nanofilaments with Platelet Structure
CNF-SC	Carbon Nanofilaments with Screw Structure
CNT	Carbon Nanotube
C_p	Specific heat
Cr	Chromium
CTE	Coefficient of Thermal Expansion
Cu	Copper
C_v or VC	Vitreous Carbon
d	Thickness
D	Diffusion Coefficient
Δ T	Temperature difference
DSC	Differential Scanning Calorimetrie
E	Electric Field
EDX	Energy Dispersive X-Ray Analysis
ϵ	Electric Permittivity
FC	Future Carbon GmbH

g	Acceleration of Gravity
γ_s or γ_{sv}	Surface Tension solid - vapor
γ_{sl}	Surface Tension solid - liquid
H	Hydrogen
H	Magnetic Field
HCHO	Formaldehyde
HP	Hotpress
hrs	hours
HTSDD	High Temperature Sessile Drop Device
In	Indium
K_i	Bulk modulus of Material i
KW	Contact Angle
L	Position of the Infiltration Front on z-axis (slug-flow model)
L_P	Sample Thickness (Parker Model)
L(t)	Infiltration depth (depending on the infiltration time)
L_a and L_c	Lengths of the graphitic domains (Jenkins-Kawamura model)
λ	Thermal Conductivity
λ_g	geometrical factor
LM	Light Microscopy
min	minutes
MMC	Metal Matrix Composite
Mo	Molybdenum
MP	Melting Point
MWNT or CNT-MW	Multi-walled Carbon Nanotube
μ	Magnetic Permeability
N	Nitrogen
n/w	Not Wetting
NASA	National Aeronautics and Space Administration
η	Viscosity
O	Oxygen
P	Pressure
P_{thresh}	Threshold Pressure
ΔP_γ	Capillary Pressure Drop (slug flow model)
Pb	Lead
Pd	Palladium
PM	Powder Metallurgy
ψ	Function depending on the infiltration depth $\psi = \frac{L(t)}{\sqrt{t}}$
P_{SPU}	Sputtering Leistung
PSU	The Pennsylvania State University
R	Ideal Gas Constant
REV	Representative Element Volume
ρ	Density
ρ_{CN}	Density of Carbon
ρ_{Cu}	Density of Copper

ρ_{CuCN}	Density of a Copper-Carbon Composite
ρ_m	Density of the Metal
R_P	Kelvin Radius
S	Saturation
SEM	Secondary Emission Microscopy
Si	Silicon
S_i	Particle Surface Area per Unit Volume
SI	Systeme International
σ_l or γ_l or γ_{lv}	Surface Tension liquid - vapor
Sn	Tin
SWNT or CNT-SW	Single-walled Carbon Nanotube
t	Time
T	Temperature
$t_{1/2}$	Half-Life Time (Parker Model of Thermal Diffusivity)
Ta	Tantalum
Ti	Titanium
TU	Vienna University of Technology
u_l	Velocity Liquid
u_s	Velocity Solid
U_{SPU}	Sputtering Voltage
v	Velocity
V_a	Volume of the Pores / Gas / Air
V_{cn}	Volume of CNFibers
V_f	Volume Fibers
VGCNF	Vapor Grown Carbon Nanofibers
V_i	Volume of Material i
V_l	Volume Liquid
V_L	Liquid Molar Volume
W	Tungsten
W_{adh}	Work of Adhesion
W_i	Work of Immersion
wt%	Weight Percent
z	Direction of the Infiltration Flow
Zr	Zirconium

Contents

1 Introduction

In industrial and technological applications materials are often subjected to severe environmental conditions. Addressing these problems, new materials with adaptable properties play an important role in many recent research programmes. Composite materials are one big concept to combine the beneficial properties of their constituents and thereby satisfying new challenges.

Due to their specific thermal and mechanical properties metal matrix composites (MMC) have attracted attention in different fields of materials science as carbon/metal MMCs are promising candidates for prospective 'heat sinks' in electronic devices. However, it is difficult to fabricate carbon/metal composites because of the poor wettability between carbon and molten metal alloys [1].

There are countless applications for heat sink and heatspreader materials. As the building elements of micorelectronics get smaller and have to cope with growing power density, more efficient cooling systems and improved heat transfer materials will be a hot topic. Suitability for cycling temperatures will also be crucial for future materials as well as long-term stability.

Heat sink application requirements

In heat sink and heatspreader applications materials with high thermal conductivity combined with a low coefficient of thermal expansion are demanded.

Property	Cu-Mo Cu-W	Al-SiC	Cu-Be	Diamond Composites	Cu-CNFiber MMC*
Mechanical Stiffness	+	+	++	+	+/++
Thermal Conductivity	++	+	++	+++	++/+++
Thermal Expansion**	++	++	+	+	+/+++
Density	-	+++	-	++	+
Machinability	+	-	+	-	++/+++
Surface Quality	+	-	-	-	++/+++

Table I: Commercially used heatsink materials, general overview [2]

(-)...bad, (+)...good, (++)...very good, (+++)...excellent
* ...Expecting benefits from existing results, simulations and publications.
** ...adaptable to the coefficient of thermal expansion of Si and ceramics.

Materials used today fit very well to these requirements, but they also have some disadvantages, for instance high density, bad machinability or high price. Table I gives a qualitative, general overview about commonly used materials.

For certain applications these materials show some disadvantages. Especially in several electronic applications (e.g. laser diodes or computer chips (figure 1)) the machinability in connection with surface quality is a topic, where the copper-carbon composite material would offer a big advantage.

Figure 1: A thermal heat sink device for use in integrated circuit packaging technology fabricated by NASA. The Cu/Carbon nanotube composite is located on the backside of the chip [3].

Carbon reinforced MMCs

Miscellaneous investigations with graphite flakes and carbon fibers have been reported to show promising results [2, 4, 5]. They improve the demanded properties and evade application limitations. Due to the lack of chemical interactions between carbon and the matrix metal, the manipulation and investigation of the interface plays an essential role.

Several potentially interesting matrices, for instance nickel [6], degrade the fibers at high temperatures and therefore developement has concentrated on composites with matrices that are chemically inert towards carbon, such as tin, lead and copper [7]. The reason that these metals do not form strong bonds with carbon and do not wet it [8], leads to several problems to be addressed in the production of MMCs. How can the wetting behavior be promoted, and how to infiltrate carbon fiber preforms with these metals? One approach is to alloy the liquid metal with an element that will react with the carbon fibers to change their wettability but that will not produce serious degradation. To investigate the wetting behavior, the sessile drop technique was successfully used in various studies [9]. Another way is to functionalize the

carbon fibers themself to build a catalytically-active surface and then deposit the metal chemically on the carbon [10, 11].

For producing MMCs many different kinds of fabrication processes such as fiber-coating, gas pressure infiltration [12] or ultrasonic infiltration [13] have been studied, but in general there are two different types.

In a powder metallurgical process metal and fibers are mixed together and subsequently hot pressed. It is possible to disperse and align the fibers more or less, but the mechanical and thermal interface still remains weak.

The other method used is to infiltrate a preform or foam with the liquid metal. In case of the pressure infiltration process, the non wetting behavior of the metal/carbon system leads to very high threshold pressures which can compress or destroy the preform and thereby worsen the infiltration process.

Nanofeatured copper composites

Copper has a very high thermal conductivity, but due to its high coefficient of thermal expansion it causes severe mismatch to the substrate (e.g. Si or alumina). For applications with a high number of thermal cycles, standard copper material often is not sufficient. In some applications the high density of pure copper is a further disadvantage. An interesting system for compounds with high thermal conductivity is copper reinforced with carbon nanofibers. Assuming an interface of high quality and a proper alignment of the nanofibers (carbon nanofilaments (CNF) have a thermal conductivity of more than 1000 $\frac{W}{mK}$ in length direction and carbon nanotubes (CNT) are predicted to have a thermal conductivity of about 2000 $\frac{W}{mK}$ in length direction), this composite is predicted to exhibit excellent thermal conductivity [4]. It is shown that the wetting behavior between carbon and copper alloys containing carbide forming elements is influenced by the additives [15] and the contact angle decreases to small values, which means good to excellent wettability.

When compared to the mentioned 'regular' carbon fibers with a diameter of about 7-10 μm, nanofibers with a diameter of about 50-200 nm have a much higher surface to volume ratio and therefore the interface between the fiber and the metal gains much more importance for the resulting properties. In MMCs containing nanofilaments or nanotubes as building blocks, the interface plays an essential role in exploiting the potential of this promising reinforcement.

Many problems, which are mainly solved for MMCs containing 'regular' carbon fibers, still appear when using nanofibers as reinforcement. Besides separation, dispersion, alignment and orientation of the fibers as well as densification problems, the reproducible quality of the raw material is very important. Only rare data of the properties of carbon nanofibers are available [16].

Examples and summary

Some examples for manipulating the wettability using carbide forming elements are given in the following: In the carbon nanofiber/Cu-Cr system with a chromium content between 0.5 and 2 at.% the contact angle is found to be constantly about 40 ° irrespective of drop mass or chromium concentration in the alloy [9]. Some other carbide forming matrices like Cu-Ti, Cu-B or so called active brazing alloys (ABA) [17] also show good wettability, but often the thermal conductivity of the alloy is significantly decreased by the additives [18].

Infiltration of carbon preforms such as nanofiber foams yields some promising results and avoids the problem of clustered nanoparticles, as described above.

With varying the nanofiber content in the matrix the coefficient of thermal expansion (CTE) can be adapted easily, which makes the product flexible and even tailorable for various applications. Furthermore carbon nanofibers containing metal matrix composites can satisfy a good surface quality and an excellent machinability.

This study gives an overview on different MMC-production routines and their feasibility which involve copper-alloy composites reinforced with carbon nanofilaments and carbon nanotubes. The production routines chosen are carbon nanofeatured preform infiltration methods and chemical coating of the nanofibers with subsequent hotpressing or microwave sintering.

2 Theoretical background

In this section models for the wetting behavior of solids, the infiltration process and thermal properties of composite materials are shown. Furthermore the chemical process of electroless copper deposition is described and several effects appearing during sintering using microwaves are presented.

2.1 Surface energy

To create a surface, surface energy is required. Regarding fluids, this energy is called surface tension (γ_l or σ_l) and is defined as follows: The work needed to increase the surface area divided by this thereby arising surface area.

$$\gamma_l = \frac{\Delta W}{\Delta A}(SI - unit : J/m^2 = N/m) \tag{2.1}$$

When bringing two surfaces in contact, energy is released, which is called adhesion or work of adhesion W_{adh}:

$$W_{adh} = \gamma_s + \gamma_l - \gamma_{sl} \tag{2.2}$$

γ_s ... Surface energy of the isolated solid state body A
γ_l ... Surface energy of the isolated solid body B
γ_{sl} ... Energy resulting out of the interaction between the interfaces (solid–liquid)

The fundamentals of adhesion are the microscopic interactions between molecules with saturated chemical bonds, which one can subsume to three different groups: primary interactions (chemical bonds), quasi chemical bonds (hydrogen-bridges) and secondary interactions (Van-der-Waals bonds).

The correlation between the surface energies can be derived from the equilibrium contact angle after bringing a solid and a fluid in contact. In case of equilibrium Young's equation (2.3) gives this correlation. It allows the prediction of the behavior of a fluid on a solid surface. The numerical value of the contact angle lies between 0° for total wetting and 180° for non wetting combinations. So $\theta \geq 90°$ means bad and $\theta \leq 90°$ good wetting (see figure 2).

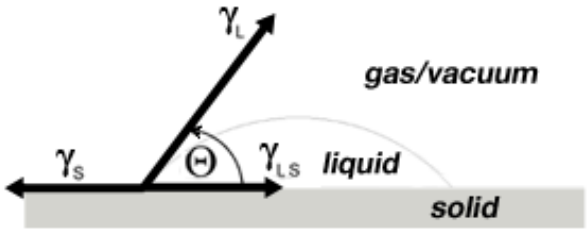

Figure 2: Contact angle between the liquid and the solid surface

A common method to determine the surface energy is measuring the contact angle. Using a fluid with known surface energy γ_l, one can derive the surface energy of the solid γ_s using Young's equation (2.3). Other experimental methods to collect γ_l of liquids are measuring the creeping height of the fluid in capillary tubes, the ring-method after Lecomte De Noüy or the investigation of surface waves.

$$\gamma_l \cdot cos\theta = \gamma_s - \gamma_{sl} \tag{2.3}$$

Inserting equation (2.2) into (2.3) the relation between contact angle and work of adhesion results in:

$$W_{adh} = \gamma_l(1 + cos\theta), \tag{2.4}$$

the Young-Dupré equation.

Table II gives some example values of W_{adh} and the contact angle for different material combinations:

Substrate	Cu at 1373 K		Au at 1373 K		Al at 1100 K	
	Θ (deg)	W_{adh} (mJ/m^2)	Θ (deg)	W_{adh} (mJ/m^2)	$\Theta^{(*)}$ (deg)	W_{adh} (mJ/m^2)
$C_v(\rho = 1.5\,\mathrm{Mg/m^3})$	139	319	135	338	139	206
$C_{mg}(\rho = 2.26\,\mathrm{Mg/m^3})$	122	611	119	595	123	383

$^{(*)}$ initial contact angle before reaction

Table II: Contact angle and adhesion of different metals on vitreous carbon (C_v) and pseudomonocrystalline graphite (C_{mg}) [19].

In non-reactive metal/carbon systems, wetting angles are very large and, as seen in Table II, the actual values differ very little for the various metals.

2.2 Infiltration process

There are several fundamental physical phenomena involved in the infiltration process, which are quite similar for all three common fiber reinforced composite materials. This includes capillary phenomena, transmission phenomena of the fluid flow, thermal- and mass transfer, mechanical properties of the preform that can be transformed during the infiltration, chemical reactions during and after the infiltration process, a.s.o.

Dealing with transport phenomena with sufficiently fine-scaled porous materials one commonly uses a continuum mechanics approach based on consideration of a representative volume (REV). This REV has to be large enough to contain representative averages of all three phases (fluid, solid, pores), but small enough to be considered as a differential element on scale of the preform [20].

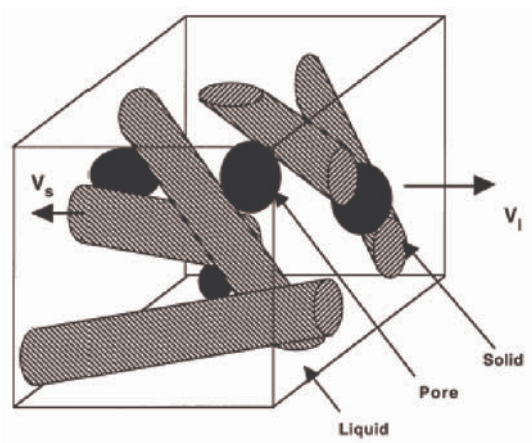

Figure 3: representative volume [20]

For the unit volume the equation

$$V_a + V_f + V_l = 1 \tag{2.5}$$

has to be fulfilled, where V_a is the pore volume (filled with gas/air), V_f the fiber volume and V_l is the volume of the liquid phase (figure 3).

To derive equations for representative properties within the REV, averaged values of the relevant parameters, such as velocity or volume fraction, are used.

This leads to the definiton of the saturation in the fluid phase [20]:

$$S = \frac{V_l}{(1 - V_f)} \tag{2.6}$$

For the empty preform the saturation S=0 and increases to S=1 when the preform is fully filled with the liquid. To simplify matters, one assumes constant densities of the liquid and solid phases for the entire experiment. In cases of reactive infiltration one has to keep an eye on this assumption and handle it with care.

In this case mass conservation is valid for the liquid and the solid phase as expressed in equations (2.7) and (2.8), where the local velocity of the solid phase (fibers) is u_s and u_l is the average local velocity of the fluid inside the pores. (see figure 3)

$$\frac{\partial V_f}{\partial t} + \nabla(V_f u_s) = 0 \tag{2.7}$$

$$\frac{\partial((1 - V_f)S)}{\partial t} + \nabla((1 - V_f)S u_l) = 0 \tag{2.8}$$

Now we assume that there is a sharp infiltration front between the uninfiltrated and the fully dense infiltrated part of the preform, which means saturation S=1 in the infiltrated part. This assumption is termed 'slug-flow' as illustrated in figure 4. A consequence of this slug-flow model is that $1 - V_f = V_l$ is valid everywhere in the already infiltrated area.

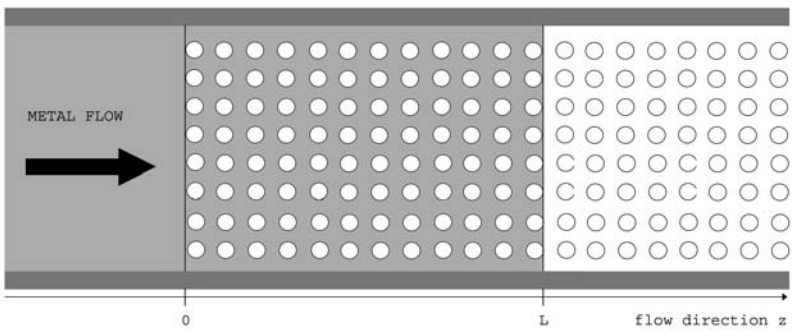

Figure 4: Schematic description of unidirectional slug-flow infiltration

Besides the definition of the representative volume (REV), the saturation and the introduction of the slug-flow model, the capillary pressure drop at the infiltration front ΔP_γ is a crucial parameter for describing the infiltration process. $\Delta P_\gamma < 0$

corresponds to wetting of the fibers by the metal, while $\Delta P_\gamma > 0$ corresponds to non-wetting.

2.2.1 Capillary law

To infiltrate a non-wetting metal into a preform a certain pressure such as mechanical or gas pressure has to be applied to the specimen during the process. Several studies have shown that for infiltration a minimum threshold pressure correlated to the fiber volume fraction V_f and the average particle diameter d is required. Wannasin [21] showed, that assuming spherically shaped particles one can calculate this threshold pressure very precicly using the capillary law (2.12).

Knowing the particle surface area per unit volume S_i of the metal matrix this minimal threshold pressure P_0 can be written in terms of the work of immersion $W_i = \gamma_{sl} - \gamma_s$ [12]:

$$P_0 = S_i W_i \tag{2.9}$$

Using Young's equation (2.3) P_0 can be related to the contact angle θ.

$$P_0 = S_i \gamma_{sl} cos\theta \tag{2.10}$$

For spherical particles with an average diameter d and a particle volume fraction V_f, S_i can be rewritten to:

$$S_i = \frac{6\lambda_g V_f}{d(1 - V_f)} \tag{2.11}$$

λ_g is a geometrical factor to consider variations from spherically shaped particles.

Using (2.10) and (2.11) the capillary law [12] is given by

$$P_0 = 6\lambda_g \gamma_l cos\theta \frac{V_f}{(1 - V_f)d}. \tag{2.12}$$

P_0... threshold pressure, λ_g... geometrical factor, (λ_g is further influenced by surface roughness, particle size distribution and some others), d... average particle diameter, V_f... particle volume fraction.

As soon as the threshold pressure can be calculated the next step is to derive the infiltration height one can expect applying a certain external pressure during the process.

2.2.2 Darcy's law

The Navier-Stokes equation describes the fluid mechanics of viscous liquids [22]. These equations explain the flow velocity and the pressure distribution in Newtonian fluids. In the case of incompressible fluids, small Reynolds numbers and assuming that the time derivative of the velocity of the fluid is much smaller than its spatial derivative, the general Navier-Stokes equation can be simplified to [12, 23]:

$$\nabla P = \eta \nabla^2 v \tag{2.13}$$

v... velocity of the fluid, P... pressure in the fluid, η ... viscosity

For most liquid-metal infiltration processes this is a reasonable assumption. One has to be aware, that in (2.13) gravitational effects were neglected. For taking these effects into account (2.13) turns into (2.14).

$$(\nabla P - \rho_m g) = \eta \nabla^2 v \tag{2.14}$$

ρ_m... density of the metal, g... acceleration of gravity

A further assumption in the Darcy equation (2.15) is that the amount of liquid laminary passing through a porous medium is directly proportional to a value characteristic for the material and directly proportional to the pressure gradient. Idealizing the flow of the pressurized fluid to be unidirectional leads to the commonly used Darcy equation for incompressible fluids flowing through porous media (2.15). One has to note that this assumption of a laminar and unidirectional flow might be physically unrealistic on a microscopic scale.

$$v_0 = -\frac{k}{\eta}(\nabla P - \rho_m g) \tag{2.15}$$

v_0 is the average superficial velocity of the fluid and k the intrinsic permeability of the preform. Assuming unidirectional, horizontal flow (flow direction is z, see figure 4 and figure 5) gravity can be neglected. So $\nabla P = \frac{dP}{dz}$ where dP/dz is the pressure gradient at the infiltration front. We also assume that v_0, defined as the average velocity over the entire volume element δV is constant i.e. $\nabla v_0 = 0$. For the permeability k one empirically found, that k of a porous medium is proportional to the square of the mean diameter d of the particulates [12] i.e. $k = a \cdot d^2$.

The superficial velocity v_0 can be related to the actual velocity in the porous medium dz/dt using the fiber volume fraction:

$$v_0 = (1 - V_f)\frac{dz}{dt} \tag{2.16}$$

It is possible to introduce a parameter change for solving the problem as a function of one variable instead of two (z,t). The quantity χ is defined as $\chi = z/\psi\sqrt{t}$ [23]. $\psi\sqrt{t}$ is acting as a scaling factor along the z axis. $\chi = 1$ shall correspond to the position of the infiltration front, $z = L(t) = \psi\sqrt{t}$.

By combining of equations (2.15) and (2.16) and integration from $\chi = 0$ to $\chi = 1$, ψ is then expressed as

$$\psi = \sqrt{\frac{2k\Delta P}{\eta(1 - V_f)}} \tag{2.17}$$

which provides – after changing to the parameter z again – the square of the infiltration height z as a function of time t and pressure difference $\Delta P = P_0 - P_a$ [12, 23]. Figure 5 shows P_0 as the pressure at the entrance of the preform at $z = 0$ and P_a as the pressure at the region just behind the infiltration front at $z = L$.

$$z^2 = \frac{2kt}{\eta(1 - V_f)}\Delta P \tag{2.18}$$

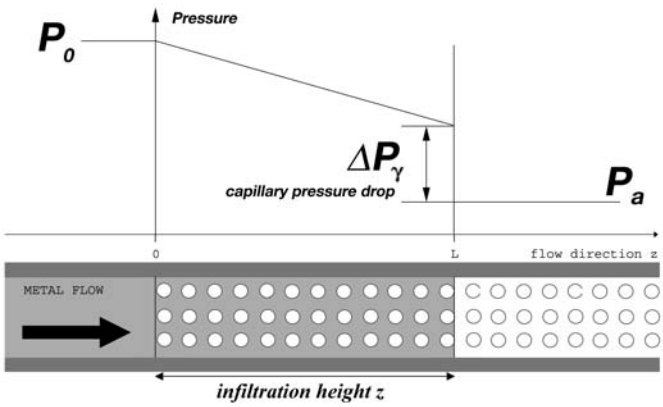

Figure 5: Schematic description of unidirectional slug-flow infiltration, showing the pressure distribution for a preform of constant permeability. [20]

2.3 Thermal properties of a composite

Regarding the complexity of a composite material, its thermal properties are relatively difficult to predict precisely. It is influenced by several factors including matrix plasticity and the internal structure of the composite, which consists of fibers embedded in a continuous metallic matrix.

For calculating the coefficient of linear thermal expansion (CTE), which is highly important for practical aims, several theoretical analyses have been presented in the literature giving expressions for the CTE of metal matrix composites.

The coefficient of linear thermal expansion (α) is defined as:

$$\alpha = \frac{1}{L_0}\frac{\Delta L}{\Delta T} \tag{2.19}$$

where L_0 is the original length of the sample and ΔL is the change in length over a temperature interval ΔT.

One of the simplest and also frequently used approches for calculating the CTE for a composite containing spherically shaped particles is the method of Turner [24, 25, 26]. This model assumes that the internal stress system in a mixture is such that the stresses are nowhere sufficient to disrupt the composite. With the volume fraction V and the bulk modulus K, the CTE of the composite (α_c) is obtained as:

$$\alpha_C = \frac{\sum_i^n \alpha_i V_i K_i}{\sum_i^n V_i K_i} \tag{2.20}$$

i . . . indicates the various involved materials.

For predicting the CTE of unidirectionally reinforced fiber composites several models have been developed. According to Schapery [27] and Chamis [28], the CTE for a fiber composite reinforced in longitudinal direction is given by:

$$\alpha_{\|} = \frac{\alpha_f V_f E_f + \alpha_m V_m E_m}{V_f E_f + V_m E_m} \tag{2.21}$$

E . . . Young's modulus, V . . . volume fraction, and the subscripts '$\|$' stands for the composite in longitudinal direction, 'f' represents the fiber and 'm' the matrix, respectively.

Schapery also gives the CTE of a fiber composite in the transverse direction as:

$$\alpha_{\perp} = (1+\nu_m)\alpha_m V_m + (1+\nu_f)\alpha_f V_f - \alpha_{\parallel}\nu_c \tag{2.22}$$

$$\text{and} \quad \nu_c = \nu_f V_f + \nu_m V_m$$

where ν is Poisson's ratio and the subscripts '$\perp$' and 'c' stand for the composite in the transverse direction and the composite respectively.

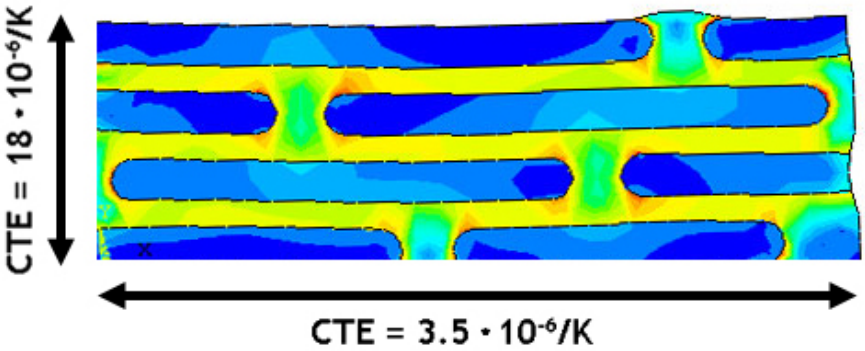

Figure 6: Simple CNF-MMC model showing thermal expansion and relative stress qualitatively for ΔT 200 K, ANSYS modeling

Besides these models finite element modeling was used to visualize the qualitative behavior of a fiber reinforced composite at elevated temperatures, here obtained by ANSYS. For this, the following material parameters were used to describe the carbon nanofiber – copper composite: Carbon nanotubes (special sort of carbon fibers, see section 3.1) with a Young's modulus of 1500 GPa [29] and thermal conductivity (α_{CNF}) of 2000 W/mK in the longitudinal direction [2]. It is important to note that this high thermal conductivity of the nanotubes is expected in the longitudinal direction only, since carbon nanotubes are not isotropic! The coefficient of thermal expansion was assumed to be negligible for the carbon nanotubes [29]. The copper matrix is characterised by $\alpha_{Cu} = 400$ W/mK and a CTE of $17 \cdot 10^{-6}/K$.

For modeling purposes, the composite was subjected to a uniformly distributed temperature difference of 200 K.

The CTE of the composite in longitudinal direction was calculated to be reduced to $3.5 \cdot 10^{-6}/K$ (figure 6). With adjusting the carbon nanofiber volume fraction the CTE of the composite can be adapted to the one of Silicon (CTE of 3–6 $\cdot 10^{-6}/K$ [30]).

2.4 Electroless copper deposition

As described above, the wetting of carbon nanofibers by liquid metals is very bad. Ebbesen et al. [31] found, that only liquid metals with surface tensions of 100–200 mN/m^2 and lower will wet the surface of carbon nanofibers. This has led to the idea of modifying the nanofiber surface by using decoration methods. Within this the surface is modified by oxidation in order to obtain nucleation of metals on the carbon nanoparticles. A chemical method of depositing metals onto the oxidized nanofiber surface is electroless plating. In this study a two-step method was accompished. Before plating with copper the oxidized carbon nanofibers are subjected to further pretreatment described below (sensitization and subsequent activation). The method introduces catalytic nuclei (Palladium) onto the non-catalytic surface.

Figure 7 shows the four steps to be accomplished for a successful electroless copper coating. Because sensitization and activation are performed in two seperated steps, this method is called two-step process.

Another approach uses one single sensitization-activation bath. This single-step method is described by Ang et al. [10].

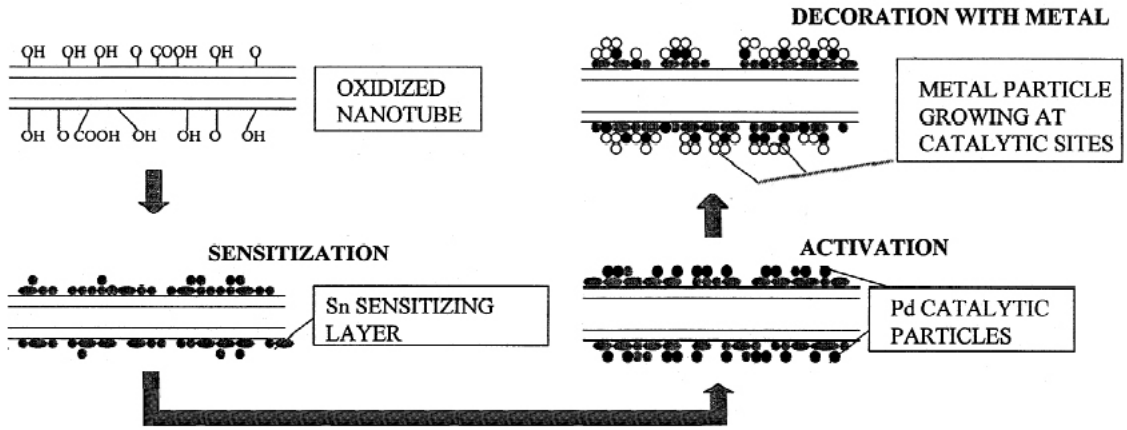

Figure 7: The stages in the electroless plating process employing the two-step sensitization-activation approach [10]

Sensitization

In the first step after cleaning the nanofibers their surface is sensitized with a Tin (Sn) layer which enhances Palladium (Pd) adsorption in the following activation step and fortifies the binding strength of Pd to the surface.

Age of $SnCl_2$–HCl sensitizing solution	Appearance of sensitizing solution	Nature of the sensitized and activated fibers	Nature of the Cu deposits after 5 min immersion in Cu bath
1 h	White, cloudy mixture with a yellowish tinge. Separates on standing to give a white precipitate and light yellow supernatant	Sensitizer does not wet the nanofiber surface well. Low density of Pd particels on the surface	Cu grows as cone-like aggregates on some nanofiber surfaces. Cu aggregates are made up of sperical particles (⌀ ≈3 nm)
72 h	Pale yellow slightly opaque solution	Sensitizer wets well. Consequently, Pd particle density is very high (Pd particles ≈3 nm in diameter)	Some of the nanofibers are densely coated with Cu particles ≈3 nm in diameter
144 h	Yellow solution	Sentiziser does not wet the surface well. Pd particles (6–12 nm in diameter) grow on the sensitized areas	Cu grows upon the Sn and Pd islands. Little mounds of Sn, Pd and Cu deposit on the nanofibers, density of deposits is relatively low

Table III: Aging influence of the $SnCl_2$–HCl sensitizing solution on the Cu deposition distribution [10].

Sensitization means adsorption of Sn^{2+} ions on the carbon surface. For the sensitizing solution 0.044M $SnCl_2$ is diluted in 0.12M HCl. Important for a homogeneous coating of the carbon nanofibers is the appropriate aging of this solution. Research done by Ang et al. [10] showed, that the copper decoration is strongly corresponding to the age of the sensitizing solution. Table III lists this correlation and figure 8 shows the sensitizing solution for various aging times. The authors found best results with densely coated carbon nanofibers for a sensitizer aged for 3 days. Longer as well as shorter aging times lead to worse results.

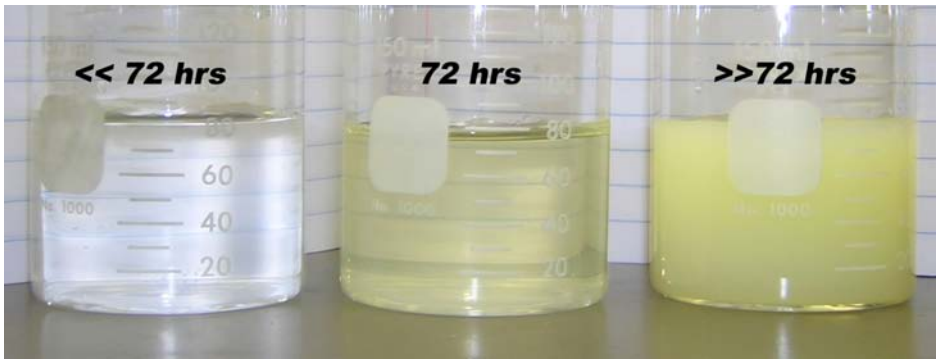

Figure 8: $SnCl_2$ sensitzing solution for various aging times

The mechanisms involved with sensitization are still under discussion, but most authors believe that Sn(IV) in the aged sensitizer forms a colloidal dispersion which entraps Sn(II) (presumed active agent). It is the nature of Sn(IV) to form colloidal polymeric species which determine the surface activity of the sensitizer. Initial aging of the sensitizer is necessary to increase the Sn(IV) concentration and to form the colloidal active species. However, prolonged aging allows continued growth of the colloidal polymeric chains until their surface activity ceases [10].

Activation

The catalytic pretreatment of nonconductive surfaces for the subsequent coating by metals is called activation. In this step the already sensitized nanofibers are dispersed in a 0.0014M $PdCl_2$ solution diluted in 0.12M HCl. The Sn^{2+} ions, which have a relatively low redox potential, reduce the Pd^{2+} ions to Pd^{0+} (metallic state). With a dense Sn layer from the sensitizing step one can expect a similar arrangement for the Pd atoms wich will catalyse the metal deposition in the following step.

Copper deposition

After successful pretreatment of the fibers they are transferred to the copper plating bath. The composition of the solution for depositing the copper ions on the substrate is as followed:

- 1.9 g $CuSO_4 \cdot 5\ H_2O$
- 5.0 g Potassium Sodium Tartrate $\cdot$ 4 H_2O ($KOCO(CHOH)_2\ COONa \cdot 4\ H_2O$)
- 10 ml Triethylamine
- approx. 4 ml Formaldehyde (HCHO)
- 400 ml H_2O distilled
- 0.8 g NaOH and Formaldehyde to adjust the pH-value to pH 12.5

The copper ions deposit at the catalytic sites where the Pd atoms are located. Formaldehyde acts as the reducing agent.

In the alkaline copper plating solution Formaldehyde decomposes to:

$$2\ HCHO + 2\ OH^- \rightarrow 2\ HCO_2H + H_2 + 2e^-$$

Besides this another reaction takes place:

$$HCHO + 2\ OH^- \rightarrow H_2C(OH)O^-$$

$$H_2C(OH)O^- + OH^- \rightarrow HCO_2^- + H^-_{adsorbed} + H_2O$$

During the coating process stabilizers prevent the not activated surfaces (e.g. beaker walls) from the metallization by copper. These additives also prevent the plating bath from decomposing.

Another important parameter for the copper coating behavior is the pH-value of the Cu bath. Experimental studies showed, that with a pH-value around pH 12 most of the carbon nanofibers are densely decorated with copper [10, 32]. Studies on the electroless copper bath by Bindra et al. [33] proposed a mechanism of the anodic reaction as shown below:

$$HCHO + H_2O \leftrightarrow H_2C(OH)_2$$

$$H_2C(OH)_2 + OH^-_{adsorbed} \leftrightarrow H_2C(OH)O^-_{adsorbed} + H_2O$$

$$H_2C(OH)O^-_{adsorbed} \leftrightarrow HCOOH + 1/2H_2 + e^- \text{ (rate determining step)}$$

$$HCOOH + OH^- \leftrightarrow HCOO^- + H_2O$$

The rate determining step thus depends on the OH^- concentration, accounting qualitatively for the observed pH dependence [10].

In order to keep the copper ions in the alkaline solution complexing agents like Potassium Sodium Tartrate are used. However the complexing agent concentration influences the copper deposition by reducing the deposition rate significantly.

2.5 Microwave sintering

Heating and sintering samples with microwaves is a rather new method in the field of materials processing. In the past years it was shown, that this method is useful for various applications (e.g. sintering of ceramic materials) and that it saves time and energy compared to conventional heating [35].

The sintering process can be devided into three phases, the heating pase, the holding phase and the cooling phase. During the holding phase the compacted powder particles connect with each other forming a so called sinter neck. This process forms a stable, solid, but porous sinter body. For each material exists a certain temperature interval where sintering results in the desired properties. Using conventional heating, sometimes long time periods are required for instance to avoid too strong mechanical stresses, which can make the process very expensive and energy consuming.

Compared to conventional heating, microwave heating is a very rapid heating process, which requires short holding times and does not just use thermal energy as the heating effect, but also nonthermal energy e.g. molecular excitation [36, 37, 38].

Another important difference between conventional and microwave heating is the temperature profile inside the sample during the process. Conventional heating heats the sample from the outside, which means it often takes a long holding time to reach the required temperature in the inside of the sample, while the outer regions stay in the hot zone for the entire time. Microwaves heat the sample from the inside, which gives a much more homogeneous temperature distribution (figure 9). Furthermore different materials can be heated selectively, even within one sample.

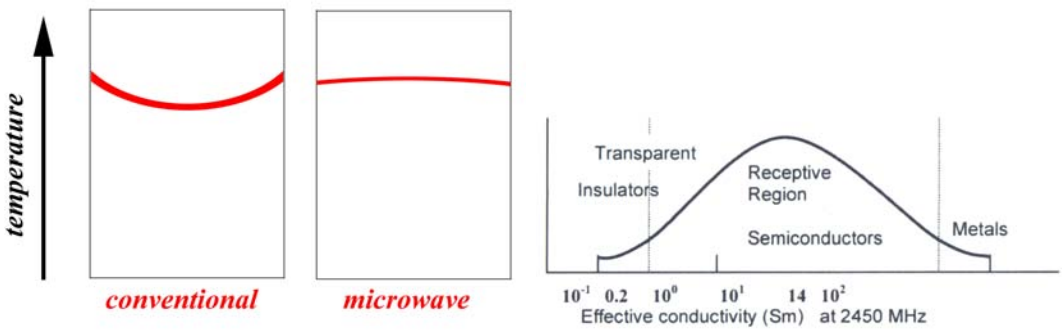

Figure 9: Temperature profile for conventional and microwave heating [35]; Microwave absorption by different materials [39]

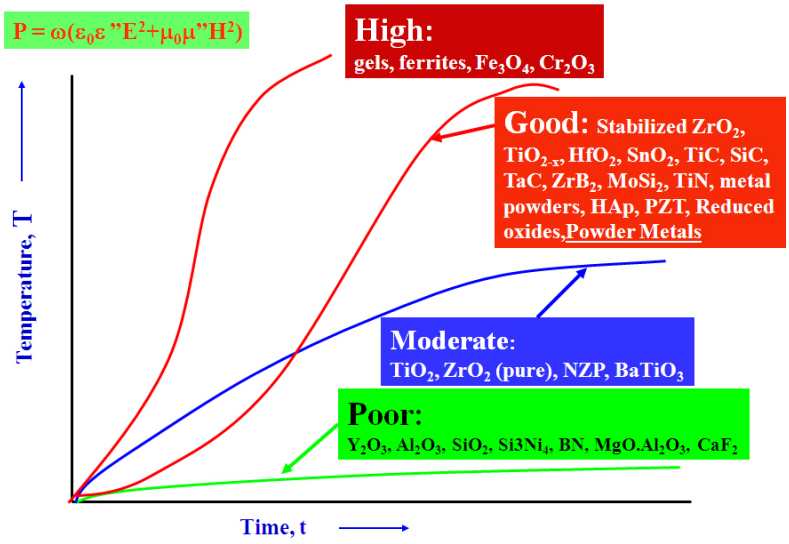

Figure 10: Microwave absorption behavior of various materials [36]

All conventional heating processes involve thermal energy for transport mechanisms leading to sintering. The diffusion coefficient D at the grain boundaries is about 100 times larger than for volume diffusion, which makes boundary diffusion the principal effect.

The heating effect of microwaves is based on dielectric losses, magnetic permeability losses, eddy currents, etc. The heating power density in the microwave field is:

$$\dot{q} = 2\pi\nu(\epsilon_0\epsilon^{''}E^2 + \mu_0\mu^{''}H^2) \tag{2.23}$$

Various materials exhibit different absorption characteristics in the electric and the magnetic field. In a composite material this effect can lead to an anisothermal heating of the sample (figures 10 and 11).

In a microwave oven with standing waves, the magnetic and electric field are spatially seperated. This fact can be used for selective heating as shown in figure 11.

The so called microwave effect is an issue in microwave processing that facilitates rapid sintering. This effect summarizes athermal contributions for enhancement in reaction kinetics and material diffusion, which lead to new reaction products and rapid sintering.

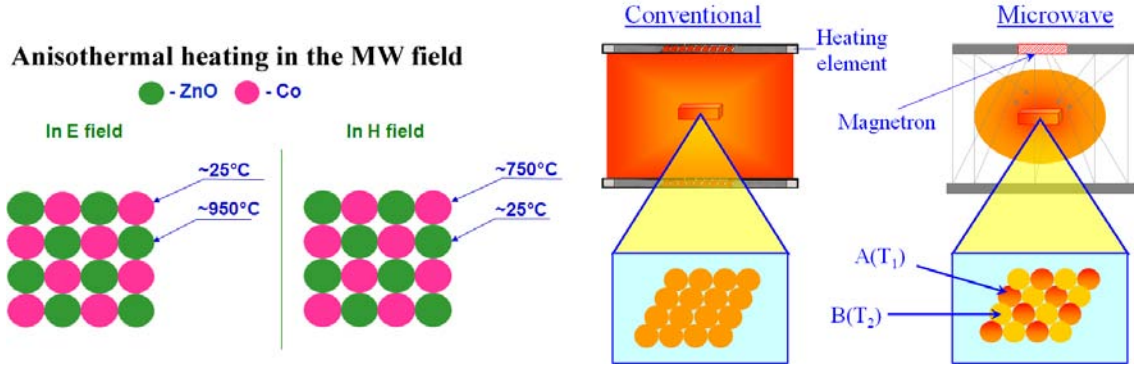

Figure 11: left: Anisothermal heating in the microwave field; right: Microwave heating compared to conventional heating [36]

Several proposed theories explain the microwave effects:

- Ponderomotive Force Interaction: Microwave-excited ionic currents become locally rectified (near the particle interface), giving rise to an additional driving force, other than thermal energy, for mass transport (Booske et al. [40]).
- Materials with substantial amount of porosity: At convex surfaces of the pores the electric field is fortified, providing a non-ohmic and a localized plasma contribution to the driving force, which results in pore removal and thereby accelerating material diffusion (Willert-Porada [41]).
- Anisothermal heating caused in two different phases of widely varying microwave absorption characteristics would provide a strong driving force to cause enhancement in reaction kinetics followed by sintering (Peelamedu, Roy and Agrawal [37, 38]).

To summarize the differences, isothermal (conventional) heating is a uniform heating, the exchange of the species is mutual, reaction kinetics are slow and low material diffusion rates occur. Anisothermal (microwave) heating is a selective heating resulting into non-uniform heating and temperature gradients which means selective exchange of the species. The reaction kinetics are rapid and the material diffusion rates are high.

Microwave sintering is quite well established in scientific laboratories, but the technology is not converted to industry conditions yet [35].

3 Materials used in this study

3.1 Carbon nanofibers

According to their growth modes and to the arrangement of the graphene layers, different filamentous nanocarbons are summarized under the term 'carbon nanofiber'. Sometimes the term carbon nanofiber is understood as carbon nanofilaments (CNF) in comparison to carbon nanotubes (CNT). In this study the term "nanofiber" is used as a summarizing term for nanofilaments and nanotubes. Carbon nanofilaments (CNF) exhibit various growth conditions and mechanisms, resulting in different filament morphologies such as seen in figure 12 and figure 13. Fishbone or herringbone structures for example are graphene sheets arranged in an angle of about 30 degrees with respect to the fiber axis. Carbon nanotube (CNT) structures are shown in figure 14 [42, 43, 44].

The carbon nanofilaments used in this study were produced by Electrovac AG [46] under specification HTF110FF-HHT.

Growth mechanism

In general carbon nanofibers are grown by depositing carbon from a carbon-containing gas mixture using fine metal particles as a catalyst. Nanostructures such as fullerenes and nanotubes sometimes do not need a catalyst to grow and are basically wrapped graphene layers, as described below. For nanofilaments, depending on the catalyst, uni-directional growth is found with the catalyst at the tip or at the base. Bi-directional growth means simultaneous growth in two opposite directions with the catalyst in the middle. Growing could also be in more than two directions called "octopus nanofilament", or a large catalyst particle splits into several smaller parts continuing growth into various directions [42], figure 12.

Three main processes are used to synthesize carbon nanostructures: catalytic chemical vapor deposition (CCVD), arc-discharge and laser ablation.

The first process produces all sorts of carbon nanostructures. For synthesizing nanofilaments with the CCVD method a boat containing a metal catalyst is positioned in a tube furnace, which is fed by a carbon containing gas. As described in

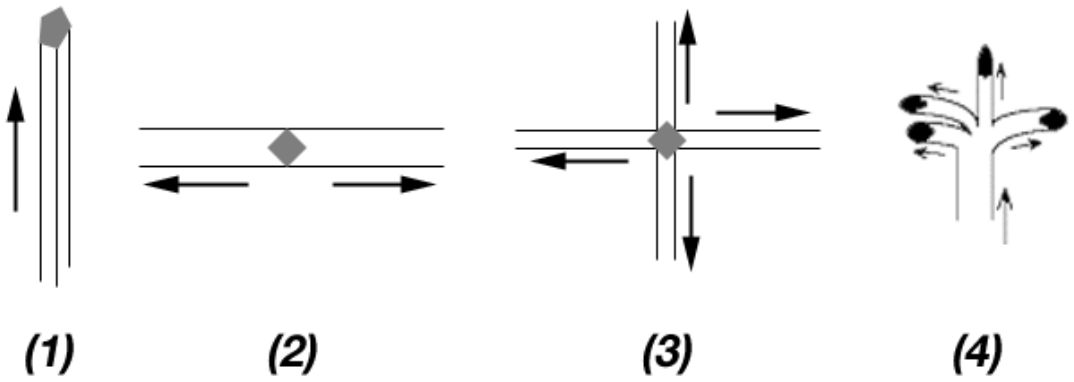

Figure 12: Morphologies of carbon nanofilaments (CNF's). (1)...unidirectional, (2)...bidirectional, (3)...multidirectional ("octopus") and (4)...dendritical growth.

detail in the following paragraph, the carbon is deposited on the catalyst surfaces which grow the nanofiber.

In case of the arc-discharge process, an arc discharge is ignited between two graphite rods that produces different carbon nanostructures at one of the electrodes. Depending on various parameters e.g. gas atmosphere, pressure or the location in the reactor, single-walled nanotubes, multi-walled nanotubes and fullerenes can be collected.

For producing nanotubes the laser ablation method is used. A furnace is loaded with a graphite target and a catalyst. The target is irradiated by a laser beam. The resulting "atom soup" rearranges, forming single- and multi-walled nanotube structures depositing in the cooler zones at the end of the tube furnace with high yield.

Carbon nanofilaments

Carbon nanofilaments (not nanotubes in this case) are typically produced via a catalytic chemical vapor deposition (CCVD) process. Their average diameter lies between 150 nm and 300 nm. Their structure is based on parallel stacked nanoscale graphene planes, which can show different forms. Figure 13 shows examples of the platelet structure (CNF-PL), the herringbone structure (CNF-HB) or the screw structure (CNF-SC).

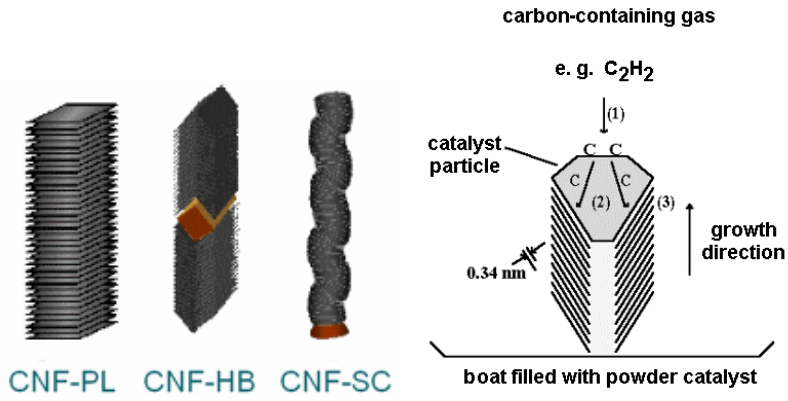

Figure 13: Different forms of carbon nanofilaments: (from left to right) platelet structure (CNF-PL), herringbone stucture (CNF-HB) and screw structure (CNF-SC) [43], CCVD unidirectional growing mechanism [42]

Their growth in this quite complex form can not be described with one simple mechanism, and there is a large number of different carbon nanostructures formed during CCVD. There are several growth mechanisms accepted for CNFs, depending on the catalytic particle used. The following model shows the growth mechanism for a one-dimensionally growing carbon nanofilament assisted by one metal catalyst particle (see figure 13).

The tube furnace is loaded by a boat containing metal catalyst powder and heated to moderate temperatures in the range of 500 °C to 1000 °C. The carbon containing gas is dissociatively adsorbed at the catalyst surfaces. The adsorbed carbon atoms go into solution and diffuse through the catalyst particle. The carbon will precipitate at the other side (rear) of the catalyst particle in the form of filamentous carbon. Multiple graphene layers are formed and the nanofilament is growing until the catalyst is deactivated, e.g. by coating with amorphous carbon [42].

For the catalytic chemical vapor deposition usually gas mixtures with acetylene, ethylene or carbon monoxide together with hydrogen and helium are used combined with nickel or nickel/copper systems. Besides catalysts in powder form, so called supported catalysts – prepared by loading different porous substrates with a metal catalyst – are also used for carbon nanofilament synthesis.

In as deposited CCVD synthisized CNFs the catalytic metal particles are still present and washing with HCl or oxidizing acids helps to remove these catalysts. This step also dissolves the amorphous carbon frequently present in the raw product. The different nanostructures are seperated using filtering techniques. After treatment

sometimes also includes treatment in activating or passivating gas atmospheres as well as heat treatment [42].

Carbon nanotubes

Besides carbon nanofilaments (often sloppy called nanofibers) carbon nanotubes (CNT) are cylindrical tubes on microscopic scale. First images of 50 nm diameter carbon tubes were published in 1952 Radushkevich and Lukyanovich but in the literature the discovery of the nanometer sized tubes composed of graphitic carbon is attributed to Sumio Iijima of NEC Laboratories in 1991.

CNTs are allotropes of carbon, basically wrapped layers of graphite (called graphene) which are typically capped with the hemisphere of a spheric fullerene (buckyball) at each end. CNTs belong to the structural family of fullerenes, which actually also includes buckyballs. The diameter of these cylindrical nanotubes is about 5–30nm, which means about 50.000 times smaller than the width of a human hair, and the lenght can reach several millimeters [42, 43]. This results in a very large aspect ratio, which exeeds 10.000. As cylindrically structured carbon molecules these CNTs exhibit novel properties such as extraordinary strenght and unique electrical and thermal properties, that make them potentially useful in a wide variety of applications.

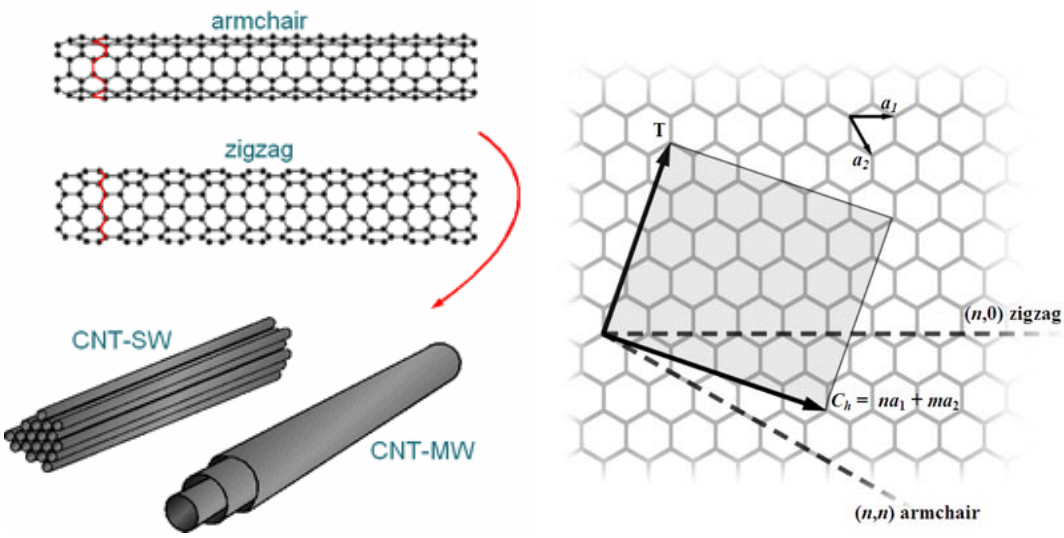

Figure 14: Single-walled and multi-walled carbon nanotubes [43, 44]

Mainly two types of nanotubes have been produced; single-walled nanotubes (CNT-SW or SWNT) and multi-walled nanotubes (CNT-MW or MWNT). As shown in figure 14 single-walled nanotubes are consisting of just one graphene layer. Regarding the honeycomb structure there are several possibilities to roll up the pane to a seamless cylinder. Using a pair of indices (n,m) to describe the directions of the cutting lines. For (n,0) one receivs a structure called 'zigzag', if n=m the resulting structure is called 'armchair', all other combinations are called 'chrial'.

Single-walled carbon nanotubes show some special electrical properties which they do not share with multi-walled carbon nanotubes. Therefore SWNT's are very interesting materials for downscaling electronic divices. CNTs exhibit outstanding mechanical properties as well.

As their name says, multi-walled carbon nanotubes consist of multiple layers of graphene. There are two models, one based on a concentric arrangement of cylinders of SWNTs and the other based on one single sheet of graphene rolled around itself several times. The latter could be compared to a rolled up newspaper.

The differently substructured types of CNTs are the result of the process used producing them and show different behavior in respect to their physical properties, for instance regarding their semiconducting properties [42, 43, 44].

Carbon nanofoams and nanofelts

In this study felts consisting of carbon nanofibers were used as a building block for the metal matrix composite (MMC). These felts are produced by Future Carbon GmbH, Germany [43]. Carbon nanofiber foams from Future Carbon (figures 15 and 16) are based on CNF-HB filaments (see figure 13) with a diameter of about 300 nm, BET-surface of about $60\,m^2/g$ and a poriosity of about 95 % – 97 %. BET stands for a theory by Brunauer, Emmet and Teller for measuring the surface area by gas adsorption. For a detailed explaination see section 4.1.

One material based on CNT-MW is Bucky-Paper [43]. Bucky-Paper are light, flexible sheets of non-woven pure carbon nanotubes with enhanced electrical and thermal conductivity with and without binders or other additives.

On carbon nanotube (CNT) foams two different after treatments are performed by Future Carbon. Thermal annealing or functionalizing with OH groups shall improve

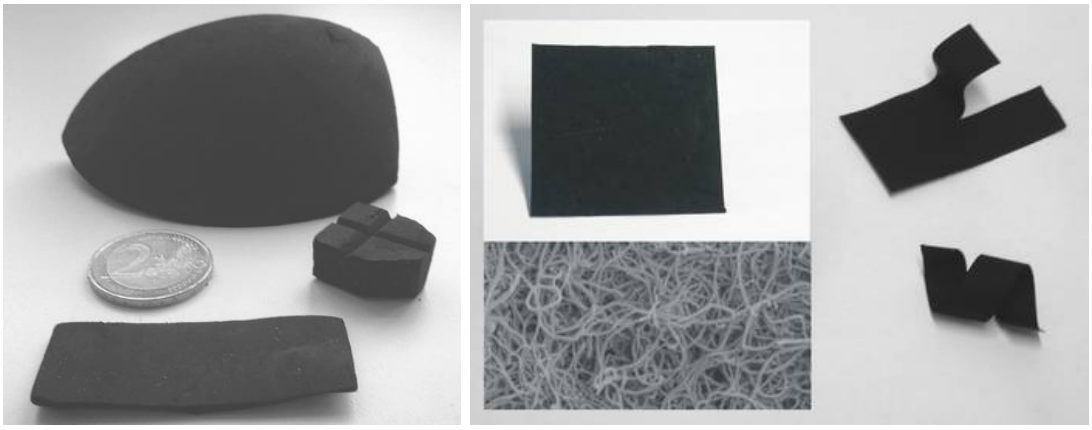

Figure 15: CNF-HB foam (left) and Bucky-Paper from Future Carbon [43]

the wetting behavior for metals. The CNTs have an average diameter of 15 nm and a BET-surface of about 200 m^2/g.

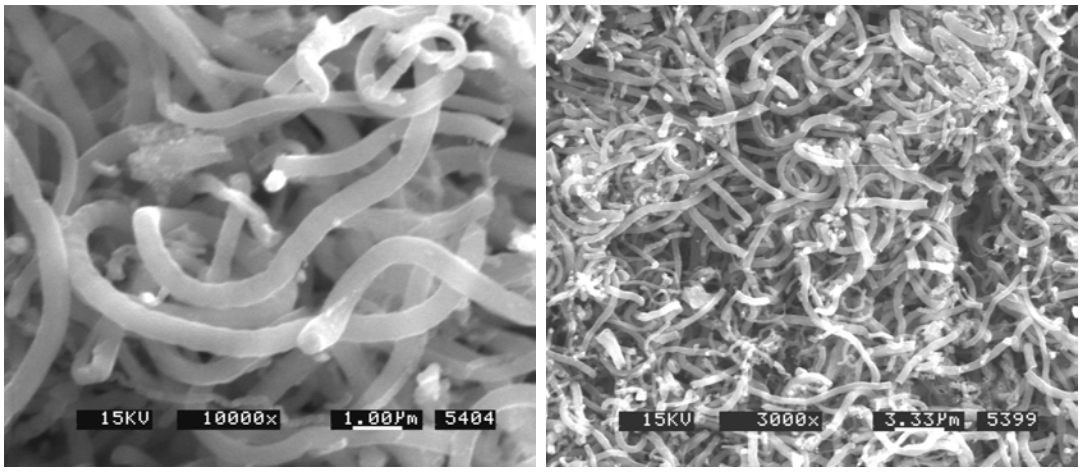

Figure 16: Scanning Electron Microscope images from the carbon nanofilament foam with herringbone structure (CNF-HB). SEM CISP

3.2 Glassy carbon

Small plates of Sigradur (glassy carbon) produced by HTW Hochtemperatur Werkstoffe GmbH, Germany, were used in most of the wetting angle experiments in this study. Glassy carbon Sigradur type G is highly temperature resistent in inert gas or vacuum atmospere up to 3000 °C. It is an example of a non-graphitizing carbon which means it is not transforming into crystalline graphite even at temperatures of

3000 °C and above. Besides this high thermal stability it is extremely resistent to chemical attacks e.g. acids. Glassy carbon is also highly impermeable to gases.

Since glassy carbon was first produced in the early 1960s its structure has been a subject of research. The model proposed by Jenkins-Kawamura, illustrated in figure 17, has been quite widely accepted. 2003 Harris has proposed another model that suggests that glassy carbons and other non-graphitizing carbons may have fullerene related microstructures [45].

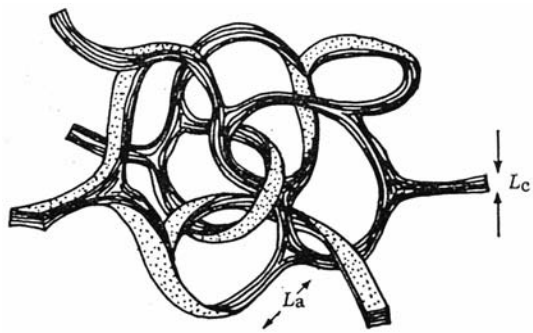

Figure 17: The Jenkins-Kawamura model of glassy carbon. L_a and L_c are the lengths of the graphitic domains perpendicular and parallel to the graphite c axis [45].

3.3 Metal Matrix alloys

Several materials were used for the wetting angle and infiltration experiments in this study. Besides pure metals like copper the behavior of metal alloys was investigated using the materials in form of powders, foils and bulk.

For most experiments the basic metal was copper often combined with carbide forming additives in the amount of about 0.5 – 5 wt%. The goal of adding elements to copper is to improve the interface between the carbon and the metal, because in case of pure copper the C/metal system lacks interactions between the two materials, resulting in very bad wetting properties. In the molten state, the additives diffuse to the carbon interface and react forming a carbide layer. This carbide interlayer shows excellent wetting with copper and results in an interface with improved quality concerning mechanical and thermal properties.

In this study the effect of carbide forming additives like e.g. chromium, titanium, boron or molybdenum on the wetting and infiltration behavior of the alloys on

Name	Nominal Composition Percent (wt%)	Liquidus temperatur (°C)	Solidus temp. (°C)	thermal conductivity (W/Km)
Cu	Cu – 100	1085	1085	398
CuCr1Zr	Cr – 0.5-1.2 Zr – 0.03-0.3	1084		
Copper-ABA*	Cu – 92.75 Si – 3 Al – 2 Ti – 2.25	1024	958	38
Ticusil*	Ag – 68.8 Cu – 26.7 Ti – 4.5	900	780	219
Cusil-ABA*	Ag – 63.0 Cu – 35.25 Ti – 1.75	815	780	180
Silver-ABA*	Ag – 92.75 Cu – 5.0 Al – 1.0 Ti – 1.25	912	860	344

*Active Bracing Alloys by Wesgo Metals [17]

Table IV: material properties

carbon nanofibers as well as on the thermal properties of the resulting MMC was investigated. Table IV shows some examples of prefabricated materials and their physical properties used for infiltration experiments.

Introducing the carbide forming additives can either be done by pretreating (for instance by coating) the nanofibers with these elements and/or modification of the matrix for instance via alloying [16].

4 Experiments

This section gives an overview on the experiments performed to investigate the wetting and infiltration behavior of carbon nanofibers by copper and some selected alloys. It is devided into three main parts, (1) the characterisation of the system and the used materials, (2) infiltration experiments on prefabricated foams/felts, and (3) producing MMCs using a powder metallurgical approach.

For producing a Metal Matrix Composite several problems have to be addressed, which are listed in table V. The difficulties are quite similar to those which appear in the carbon fiber system but are usually more critical. This study addresses two of these topics, the influence of carbon forming elements on the wetting behavior and the separation/dispersion of the short fibers in the metal matrix.

Due to the size of carbon nanofibers and carbon nanotubes the nanoparticles stick together and form clusters, which cannot be dispersed sufficiently during a milling process even when using surfactants. One approach investigated in this study is coating the particles with copper using an electroless plating technique. The completely coated particles could be treated as copper particles. A homogeneous distribution would result. In this study it was found to be sufficient, that the growing copper particles build a network within the carbon nanofibers and hold them appart. Complete coating was not required for an improved dispersion in the final product.

The other approach studied is to use prefabricated carbon nanofiber/nanotube foams or felts. Within these materials the nanoparticles are homogeneously distributed. This preform is infiltrated with the matrix metal. One of the main difficulties in these experiments is the very low thermal conductivity of the foams. In several experiments the foam itself proved to be an excellent thermal insulator.

Carbide forming elements where added to the matrix metal to improve the wetting.

A cumulative protocol with all investigated samples and experimental series can be found in the appendix.

Problems	**CarbonFibers (dia:10μm, 100-500μm)**	**CarbonNanofibers (dia:100-200nm, 1-100μm)**
Selection of suitable raw materials (different suppliers & qualities)	Material properties for different carbon fibers are available; measurement of properties possible too (even for transversal direction)	Characterisation of CNF properties is not easy; limited availability; there are different suppliers, but it is difficult to get reproducible quality
Separation and dispersion of short fibers in the matrix material	Optimisation of conventional blending techniques is sufficient; coating of fibers provides an advanced solution; fiber breakage has to be taken into account	To coat the CNFs is one of the solutions to obtain a good dispersion in the matrix; simple mixing has limitations (especially fiber alignment)
Alignment/ Orientation/Anisotropy	Fiber aspect ratio of 1:10 to 1:100 results in an orientation of the fibers during PM processing $\Rightarrow$ anisotropy of properties	Alignment of CNFs during PM processing is not confirmed yet; alignment by extrusion is possible
Densification of the composite	Optimisation of processing conditions with regard to densification and interfacial reactions	Remaining porosity is higher; interface reactions are not the same as for carbon fibers; severe reactions must be avoided
Interface	Interface plays an important role for mechanical and thermophysical properties	Interface plays an essential role to exploit the potential of the reinforcement

Table V: Problems to be addressed producing MMC's, comparing differences between carbon fibers and carbon nanofibers [2]

Characterisation of the materials used in this study

4.1 CNF/CNT characterisation

In order to get a better knowledge about the carbon nanofiber felts and the carbon nanotube felts from Future Carbon GmbH, several experiments where performed and the following characteristic properties of these materials where determined: Porosity, surface area, pore volume, thermal behavior (table VI and thermal diffusivity as well as the infiltration behavior of distilled water. These properties are important keys to understand the structure and formation of the materials. They also indicate potential applications.

Surface area and pore volume

One important property for powder metallurgical materials, nanomaterials, fibers and all kinds of porous materials is the BET surface area. BET stands for the three scientists Brunauer, Emmet and Teller, who optimised the theory of measuring the surface area using adsorption of gas molecules on solid surfaces. This theory extends the Langmuir theory to a multilayer adsorption, assuming that gas molecules physically adsorb on a solid in layers infinitely with no interaction between each adsorption layer. The Langmuir theory can be applied to each layer. Measuring the number of gas molecules adsorbed by the solid surface one can calculate its specific surface area [47].

$$S_{BET} = \frac{V_M \cdot N_A \cdot A_M}{M_V} \tag{4.1}$$

S_{BET}... BET surface area, V_M... adsorbed gas quantity, N_A... Loschmidt number (Avogadro), A_M... cross sectional area occupied by each adsorbate molecule (nitrogen: assumed to be 0.162), M_V... gram-molecular volume (for nitrogen 22414 ml)

The pore volume was calculated using the BJH method by Barrett, Joyner and Halenda [48] which accounts for capillary condensation in the pores. It uses the Kelvin equation (4.2) to correlate the relative pressure of nitrogen in equilibrium with the porous solid, with the size of the pores where capillary condensation takes place.

	S_{BET} (m^2/g)	S_{ext} (m^2/g)	V_{BJH} (cm^3/g)	V_{TOT} (cm^3/g)	V_{μ} (cm^3/g)	PS_{BET} (A)	PS_{BJH} (A)
CNF-HB	73.67	80.94	0.081	0.074	0.0048	40.28	48.28
CNT-ann	250.26	231.82	0.503	0.489	0.0076	78.21	70.72
CNT-OH	244.80	266.92	0.539	0.504	0.0126	82.35	72.23

Table VI: Measurements for adsorption and desorption isotherms on CNF-HB, CNT-annealed and CNT-OH

S_{BET} is the BET surface area, S_{ext} the external surface area, V_{BJH} the BJH adsorption cumulative pore volume of pores between 1.7 and 300 nm, V_{TOT} is the total volume adsorbed determined at p/p_0=0.97466840, V_{μ} the micropore volume, PS_{BET} the adsorption average pore diameter by BET and PS_{BJH} the BJH adsorption average proe diameter.

$$R_P = \frac{\frac{-2\sigma V_L}{RT}}{ln(p/p_0)} \tag{4.2}$$

Kelvin equation: R_P... Kelvin radius, σ... surface tension of N_2, V_L... liquid molar volume, R... ideal gas constant, T... temperature in Kelvin, p... equilibrium and p_0... saturation pressure of the adsorbats at the temperature of adsorption.

The micropore volume and the micropore area were estimated using the thickness-plot (t-plot) method [49]. The volume of gas absorbed, which is measured during the analysis, is plotted against the statistical thickness [50] of the adsorbate molecular film.

Thermal behavior

All experiments with carbon nanofeatured foams/felts in this study have shown that it is very difficult to heat these foams. To reach the melting temperatures of the metal alloys a big amount of heat is required if the solid metal is located on top of the foam. Due to their high porosity the foams contain lots of gas, which has to be heated as well. This could be one explaination of their highly thermally insulating property. In case of experiments in vacuum, the vacuum is a good thermal insulator too.

Differential scanning calorimetry (DSC) was performed on the foams to invistigate if any exothermic or endothermic reactions take place in the sample. The DSC method is a thermoanalytical technique to determine the difference in the amount

of heat required to increase the temperature of the sample and a reference, measured as a function of temperature. The CNF/CNT foams did not show any reforming or restructuring behavior.

For further characterisation of the thermal behavior of the foams, it was tried to measure the thermal diffusivity. For these experiments a laser flashline 5000 from Anter inc. was used. The samples were heated up to 250°C under ultra high purity argon atmosphere. For calculating the thermal diffusivity several complex mathematical evaluation models are in use. A simple model for understanding the process is the Parker model.

The thermal diffusivity α is related to the thermal conductivity λ, the specific heat C_p and the density ρ as follows:

$$\alpha = \frac{\lambda}{\rho\, C_p} \quad [m^2 s^{-1}] \tag{4.3}$$

According to this definition, the thermal diffusivity affects each conductive transient heat transfer process within the medium.

After stabilizing the sample temperature at the desired point T_0, in the flash method a nearly instantaneous pulse of energy is deposited (usually by laser) to the front face of the sample. The temperature increase $\Delta T(t)$ is measured at the rear surface and recorded as a function of time. From this thermogram the thermal diffusivity is calculated using the method proposed by Parker, which is assuming no heat loss during the process (isotropic and adiabatic sample). The model uses the sample thickness L_P and the time $t_{1/2}$, at which the sample has reached the half of the maximum temperature increase, for deriving:

$$\alpha = 0.1388\, \frac{L_P^2}{t_{1/2}} \tag{4.4}$$

The laserflash method applied to the CNT Buckypaper yields a thermal diffusivity slightly below $2\,\mathrm{mm}^2/\mathrm{s}$ at $50\,°\mathrm{C}$.

Measuring the thermal diffusivity of a CNT felt, which was pretreated for oxidizing with OH-groups, resulted in a value of approximately $2.3\,\mathrm{mm}^2/\mathrm{s}$ (see figure 18).

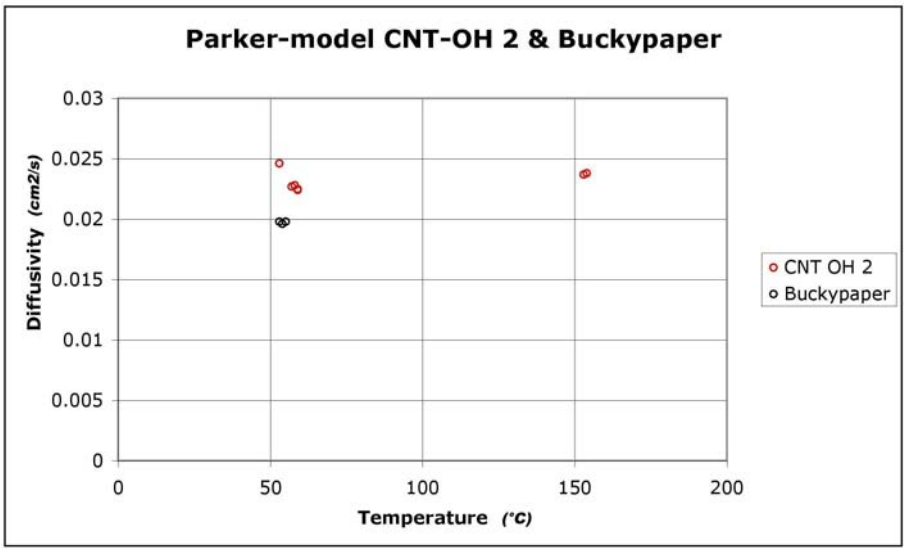

Figure 18: Diffusivity CNT-OH foam and CNT Buckypaper

Evaluating the experimental data, the nanopreforms exhibit stable behavior up to 150°C. For higher temperatures the gradient plot becomes very spiky. Mathematical fitting of the data proposes a slightly ascending behavior.

Ultrasound assisted water infiltration

For the chemical copper coating experiments of the carbon nanofiber foams the behavior in respect to the infiltration by water was investigated. A simple experiment was designed to show the difference in water infiltration versus time for the CNF-HB foam in two different conditions. Two baths with distilled water were prepared and the CNF-HB foam was carefully submersed for a certain period of time. One bath was agitated with ultrasound.

A commercially available ultrasonic bath from Bransonic inc. "5500 Branson" was used. The ultrasonic power of this cleaning unit is 135 W at 42 kHz.

After 5 min the initial weight and the final weight of the foams were compared and it was found that the sample in the ultrasonically agitated bath absorbed about 4 times the amount of distilled water compared to the sample in the plain water bath. This result was used to support solution infiltration by ultrasound into the foams during the electroless copper plating process (section 4.6). No damage of the CNF preforms caused by the ultrasonic treatment was found.

4.2 Wetting angle measurements

Wetting angle measurements were performed for several carbon/metal systems. Using glassy carbon 'Sigradur' and the different carbon FC nanofoams/felts as substrates, investigations were performed with several copper alloys containing different amounts of carbide forming additives.

4.2.1 Experimental setup

For the experimental setup a high temperature sessile drop device (HTSDD) for measuring contact angles under high vacuum (10^{-3} Pa) constructed by Bernhard Schwarz (Vienna University of Technology, Austria) [51] was used. In the HTSDD the sample is heated by resistive heating. It is resting on a sheet of tantalum, which is clamped on both ends and which is subjected to a high electrical current. The high current feedthroughs are water-cooled which allows to reach temperatures up to 1100 °C for 1 – 3 minutes. For monitoring the melting event a camera is installed and connected to a computer. A software tool allows to chart the received data and to evaluate the contact angle. This software also supports taking a series of pictures during the process for analysing the experiment over time.

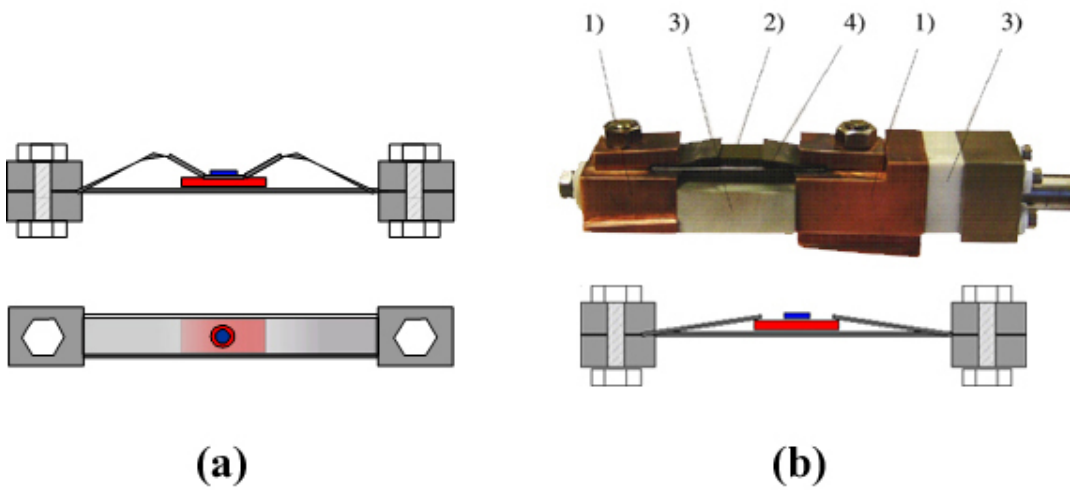

Figure 19: Experimental setups for wetting angle measurements: for foams (a); for Sigradur plates (b). Both setups were used in the HTSDD and in the high vacuum coating plant respectively. (1) Copper current feedthrough, (2) sample, (3) ceramic spacer and (4) Ta heating foil. [51]

Some of the experiments were also performed in a high vacuum coating plant, where longer heating periods were possible, but no automated vision system could be used for documenting the observations. In this case the samples were only evaluated after the experiment.

The setup in figure 19 shows that the substrate is put on the tantalum (Ta) foil and then a small piece of metal (usually 5 – 10 mg) is put on top of the substrate. The substrate is fixed with clips against unwanted movements.

4.2.2 Measurements on Sigradur

All contact angle experiments are performed under high vacuum of 10^{-3} Pa using the devices described above. The heating of the samples was done very quickly within 1 – 2 minutes and, after the holding time, the samples cooled down slowly to room temperature within 30 minutes.

Metals

For the MD series Sigradur G is used as a substrate and different copper alloys were investigated. Several metals like indium, aluminum, silver, copper, tin and lead were tested for their wetting behavior on Sigradur, but none of them showed a wetting angle smaller than 120 °.

CuB alloys

Interesting results were achieved for alloys containing boron. While no significant wetting (contact angle is about 170 °, figure 21) is observed for these alloys, the melting pearl shows a good bonding to the substrate. A slight neck is seen at the triple line, which means there is no progressive wetting-promoting layer. When removing the melting pearl a crater is left in the substrate at the interface. Similar behavior was observed by Froumin et al. [52] for copper on a B_4C substrate (figure 20). Boron also exhibits interesting behavior at the infiltration experiments with carbon nanopreforms as shown later.

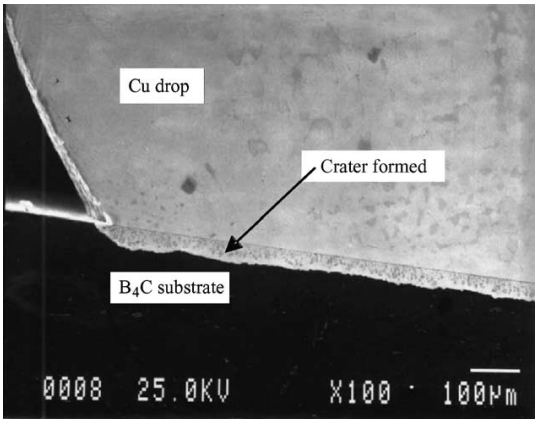

Figure 20: Cross-section of the interface between unalloyed Cu drop and boron carbide. Notice the high contact angle and the crater formation [52].

CuCr alloys

For the industrial alloy CuCr1Zr the final contact angle after about 3 minutes is measured to be about 60 °. Voitovitch et al. [9] have shown, that in the CNF/CuCr system with chromium contents between 0.5 and 2 at.% the contact angle is about 40 ° irrespective of drop mass or chromium concentration in the alloy. Compared to the experiments in this study, Voitovitch et al. found that receiving the final euquilibrium contact angle in reactive systems needs leaving the sample at melting temperature for several hours. This was not possible in the present device, but the tendency is clearly seen within the first minutes.

Active Brazing Alloys

The Active Brazing Alloys CopperABA and Ticusil from Wesgo Ceramics GmbH show excellent wetting on Sigradur with a contact angle between 15 ° and 0 °, so these materials were also used for the infilitration experiments on the carbon nanofiber foams.

4.2.3 Measurements on CNF-HB

For the wetting and infiltration experiments with CNF-HB foams a slightly different setup was used (see figure 19 (a)). A tantalum clip with a hole was chosen to fix the foam at a certain place and the clip is tightened enough to squeeze the foam slightly, so that a small part of it sticks out through the hole. Due to the smaller

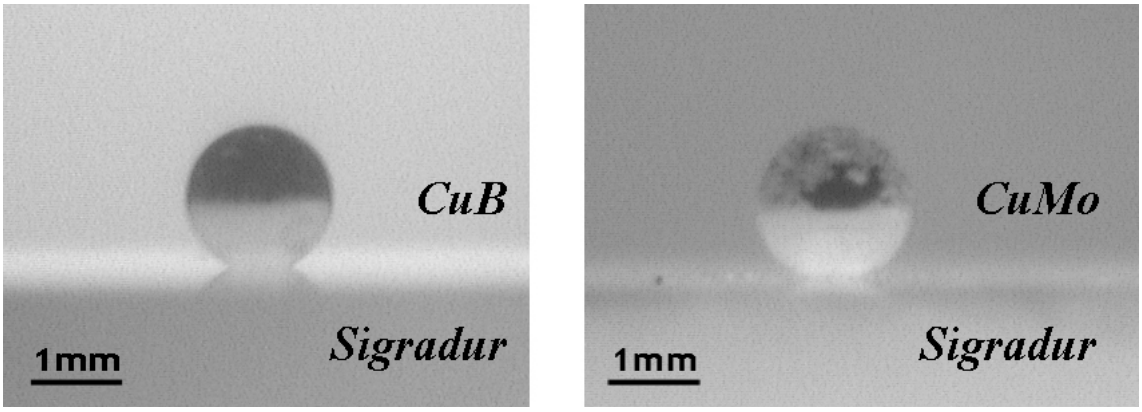

Figure 21: CuB and CuMo on Sigradur at melting temperature, TU-Wien

cross section in the area of the hole, this part is heated more strongly. This setup helps to reach the required temperatures despite of the very bad heat conductivity of the CNF-HB foam.

Testing series MA for wetting behavior of different metals (In/Sn/Pb/Bi) on the CNF-HB foam show no significant wetting. Also chromium alloys, titanium alloys as well as the Active Brazing Alloy copperABA, which had shown good wetting on Sigradur, exhibit contact angles of >140 ° on CNF-HB. Only Ticusil shows excellent wetting with a contact angle below 10 °. (series MB and MC)

The reason for the non wetting behavior of Cr and Ti-alloys and copperABA could be the strong surface tension of copper leading the melting pearl to just rest on the tips of the fibers having not enough contact area for the carbide forming process to take place.

To solve this and promote the wetting process, the foam was coated with a thin sputtered layer (100 nm) of titanium, TiN or molybdenum (10^{-4} Pa, RT, P_{SPU}=200 W, U_{SPU} ≈360 V, Ar atmosphere). With this thin layer of carbide forming material, the wetting of copperABA was induced. No effect could be noticed for other alloys.

Results of series MA – MD are given in table VII

sample	result	date	series
CNF-In	not wetting MP:156°C	24.01.2007	MA
CNF-Sn	n/w (MP: 232°C)	24.01.2007	MA
CNF-Bi	n/w (MP: 271°C)	24.01.2007	MA
CNF-Pb	n/w (MP: 327°C)	24.01.2007	MA
CNF-CuCr1Zr_4	not wetting (n/w)	26.01.2007	MB
CNF-CuMo HP1177/155	n/w	31.01.2007	MB
CNF-CuB HP1177/157	n/w	31.01.2007	MB
CNF-CuABA	n/w	07.02.2007	MB
CNF-Ti100-ABA (120nm Ti)	120nm Ti-layer, excellent wetting	08.02.2007	MC
CNF-Ti100 CuCr1Zr_2	100nm Ti, not wetting, melting pearl sticks on the foam	27.02.2007	MC
CNF-Ti100-CuABA_2	excellent wetting	28.02.2007	MC
VC-CuMo_b1 HP1177/155	not wetting (n/w)	31.01.2007	MD
VC-CuCr_b1/b2 HP1177/156	n/w	31.01.2007	MD
VC-CuCr_b3 HP1177/156	n/w, popped away	20.02.2007	MD
VC-CuB HP1177/157	wetting angle approx. 170°, Pearl sticks, breaks piece from the substrate (crater)	31.01.2007	MD
VC-CuCrB2_b1 HP1177/159	n/w, pearl sticks forming a crater	10.02.2007	MD
VC-CuCrB2_b2 HP1177/159	n/w, pearl sticks tight forming a crater	20.02.2007	MD
VC-CuTiB_b1	n/w	10.02.2007	MD
VC-CuCr1Zr_b2	KW $\approx$ 60°	23.03.2007	MD
VC-CuCrZr_b2	KW $\approx$ 68°	23.03.2007	MD

Table VII: Contact angle experiments performed on Sigradur and Future Carbon nanofoams, series MA–MD

Infiltration experiments

Based on the results of the wetting angle experiments (section 4.2), several metal alloys where chosen for pressureless and external pressure assisted infiltration experiments on the carbon nano-preforms (FC).

4.3 Pressureless infiltration

4.3.1 Experimental setup

In this study two different setups for pressureless infiltration experiments where used. The first setup is similar to that for the wetting angle measurements described in section 4.2.1. As already mentioned, in this HTSDD application the sample is heated using resistive heating. The experiments were performed under high vacuum (10^{-3} Pa). (TU-Wien)

The other setup is a conventional heating furnace with a furnace vision application. This application is a digital camera looking through a mirror and triggered with a flashlight to monitor the inside of the furnace during the melting/sintering procedure. Samples can be treated under Argon, Nitrogen and Hydrogen atmospheres with this device. Experiments in this setup were performed in the Center for Innovative Sintered Products (CISP) laboratory at the Pennsylvania State University. (PSU)

In both setups it is very difficult to determine the actual temperature of the sample during the heating period. In the HTSDD setup at the Vienna University of Technology no explicit temperature measurement is implemented. The only way for knowing the sample temperature is reaching the melting temperature of the metal on the preform surface. But this does not mean, that the whole preform has this temperature. Maybe the preform is heated much more (e.g. Bucky paper) or much less (e.g. CNF-HB foam). In this setup one time a thermocouple was used to measure the temperature of a heated CNF-HB foam. Because of the sponge-quality of the foam, the thermoelement was pressed into it. The heating element, tantalum, was glowing in white light, so the temperature was estimated to be 1300 – 1500 °C. The measurement on the thermocouple was only about 300 °C after approximately 2 minutes of heating. (This is the maximum time that can be performed with the HTSDD at these temperatures.)

At the PSU the temperature was not measured seperately, the whole furnace was heated to the desired temperatures and different holding times where performed to give the sample time to heat up. Several results lead to the assumption, that very often the sample was much cooler than the estimated temperature. A direct measurement of the sample temperature was not possible for the conventional furnaces. For the experiments with microwave heating an Infrared Pyrometer was used to determine the actual sample temperatures.

4.3.2 Bucky paper, series ME

As already mentioned, bucky paper produced by Future Carbon GmbH contains 100% multiwall carbon nanotubes with a paper thickness of some 100 μm.

For the experiments the bucky paper was cut into 5 mm×5 mm pieces and fixed on the tantalum sheet (setup figure 19 (b) and figure 22). Infiltration studies were done with CuCr1Zr and copperABA with the result of non wetting behavior for CuCr1Zr and good wetting and infiltration for copperABA. The copperABA foil was cut into pieces of 5 – 10 mg, put on the substrate and heated to the melting point of copper.

As soon as the melting temperature was reached, the sample was held at a temperature of about 1100 °C for another 3 minutes. During this time the contact angle of the melting pearl decreases continuously and the alloy gradually infiltrates the CNT paper. After about 60 seconds the whole alloy is absorbed and the experimental series showed, that after further 2 minutes the alloy reaches the lower surface of the substrate.

The whole experiment was accomplished under high vacuum (10^{-3} Pa) and is shown in figure 23.

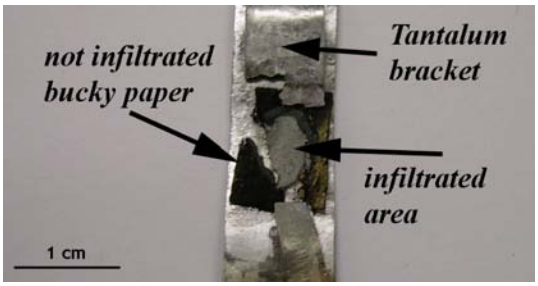

Figure 22: Bucky paper infiltrated with CuABA

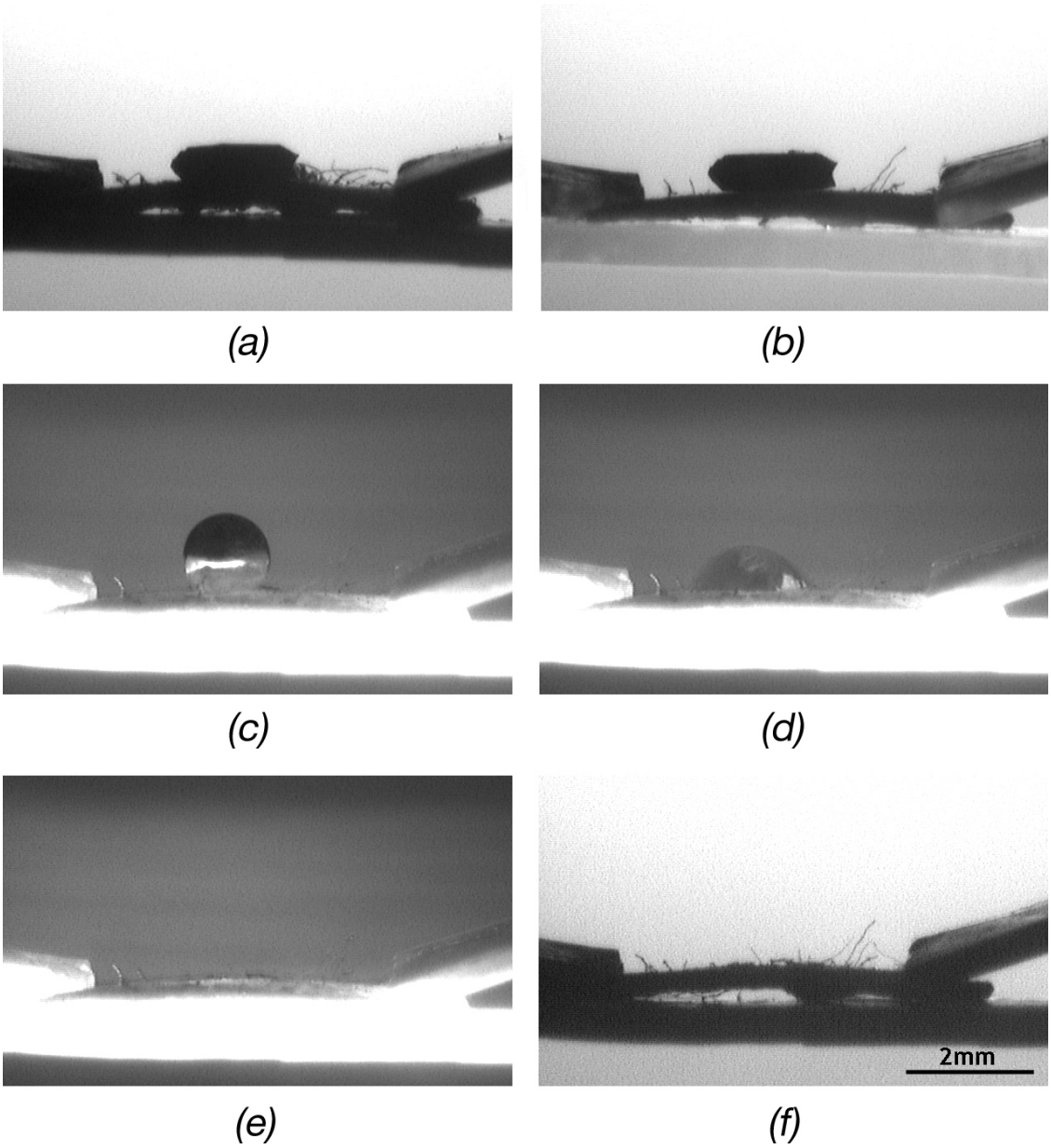

Figure 23: infiltration process, Bucky Paper, TU-Wien

(a)... CNT paper before heating

(b)... heated to approx. 900 °C

(c)... at about 1100 °C

(d)... CNT paper 10 seconds after the infiltration process has started

(e)... after 60 seconds

(f)... shortly after the infiltration

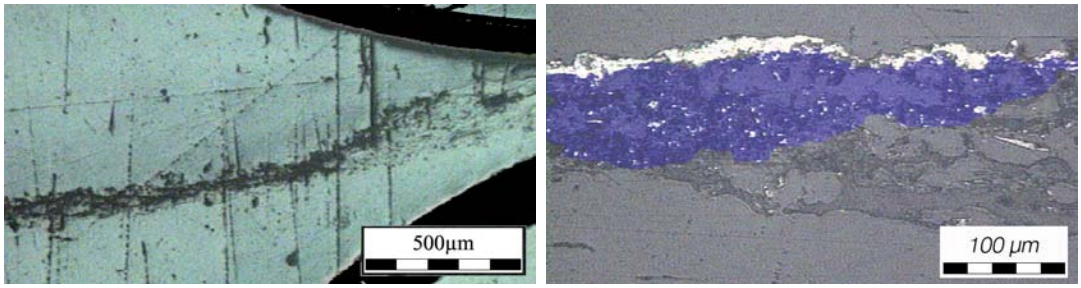

Figure 24: Bucky paper infiltrated with CuABA, LM 50x (left), LM 200x (right)

For further investigation the infiltrated Bucky paper was embebbed into epoxy resin and a cross section of the infiltrated area was studied by optical microscopy (LM) as well as scanning electron microscopy (SEM). The images show a homogeneous infiltration for the entire cross section, but energy dispersive X-ray analysis (EDX) does not show any copper left (figures 27 and 28). Several Silicon containing crystals were formed in the infiltration area (figures 25 and 26). The reason of the disappearance of the copper is not clear yet. Due to the high temperatures held over about 3 minutes, taking fractional vaporization into account, the percentage of copper in the alloy will be reduced to about 50%, but because of the complete vanishing there has to be an additional effect. (CuABA contains 92.75 wt.% Cu, 3 wt.% Si, 2 wt.% Al and 2.25 wt.% Ti.)

As described above, the heating process of the substrate was very tricky and a direct temperature measurement was not possible. Regarding the effects which showed vanishing of copper in the Bucky Paper infiltration experiments, it is believed, that the temperature was not stable during the experiment and reached much too high maximum values. As soon as the infiltration front reaches the bottom of the CNT paper, the thermal contact between the heating element tantalum and the liquid metal suddenly improves, which could cause the evaporation of the copper.

At the infiltrating surface area there remains a several micrometer thick crust (figures 24 and 25) containing aluminum, titanium and silicon, but no copper.

Especially in the SEM images the carbon nanotubes with a diameter of about 20-70 nm are clearly visible (figure 26).

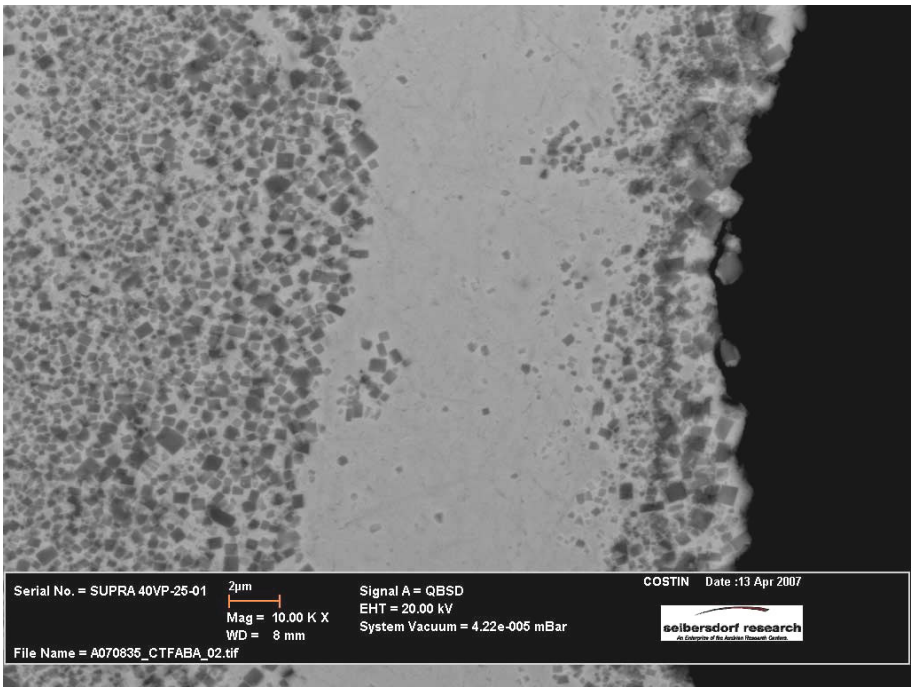

Figure 25: Bucky paper infiltration, Silicon crystals, SEM: ARC Seibersdorf

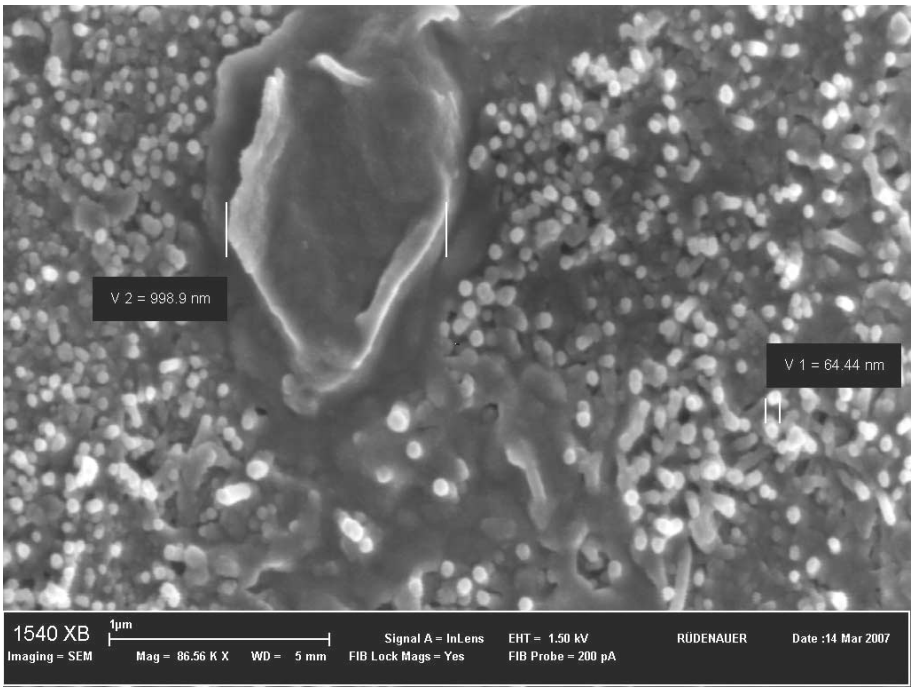

Figure 26: Bucky paper infiltration, Carbon nanotubes, Silicon crystal, SEM: ARC Seibersdorf

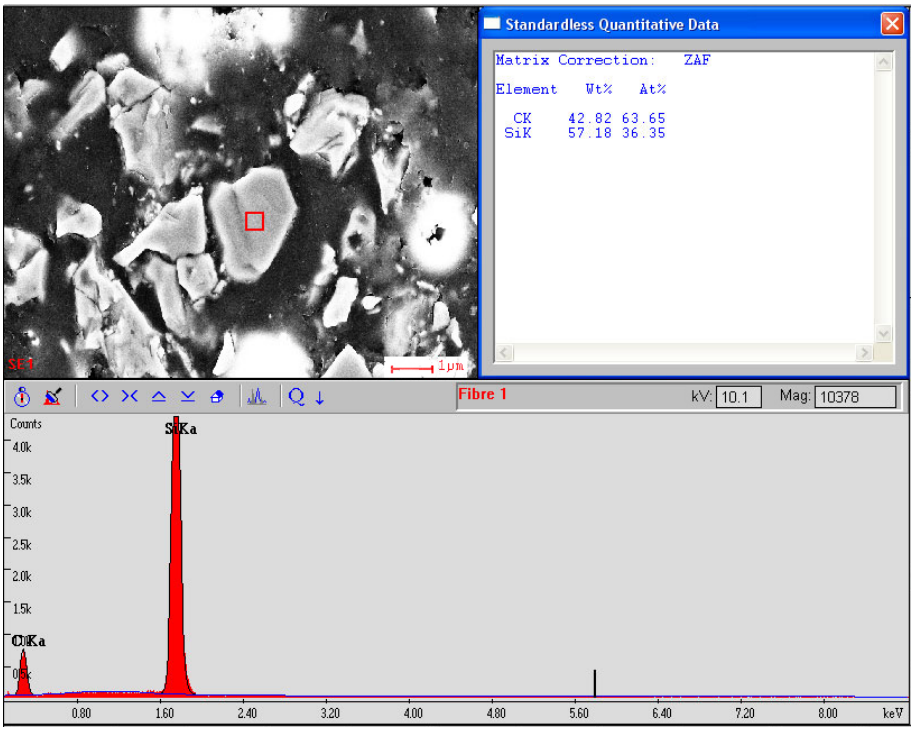

Figure 27: Bucky paper infiltration, EDX analysis, 10keV, SEM: ARC Seibersdorf

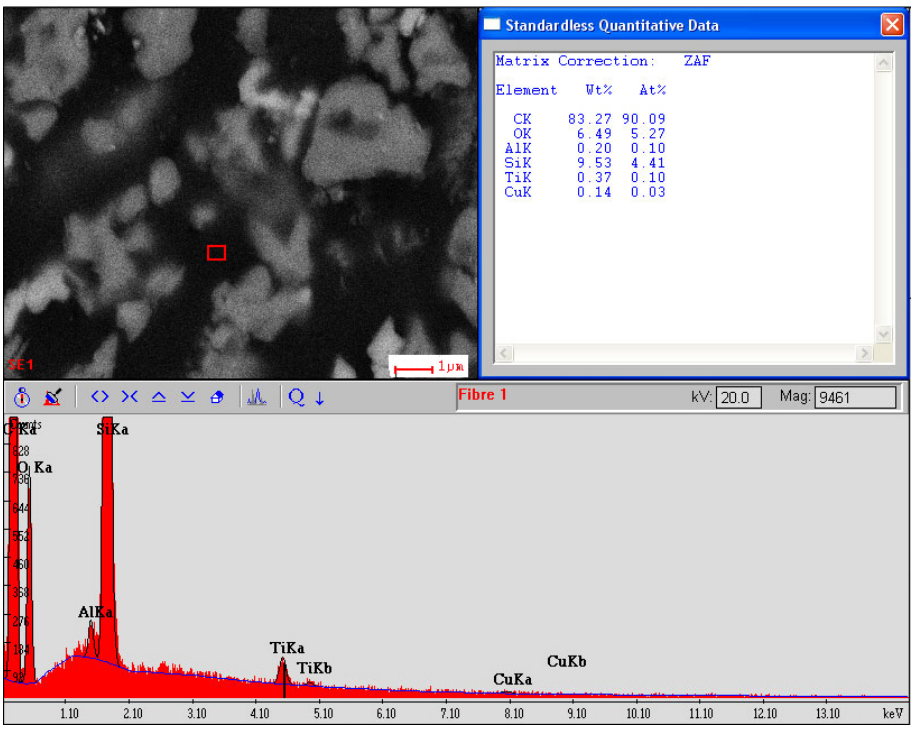

Figure 28: Bucky paper infiltration, EDX analysis, 20keV, SEM: ARC Seibersdorf

4.3.3 CNF-felts and CNT-foams, Series MF, MJ, MM

Pressureless infiltration means using just gravity and the metal mass as an 'external' infiltration force. No other external pressure was applied for these experiments. In principal the setup was quite similar to the wetting-angle measurements. It is very difficult to heat the CNT and CNF preforms of a thickness of several millimeters to the desired melting temperatures of the infiltrating metals. For investigating and comparing, two different heating methods (setups described in sections 4.2 and 4.3.1) were used to study the thermal behavior of the samples.

In setup 1 (TU-Wien) the sample was heated from the bottom side, so nearly the entire foam was at the melting temperature of the metal. Infiltration of the metal-alloys was observed in certain spots for a very small infiltration depth of at least some 10 μm. The heating cycle was very short, the melting temperature could be reached within minutes and the entire infiltration procedure was accomplished within about 5 minutes. Cooling was performed slower, the sample reached ambient temperature after 30 minutes to avoid damage from shock cooling.

At PSU the samples were heated from all sides in a conventional furnace (setup 2). The foam-substrate was still placed on the bottom, topped with a small piece (approx. 5 mg) of metal alloy. In this furnace the heating rate was 5 °C/min until the desired temperature was reached and held for a certain time (typically 2 hrs) before the samples where cooled down to ambient temperature with the same rate of 5 °C/min. When comparing with setup 1, this cycle is much longer. Setting the holding temperature slightly above the melting temperature, it was not possible to melt the metal pieces. After 2 hrs the foam was still too cold for infiltration. Setting the holding temperature far above the metal melting temperature (difference about 300 °C) melting set in, but the infiltration results were not satisfying. The alloy already decomposed and the carbide forming additives consumed the carbon fibers completely (figure 29).

To sum up these two series, spontanous pressureless infiltration on CNF-HB felts and CNT-foams (figures 30–32) was observed for regions near the contact edge line. It can be concluded that for spontanous infiltration the whole sample is not penetrated, so the metal is not sucked into the substrate. It seems that the own weight of the metal drop builds up enough pressure to infiltrate the substate in a small zone below the metal drop. All samples were heated with the metal on top of the substrate.

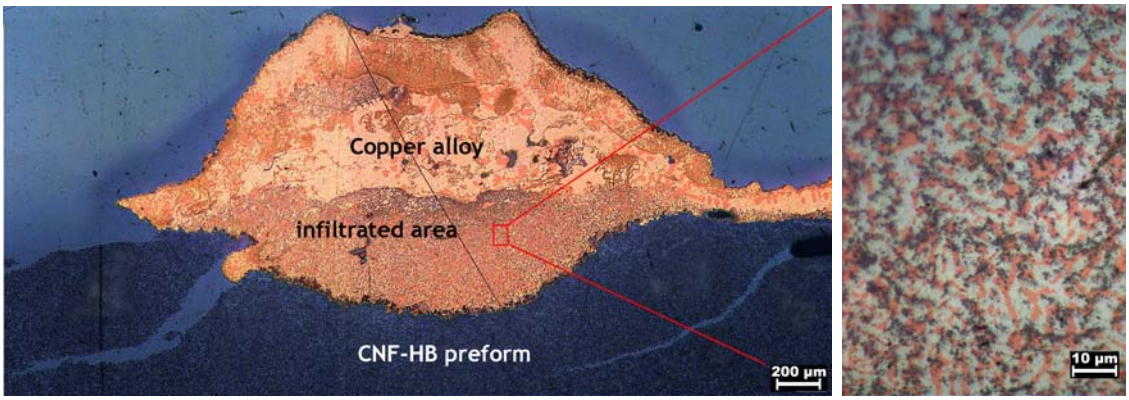

Figure 29: CNF-HB Ticusil after 1400C treatment for 2 hrs. LM: PSU

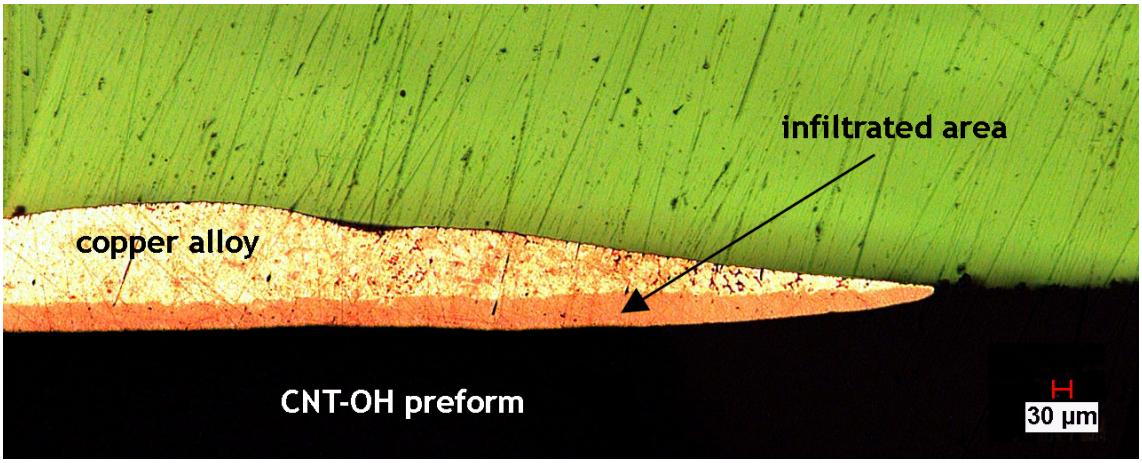

Figure 30: CNT-OH CuSil Series MJ, LM: PSU

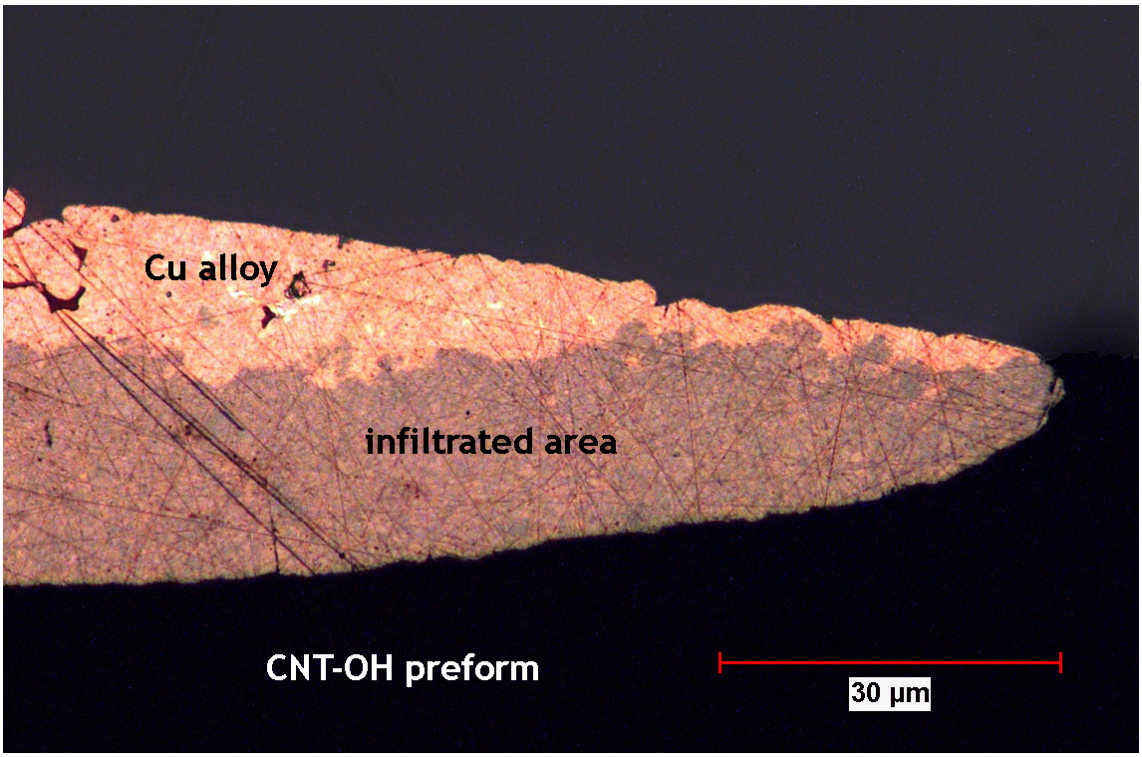

Figure 31: CNT-OH CuSil Series MJ, LM: PSU

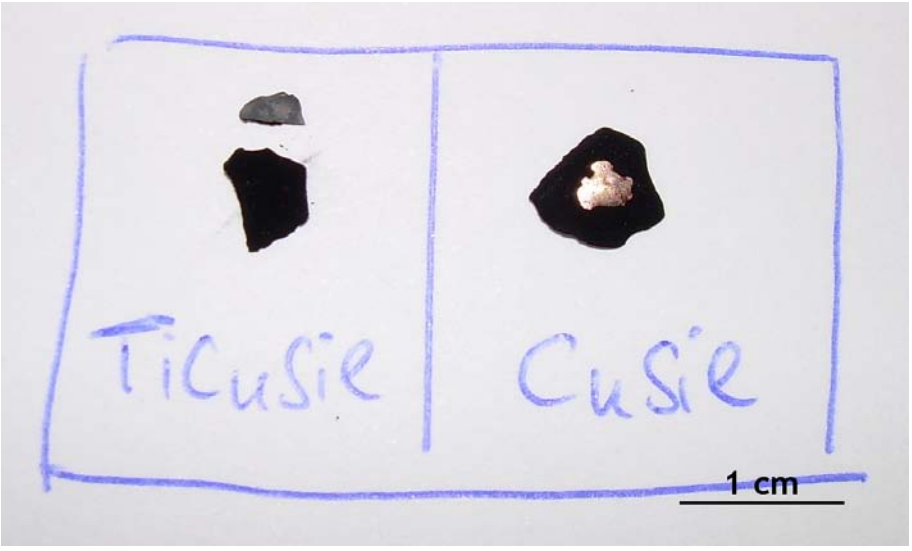

Figure 32: CNT-OH preform wetting/infiltration experiment with Ticusil and Cusil (ABA), TU

4.4 External pressure assisted infiltration

4.4.1 Experimental setup

Applying external pressure on an infiltration sample is one way to increase infiltration depth. As shown in section 2, a certain threshold pressure is required for infiltration to occur. Deviating from the assumptions made, the MMC-systems are subject to reactive wetting and compression of the foam can play a decisive role in the external pressure assisted infiltration process. This series of experiments was perfomed to study the influence of externally applied pressure on the infiltration behavior of the molten metal into carbon nanofiber felts and nanotube foams. The porosity of these substrate materials is very high (up to 98%), which means that a high amount of gas is stored within the foam. Before the matal can infiltrate the substrate, the gas has to escape. In case of too high pressure applied, the foam will be compressed and close the pores.

First experiments were accomplished in a conventional furnace, the foam was topped with the copper alloy in powder form, and compacted in a graphite crucible (pressure 1.3 tons/200 mm^2, tablet dimensions about 5 mm × ⊘ 10 mm). Sealed with a graphite plunger, they were loaded with a 2 kg weight and heated to just below melting temperature (figure 33). Reaching or exceeding melting temperature would squeeze the molten metal out of the grapite crucible.

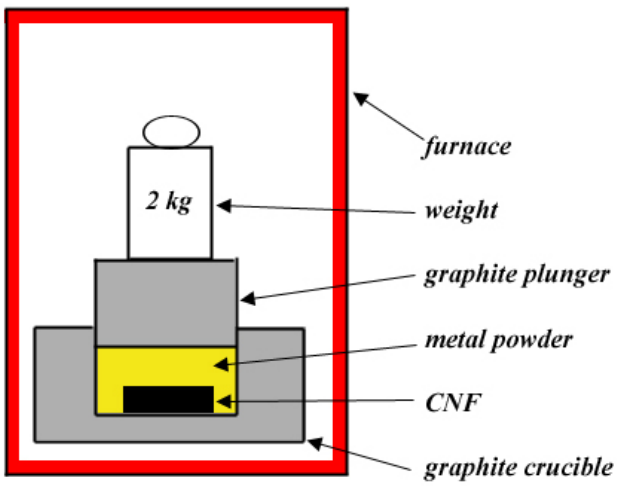

Figure 33: Infiltration setup applying external pressure (weight), ARC

For increasing the applied pressure, a series of experiments was performed in a hot

press (under argon and hydrogen atmospheres, setup figure 34). The preparation was similar to the previous experiments, the pre-compacted samples were heated in a graphite crucible using an induction coil and subsequently pressure was applied. After a holding time of 30 – 60 min at the maximum temperature the sample was cooled down and the load was continously reduced.

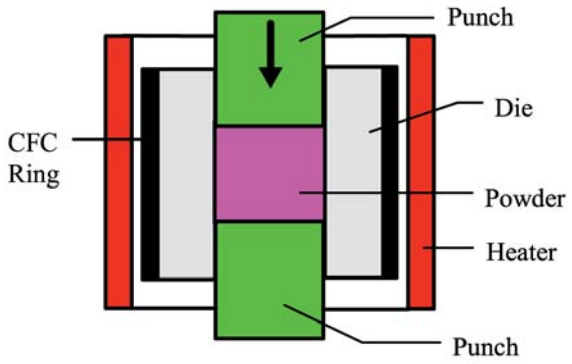

Figure 34: Infiltration setup for applying external pressure (hot press), ARC

4.4.2 Measurements, Series MF, MH, MI, MK, ML

Two series of experiments were accomplished to test the infiltration behavior of the different substrate materials CNT-felt, CNF-HB foam and CNT paper (all from Future Carbon GmbH), using various matrix alloys and differently coated substrates. Series MF was to investigate the CNF-HB foam, coated with 100 nm Ti or TiN, using copper and CuCrZr alloys. As shown in figure 33 the 10 mm diameter samples were loaded with 2 kg, the furnace was evacuated and heated to 1000 °C under H_2 atmosphere, the holding time was 30 min.

Chromium containing alloys

For the samples with pure copper as matrix no infiltration was observed. The CNF-HB sample with TiN as interlayer and CuCrZr as matrix showed some small infiltrated areas, and remaining fiber structures were determined using SEM (figure 36). The chromium was mainly found in the infiltration areas, which was clearly confirmed by EDX-analysis (figure 35). For the alloy CuCr3 with 3wt.% chromium infiltration of about 100–400 μm was observed on the CNT preform (figure 37).

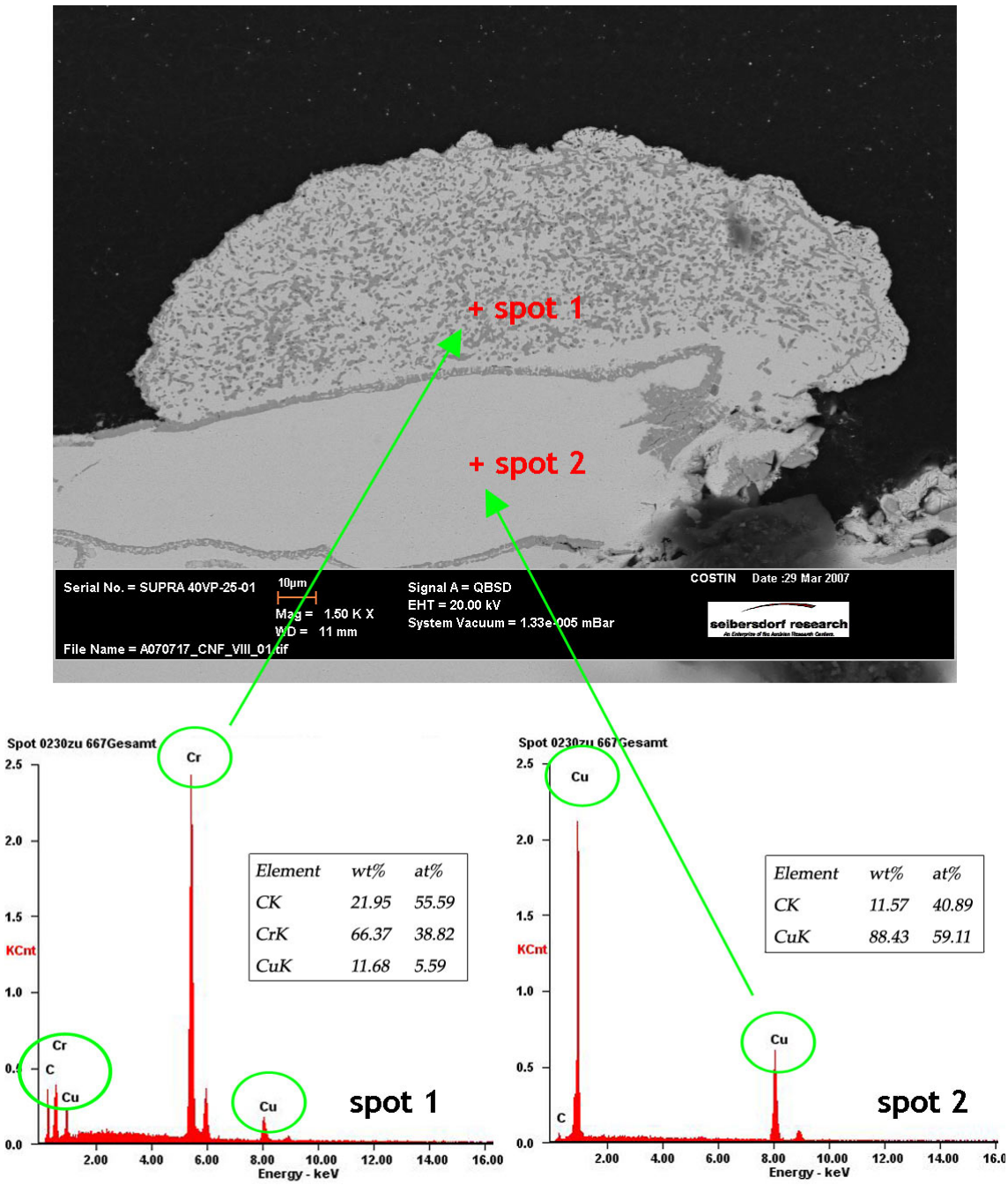

Figure 35: Series MF, CNF-HB TiN(100nm) CuCrZr, 1500x SEM: ARC

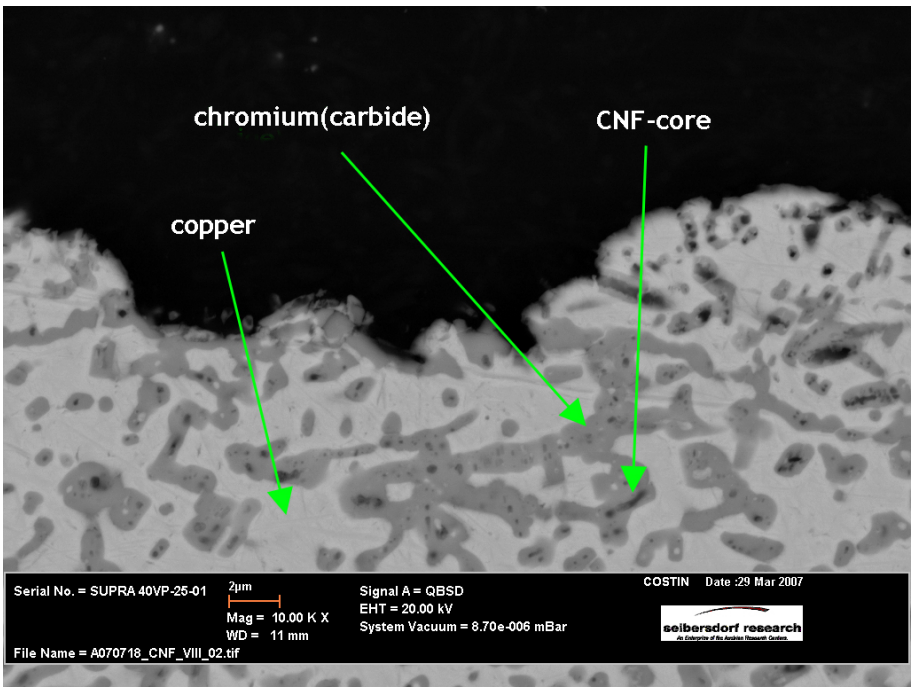

Figure 36: Series MF, CNF-HB TiN(100nm) CuCrZr, 10000x SEM: ARC

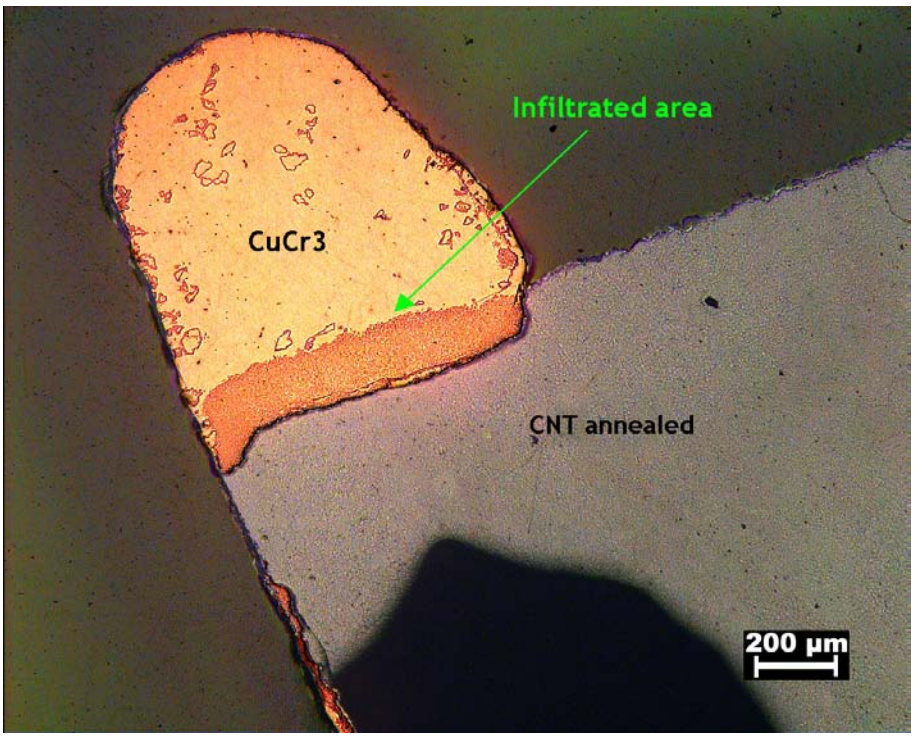

Figure 37: Series ML, CNT annealed CuCr3 (3wt%Cr) Infiltration area, LM: CISP

Ticusil on CNF-HB

For series ML the setup for the sample heating in the furnace was as shown in figure 33. The CNF-HB foam was topped with several layers of a Ticusil foil and sealed with a graphite plunger.

When investigating the infiltration zone with a depth of about 100 μm, the carbon nanofilaments with a diameter of 200–300 nm are clearly visible in the LM image (figures 38 and 39). When having a closer look at figure 39 one can see the black CNF cores coated with gray Ti carbide. In the right part of the image (here the infiltration began and the alloy had more time to react with the CNFs) the nanofibers are fully consumed. When moving in direction of the infiltration flow to the left of the image, more and more fiber cores are visible. This can also be interpreted as the states of by-and-by carbide formation or consumption of the CNFs. The white arrow in figure 39 indicates the gradient of the carbide formation.

The thickness of the carbide layer has a very strong influence on the thermal properties of the final MMC. When using Ti as the carbide forming element, this interlayer has to stay extremely thin. As soon as the carbon nanofilaments are fully consumed by the reaction, the expected properties will disappear, because the special structure of the CNFs with the promising thermal conductivity does not exist any more. When interpreting these results, the reaction time has to be shortened to get still existing carbon nanofiber structures like from the middle to the left hand side in figure 39.

For carbon nanotubes this effect becomes relevant to a greater extent, but because of the greater surface to volume ratio for CNTs the interface is of major importance too.

The optimization of the process will have to take all these results into account. Fast infiltration and slower reaction kinetics could solve this problem.

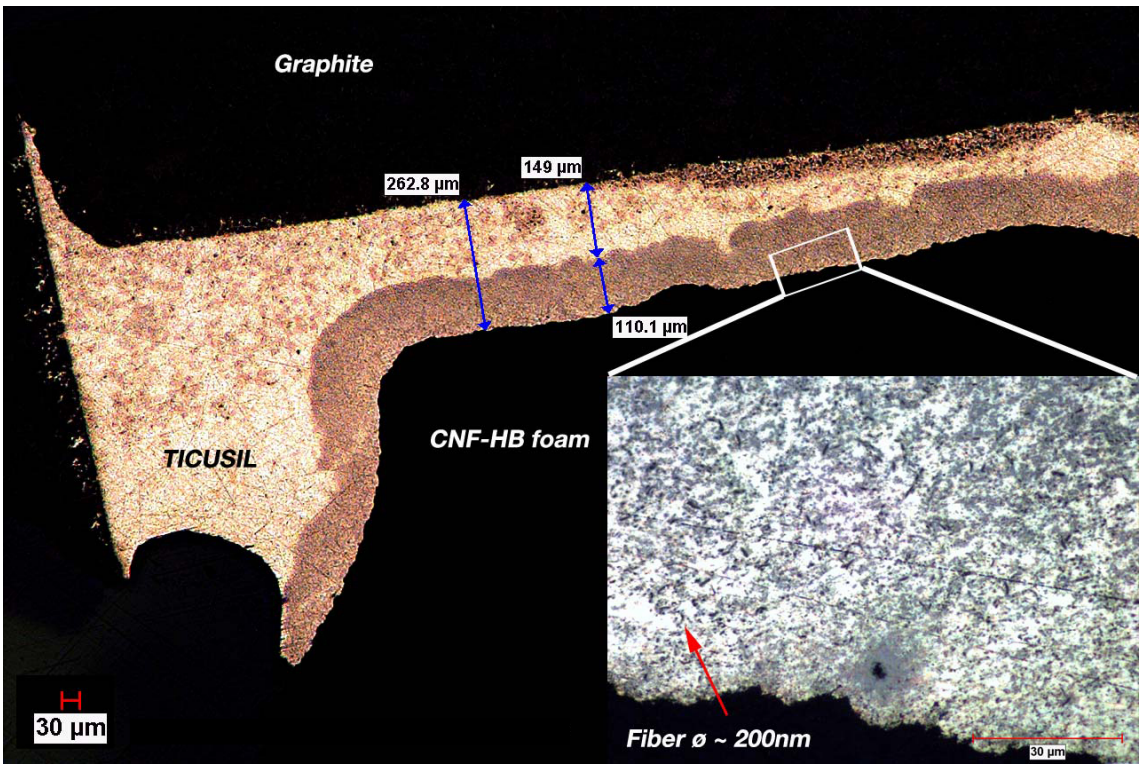

Figure 38: Series ML, Sample IN40 CNF-HB infiltrated by Ticusil. Infiltration depth is about 100 μm, 50x LM: CISP

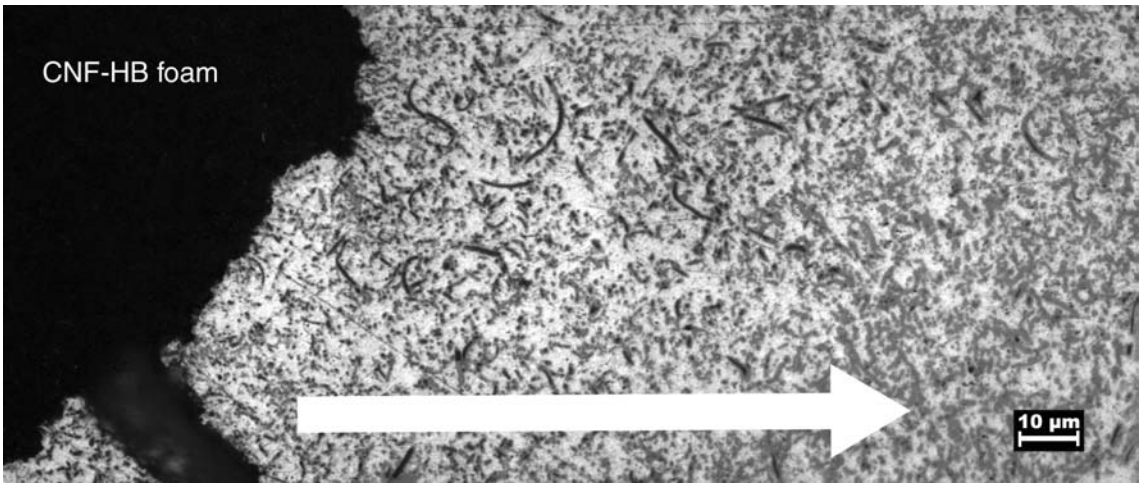

Figure 39: Series ML, Sample IN40. The white arrow indicates the gradient of the carbide formation (Infiltration flow of the metal-alloy is in the opposite direction), 1000x LM: CISP

Cu-Boron-alloys

For Boron containing Cu-alloys (CuB1 with 1 wt.% B and CuB2 with 2 wt.% B) infiltration depths of several 100 μm were observed. The experimental setup for this series is shown in figure 33.

It seems, that boron promotes the infiltration into the carbon preforms. Figures 40 – 43 show backscattered electron images of the samples IN63 (CNT-OH with CuB2) and IN66 (CNT with CuB1). Single nanotubes can not be determined, but the dark black areas are assumed to be clustered CNTs. It is possible that these clusters were present in the original preform already and connecting nanofiber bridges between them were consumed or flushed by the infiltrating alloy. Clustering due to the infiltration process is not considered to be the principal mechanism.

EDX analysis (figure 44) found boron in the gray and darker areas of the BSD-images, but not within the copper matrix (lighter areas in the BSD-images, figure 46).

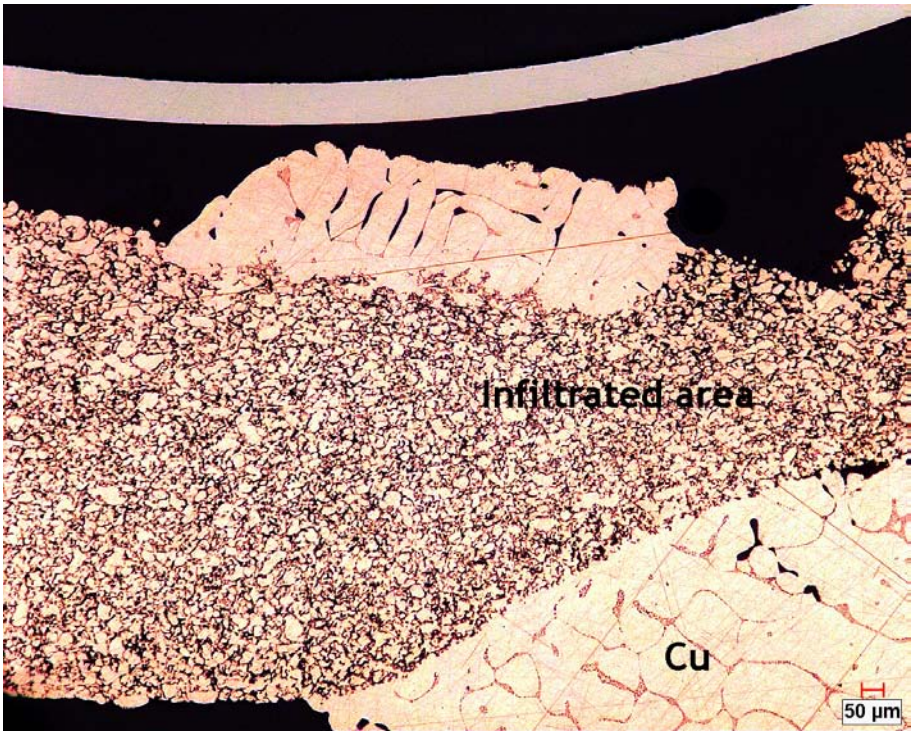

Figure 40: IN63 CuB2 infiltrated area of several 100 μm. LM: CISP

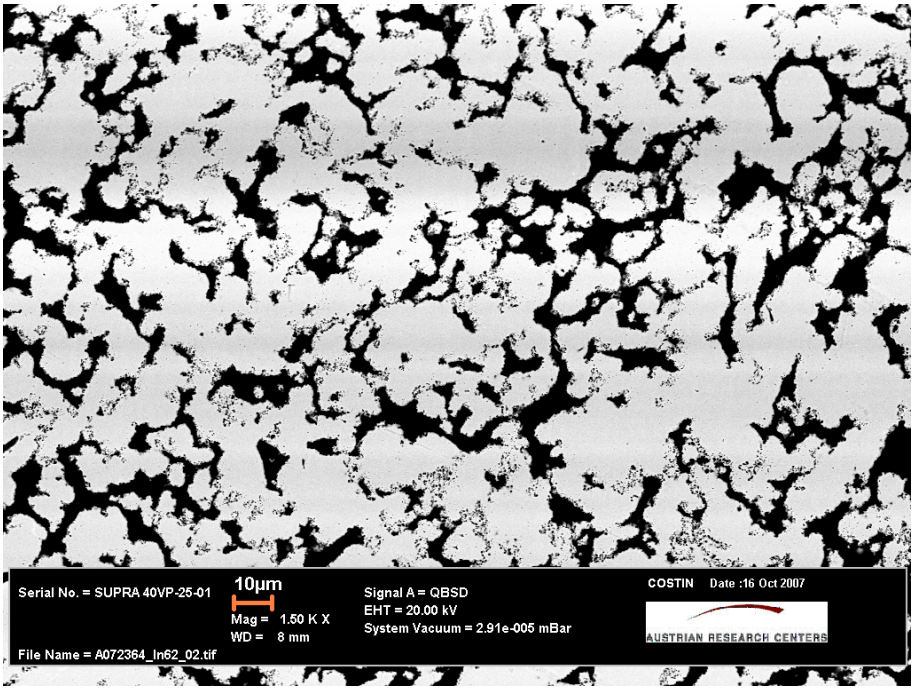

Figure 41: IN66 CuB1 infiltrated area, 1500x. BSD: ARC

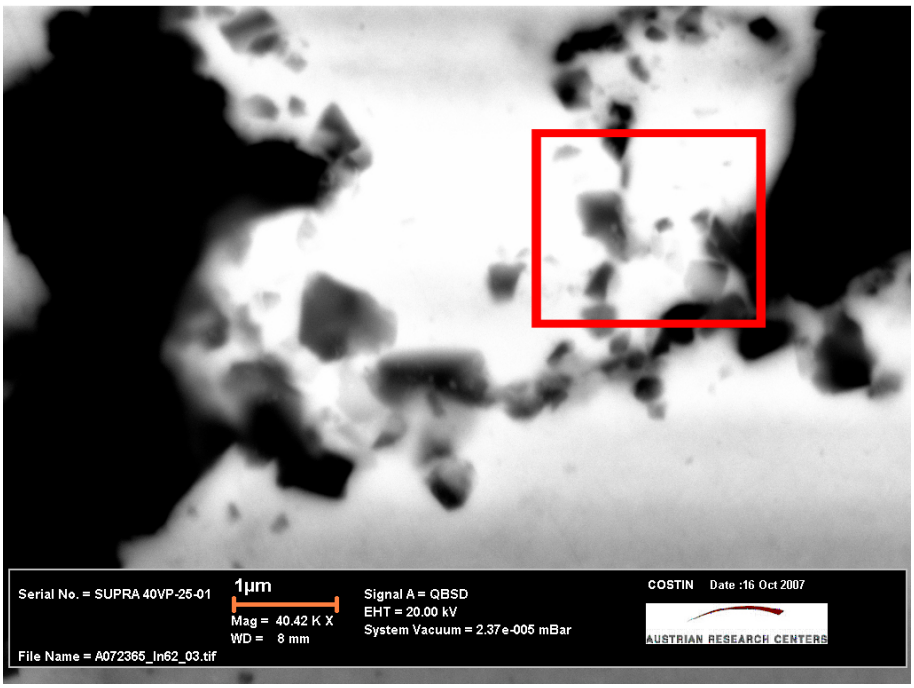

Figure 42: IN66 CuB1 infiltrated area, 42000x. The red square shows the position of figure 43. BSD: ARC

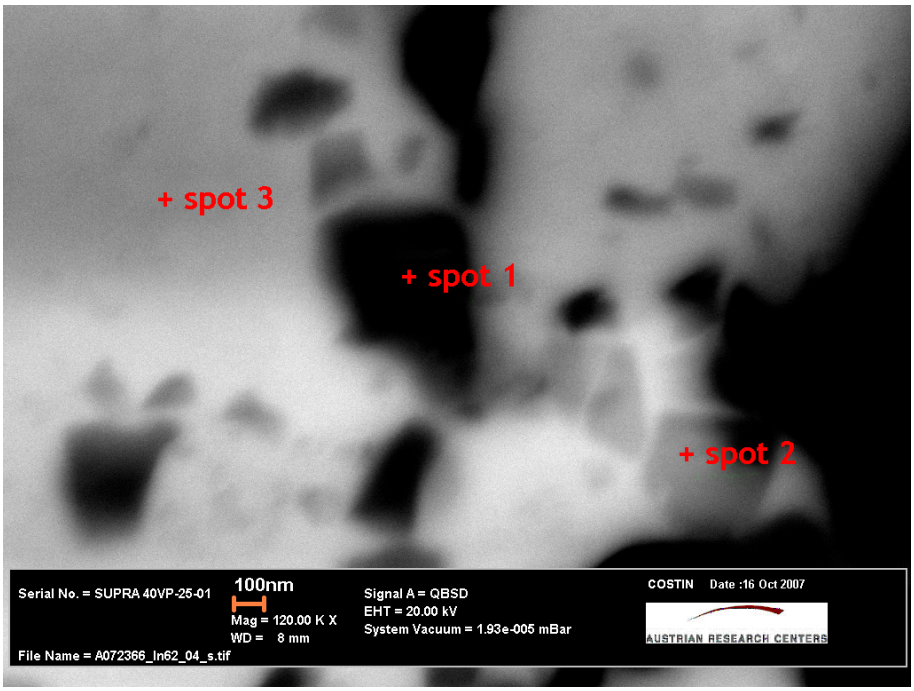

Figure 43: IN66 CuB1 infiltrated area, 120000x. Spots indicate the EDX-Scan areas. BSD: ARC

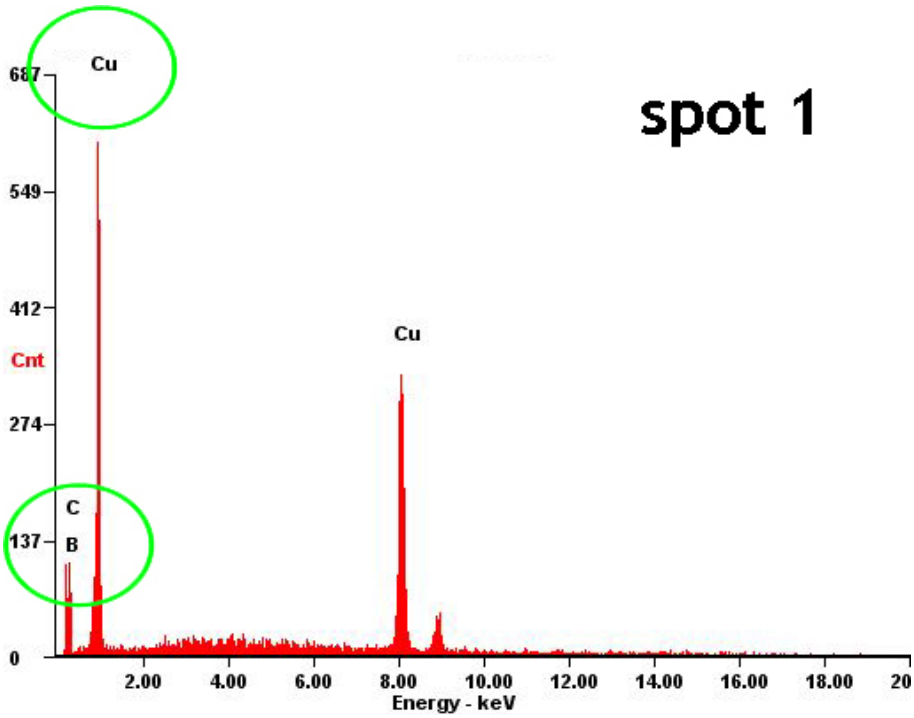

Figure 44: IN66 CuB1 EDX of Spot 1 shows not only carbon, there is copper and boron too.

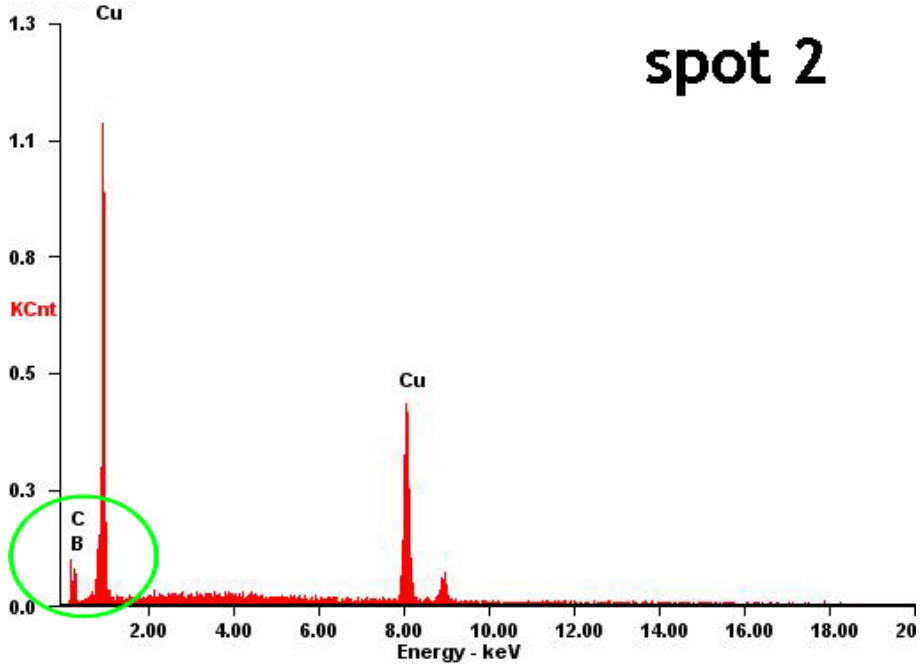

Figure 45: IN66 CuB1 EDX of Spot 2 shows similar results as Spot 1.

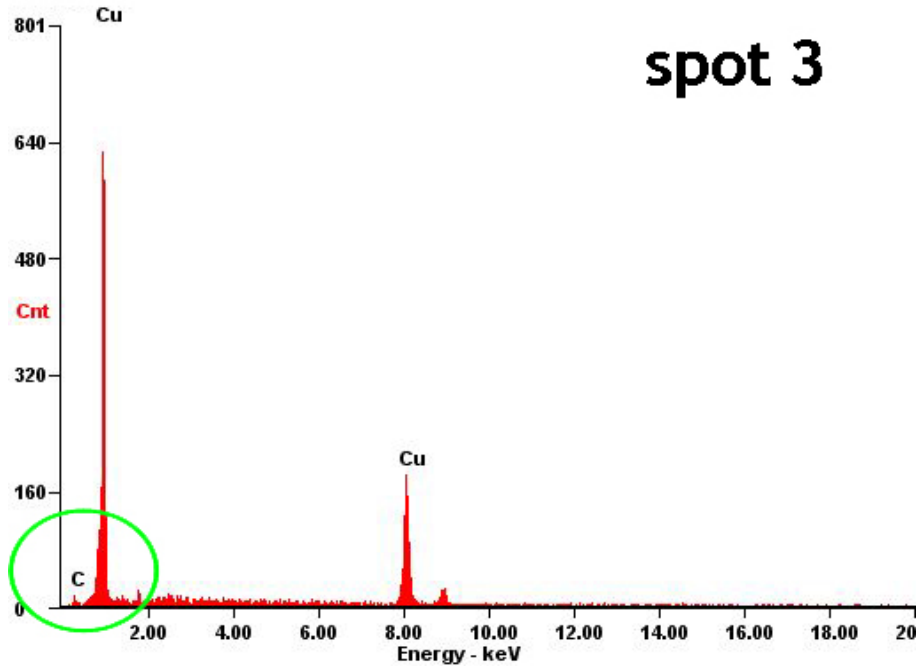

Figure 46: IN66 CuB1 EDX of Spot 3 is placed in the copper matrix and therefor only copper is found besides some carbon - no boron as expected.

Powder metallurgical approaches

Due to the severe problems in heating the nanofeatured carbon preforms and the not very satisfying infiltration depths of about 100 μm at maximum, another approach was investigated to produce Metal Matrix Composites containing carbon nanofibers. When mixing metal powders with carbon nanoparticles, clustering of the nanoparticles appears, which is undesired in heatsink materials. In order to obtain a homogeneous fiber distribution in the final product, various methods like introducing surfactants, additives, mixing, milling and coating were investigated.

4.5 Uncoated CNF, Series MG

In this chapter a powder metallurgical method is presented for producing copper carbon nanofiber composites with prefabricated, uncoated vapor grown carbon nanofibers (VGCNF). In order to achieve a uniform dispersion of the nanoparticles in the copper matrix, various dispersion and mixing techniques can be used. Different types of mixers and shakers, using milling media such as steel or ZrO_2 balls, introducing liquid dispersion support or ultrasonic agitation provide various possibilities.

In this study the powders are mixed with copper in three different ways. The volume percentage is 30 vol% for the CNFs in every sample and copper including different amounts of additives was used as metal matrix. For mixing the powders a turbula sintris mixer was used.

The different mixing routes were:

- Mixway A: Adding the surfactant Hexam to the powder and mixing in the turbula-mixer with ZrO_2 balls for 12 hours.
- Mixway B: using the Pluronic F108 in water for dispersion of the fibers, drying and then mixing in the turbula-mixer for 6 hours.
- Mixway C: Powder plus Hexam and milling for 3+12 hours.

After the mixing procedure the powder has a homogeneous gray colour. For sample preparation the powders were hot pressed using a 12 fold die (figure 47) with rectangular sample shapes (approx. 14x14x10 mm^3). This die setup offers the possibility to prepare 12 samples in one hot pressing run, which guarantees equal processing

Sample	**Total weight** of CNFs (g)	**Total weight** of Cu (g)	**Total weight** of X* (g)	**Mixing**	**Mixing time** (h)
G1	1,15	12,29	0	A	12
G2	1,15	12,29	0	B	6
G3	1,15	12,29	0	C	3+12
G4	1,15	12,12	0,1399	A	12
G5	1,15	11,77	0,4198	A	12
G6	1,15	11,42	0,6997	A	12
G7	1,15	12,12	0,2015	A	12
G8	1,15	11,77	0,6045	A	12
G9	1,15	11,42	1,0074	A	12
G10	1,15	12,12	0,089	A	12
G11	1,15	11,77	0,267	A	12
G12	1,15	11,42	0,4449	A	12

Table VIII: Series MG

G1:	Cu+30%vol.CNF	G7:	Cu+1%vol.Mo+30%vol.CNF
G2:	Cu+30%vol.CNF	G8:	Cu+3%vol.Mo+30%vol.CNF
G3:	Cu+30%vol.CNF	G9:	Cu+5%vol.Mo+30%vol.CNF
G4:	Cu+1%vol.Cr+30%vol.CNF	G10:	Cu+1%vol.Ti+30%vol.CNF
G5:	Cu+3%vol.Cr+30%vol.CNF	G11:	Cu+3%vol.Ti+30%vol.CNF
G6:	Cu+5%vol.Cr+30%vol.CNF	G12:	Cu+5%vol.Ti+30%vol.CNF

conditions (temperature, pressure, atmosphere). In order to avoid mechanical damage to the die, it is necessary that all samples have the same volume percentage. The hot pressing procedure was performed as followed:

In the first step the die is prepared with a graphite foil (0.75 mm) inserted into each sample hole of the die in order to be able to remove the samples easily after hot pressing.

After filling the powders into the die, each powder is cold compacted at a pressure of 1.3 tons on 200 mm^2.

The second step is to perform the hot pressing procedure:

1. 60 minutes evacuation
2. 90 minutes heating up to 950 °C (temperature of graphite heater), applying load 20 kN, 0.5 Pa H_2
3. 30 minutes at 950 °C, increase load to 47 kN, 0.5 Pa H_2

Figure 47: hot press 12 fold die

4. 30 minutes at 950 °C, load at 47 kN, 0.5 Pa H_2 (max. sample temp. ≈ 930 °C)
5. 120 minutes cooling down at 47 kN, 0.5 Pa Ar
6. 60 minutes cooling down, continous reduction of load

The samples where extracted from the die, the graphite foil was removed by grinding and the samples where polished. For characterisation the samples where investigated by optical microscopy and the archimedian density was determined. For comparing the measured density with the theoretical density the rule of mixture (4.5) was used.

$$\rho_{CuCN} = V_{CN} \cdot \rho_{CN} + (1 - V_{CN}) \cdot \rho_{Cu} \tag{4.5}$$

Unfortunately there are no precise density values of CNFs. The supplier of CNFs for the composites in this section (series MG), Electrovac AG, gives a value of approx. 0.15 to 0.2 g/cm^3 for the CNF. Since the CNFs have 80% purity, the additional amount of 20% is graphite with a density of approx. 2.0 g/cm^3. So the real density of the raw material is probably approx. 0.56 g/cm^3 or even higher due to additional metallic impurities. Details of density measurements can be found in the following Table IX.

For all samples of this series, the resulting fiber distribution is not homogeneous, as seen in figure 48. Cross sections investigated by optical microscopy show carbon

sample	m.air (g)	m.H_20 (g)	arch. density (g/cm^3)	theor. density* (g/cm^3)	% arch. density
G1	5,3494	4,43401	5,843847977	6,86	85,22%
G2	5,3532	4,4562	5,967892977	6,86	87,03%
G3	5,48237	4,5916	6,15464149	6,86	89,76%
G4	5,47586	4,559	5,97240582	6,86	87,10%
G5	5,66244	4,7228	6,026180239	6,86	87,88%
G6	5,27305	4,4067	6,08651238	6,86	88,76%
G7	4,73914	3,9508	6,011543243	6,86	87,67%
G8	5,39564	4,51603	6,134127625	6,86	89,46%
G9	5,48398	4,58057	6,070311376	6,86	88,53%
G10	5,49728	4,57309	5,948214112	6,86	86,75%
G11	5,68685	4,7357	5,978920254	6,86	87,19%
G12	5,8367	4,8586	5,967385748	6,86	87,03%

Table IX: Series MG, densities, (*)derived by rule of mixture.

nanofiber clusters in the entire volume of all samples.

The uncoated nanoparticels tend to agglomerate and form clusters, and the three different mixing methods during the preparation do not seem to solve this problem. One approach for a better distribution might be to use heavier balls as milling media or longer mixing periods, but then breaking or cracking of the nanofibers could occur, which is undesired. Using surfactants for deagglomeration works very well as long as the nanofibers are suspended in the liquid. After drying and mixing with the matrix powder, however they agglomerate again.

When comparing the samples with the different carbide forming additives Ti, Mo, Cr, there are some differences in the areas where the additives move to.

Cross sections of samples G4–G6 show the chromium settled in certain small areas near the carbon nanofilaments. The chromium seems to diffuse to the carbon particles. See figures 49 – 51.

In the case of molybdenum as additive (samples G7–G9) the melting temperature of molydenum was not reached during the hot pressing process. The entire surface is covered with little spots of molybdenum, but it seems not to be connected to the nanofibers. With an increasing amount of additives the spots grow in size. See figures 52 – 54.

For the samples G10–G12 titanium was used as alloying element. Titanium is diffusing to the carbon nanofibers and appears inside the nanofiber clusters. Hardly

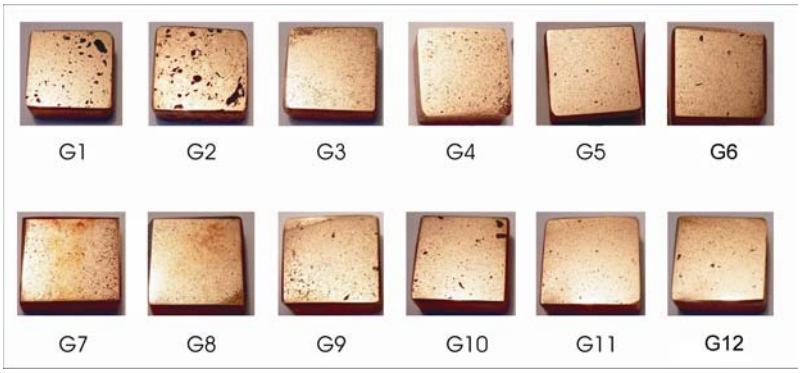

Figure 48: Series MG

any titanium can be found in the copper matrix. See figures 55 – 57.

Because of the inhomogeneus CNF distribution, the thermal properties of the produced samples were not very good. Table X lists the thermal diffusivity and the thermal conductivity of the samples in Series MG. No significant differences can be found between the samples containing carbide forming additives. The main reason for this result is again the inhomogeneous CNF distribution.

Therefore in the light of these results a method was applied to coat the CNFs chemically with copper and then adding the carbide formers plus eventually some more copper. This procedure, which improves the fiber distribution, is described in section 4.6.

Sample	Diffusivity	Thermal conductivity
G1 Cu	26,63	10,652
G2 Cu	23,21	9,284
G3 Cu	22,27	8,908
G4 Cu + 1%vol. Cr	18,73	7,492
G5 Cu + 3%vol. Cr	20,27	8,108
G6 Cu + 5%vol. Cr	no result	no result
G7 Cu + 1%vol. Mo	24,51	9,804
G8 Cu + 3%vol. Mo	25,53	10,212
G9 Cu + 5%vol. Mo	17,14	6,856
G10 Cu + 1%vol. Ti	17,14	6,856
G11 Cu + 3%vol. Ti	21,92	8,768
G12 Cu + 5%vol. Ti	20,69	8,276

Table X: Thermal diffusivity and conductivity of the samples in Series MG

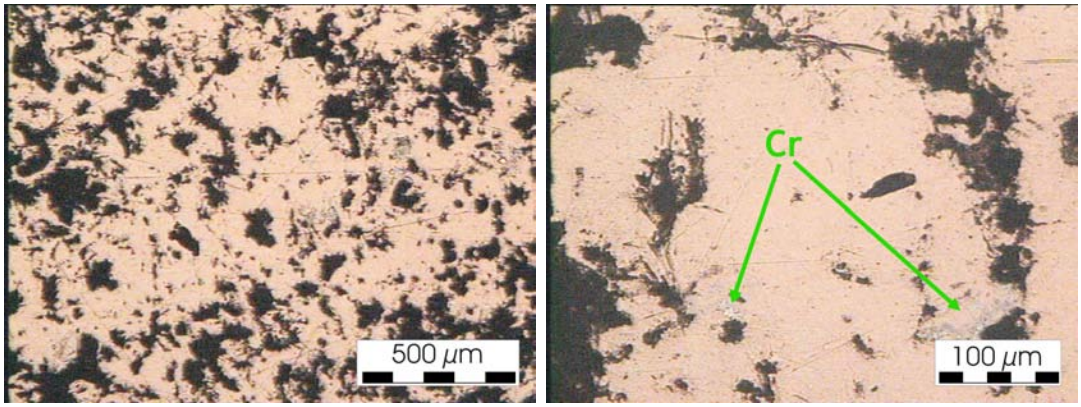

Figure 49: Sample G4 Cu+1%vol.Cr+30%vol.CNF, LM TU-Wien (50x, 200x)

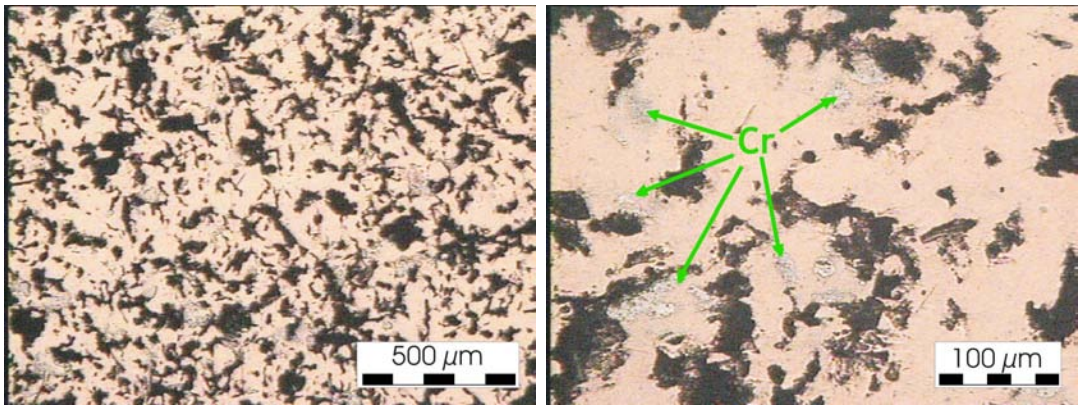

Figure 50: Sample G5 Cu+3%vol.Cr+30%vol.CNF, LM TU-Wien (50x, 200x)

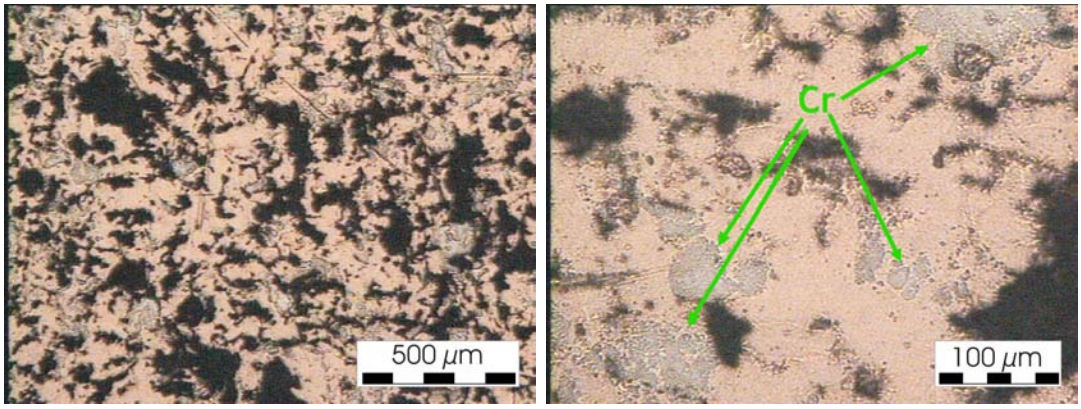

Figure 51: Sample G6 Cu+5%vol.Cr+30%vol.CNF, LM TU-Wien (50x, 200x)

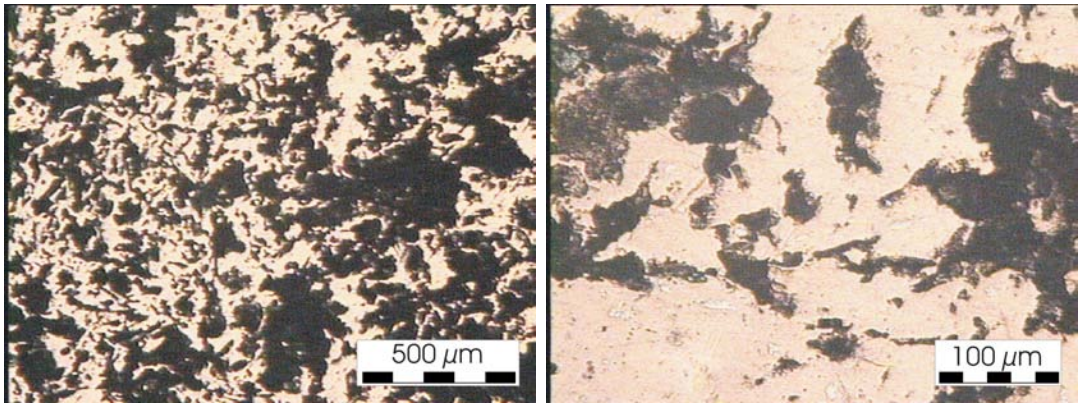

Figure 52: Sample G7 Cu+1%vol.Mo+30%vol.CNF, LM TU-Wien (50x, 200x)

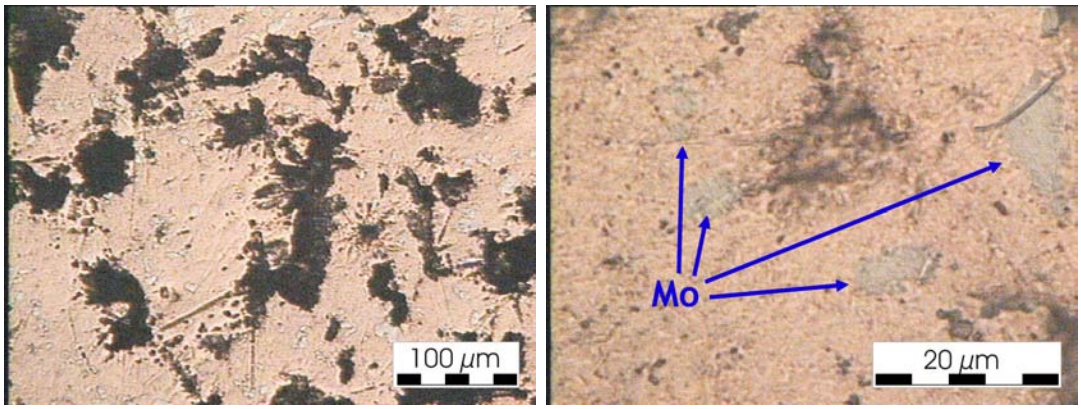

Figure 53: Sample G8 Cu+3%vol.Mo+30%vol.CNF, LM TU-Wien (200x, 1500x)

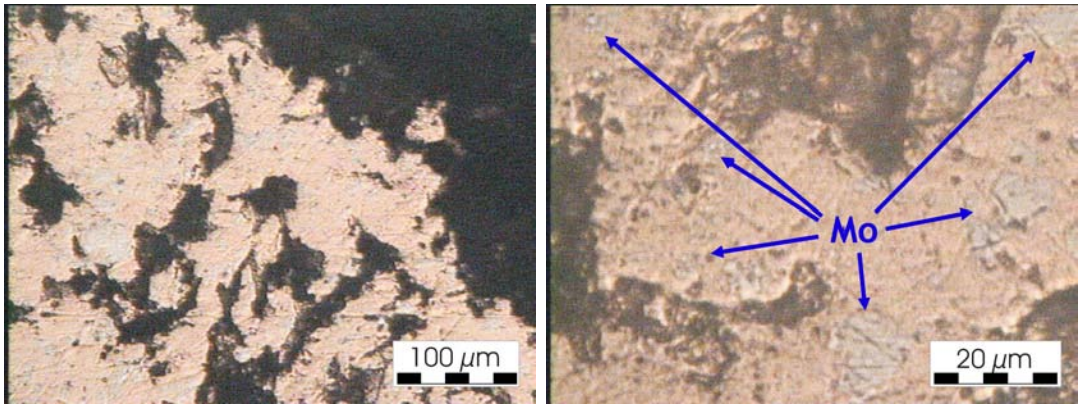

Figure 54: Sample G9 Cu+5%vol.Mo+30%vol.CNF, LM TU-Wien (200x, 1000x)

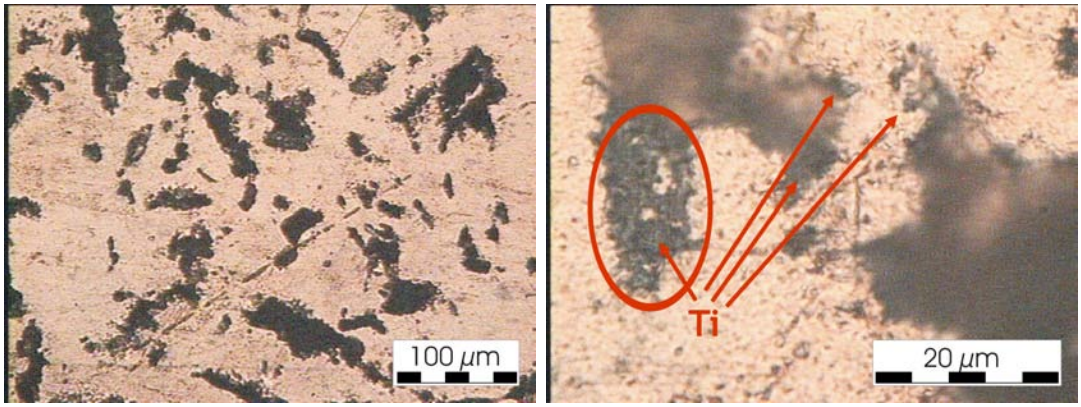

Figure 55: Sample G10 Cu+1%vol.Ti+30%vol.CNF, LM TU-Wien (200x, 1500x)

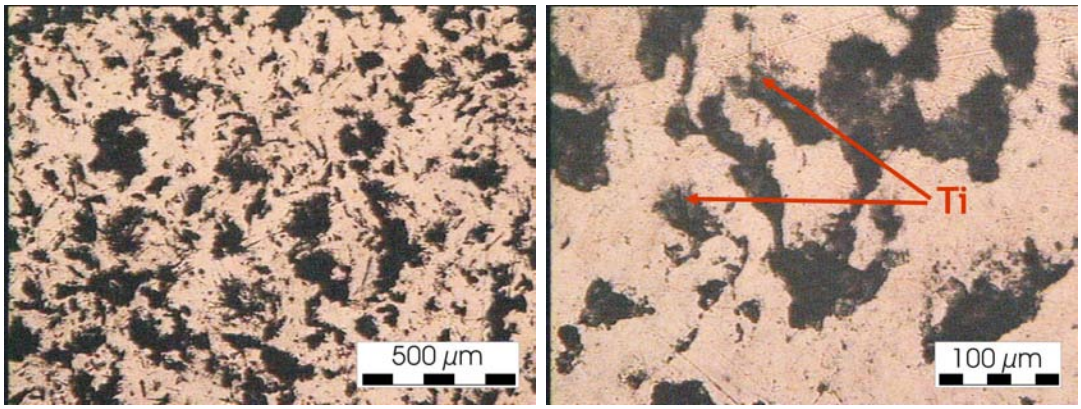

Figure 56: Sample G11 Cu+3%vol.Ti+30%vol.CNF, LM TU-Wien (50x, 200x)

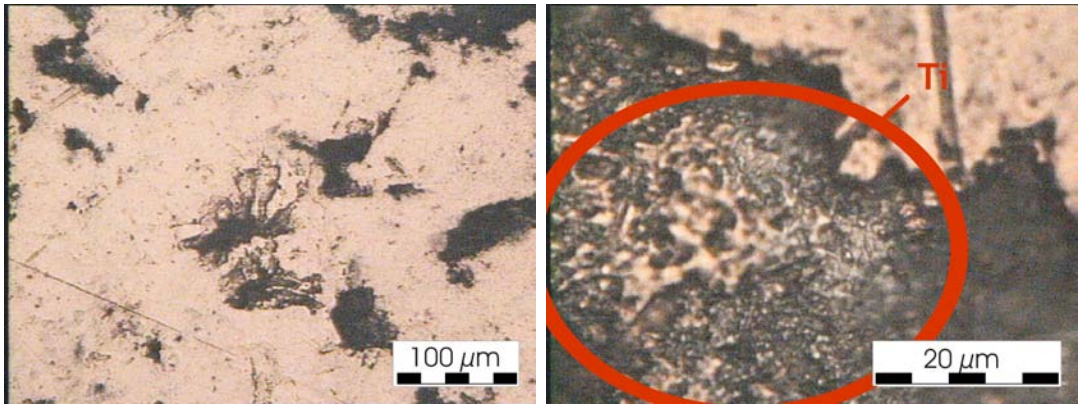

Figure 57: Sample G12 Cu+5%vol.Ti+30%vol.CNF, LM TU-Wien (200x, 1500x)

4.6 Carbon nanofibers coated via electroless copper plating

To avoid the agglomeration problem of the uncoated carbon nanofibers, a chemical coating process was performed to coat the nanofibers with copper. The coated nanofibers then behave like copper particles which could improve the distribution in the final product.

It is very tricky to get a homogeneous coating of the fibers. Mostly the result is a fine network formed by copper particles and the carbon nanoparticles (figure 58). This network seems to be sufficient to hold the nanofibers apart in the subsequent sintering process (e.g. hot pressing) and inhibits agglomeration to large clusters.

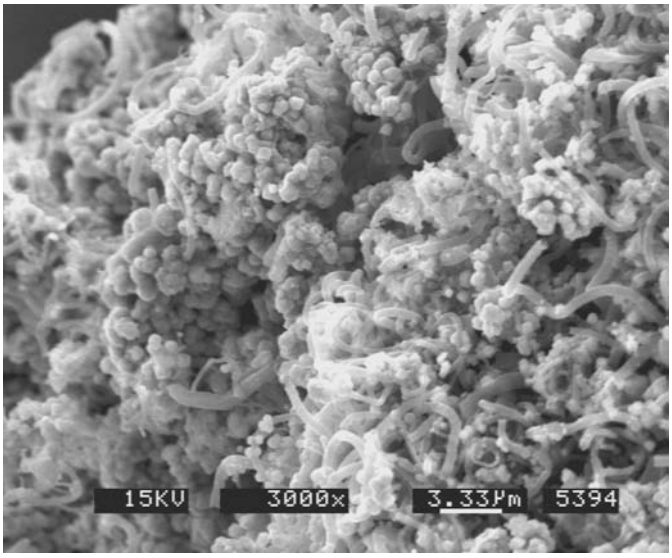

Figure 58: Copper - carbon nanofiber network after the electroless plating process, SEM: CISP

4.6.1 Experimental procedure

The electroless copper plating process used in this study follows a paper by Ch. Edtmaier and E. Wallnoefer [32] and was adjusted with previous experiments at the Center for Innovative Sintered Products, PSU [11]. The final procedure used for this study is as followed:

The desired amount of carbon nanofibers was cleaned with 70% nitric acid for about 15 minutes in order to remove contaminants and was subsequently filtered. After this pre-treatment the nanofibers were subjected to sensitization in a $SnCl_2 \cdot 2H_2O$

solution under ultrasonic agitation. In the next step activation was carried out in a $PdCl_2$ bath. For copper deposition a solution containing $CuSO_4 \cdot 5H_2O$, Potassium sodium tartrate and Triethylamine was prepared as described in section 2.4. Formaldehyde and NaOH where used to adjust the pH-value to pH 12.5. The carbon nanofibers were added to this elecroless plating solution, heated and ultrasonically agitated to deagglomerate the fibers and facilitate the copper deposition. Additionally the solution was stirred manually.

At the end of each step the carbon nanofibers were collected by vacuum filtration and finally dried after the coating procedure.

In order to optimize the coating process, parameters like the holding time, the temperatures and chemical conditions were slightly varied in the respective steps. According to Ang et al. [10] 3 days were chosen for the aging time of the sensitizing solution ($SiCl_2$ diluted in HCl). The relation between the aging time and the coating properties as well as the chemical compositions of the various used baths is shown in section 2.4 in detail. See the appendix for detailed information about all the experiments performed on electroless copper coating of the nanofibers.

4.6.2 Coating results

The final carbon nanofiber to copper weight-ratio was derived by weighing the initial nanofiber content and comparing it to the final weight of the coated particles after drying. Each filtration process gives a weight-loss that has to be appraised and subtracted from the initial weight.

Depending on several parameters (e.g. the hold time during the coating process, the bath temperature and aging, the copper-ion content in the bath and the bath composition in general) the copper:nanofiber weight-ratio was between 60:40 and 90:10. To prepare the coated nanofibers for sintering or hot pressing, the carbon nanofiber-copper ratio was adjusted by adding copper powder and the designated amount of the carbide forming additive was admixed, again using the turbula-mixer.

Several series with altering parameters were accomplished with carbon nanofilaments (CNF) and CNF/CNT preforms. The CNF raw material (HTF110FF-HHT) was produced by Electrovac AG [46] and the CNF/CNT preforms by Future Carbon GmbH. On the nanofiber preforms the infiltration behavior of the plating solution and the copper deposition performance were investigated. Assisted by ultrasound

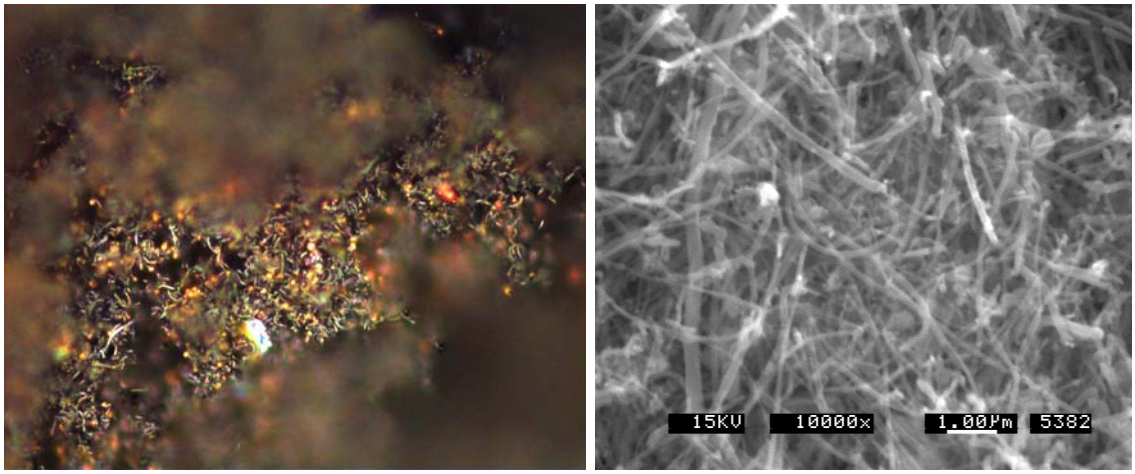

Figure 59: Copper coated carbon nanofibers Series 4 ($SiCl_2$ aged for $\approx$ 3 days), no formaldehyde. left: coated CNF-HB preform LM: CISP, right: coated nanofilaments SEM: CISP

(see section 4.1) the deposition of copper particles was possible to the depth of several milimeters, but the resulting distribution within the preforms was not homogeneous.

Formaldehyde acts as reducing agent in the plating solution, but in series 4 (figure 59) no formaldehyde was present in the solution. Compared to the other series there is significantly less copper deposited on the fibers. After filtrating the nanofibers from the plating bath, usually the solution has a pale, transparent color. Accomplishing the experiments in series 4 the solution color remains cyan, which indicates remaining copper ions in the bath. Weighing the coated fibers supports this assumption.

The experiments do not show a homogeneous coating of the CNFs or CNTs as already mentioned, but the distribution of the copper particles is very dense in certain regions. SEM images show clustered copper depositions, the denser, the higher the copper-ions concentration in the plating bath (figures 60–63).

EDX analysis (figure 61) clearly shows copper besides palladium and tin leftovers on the CNFs .

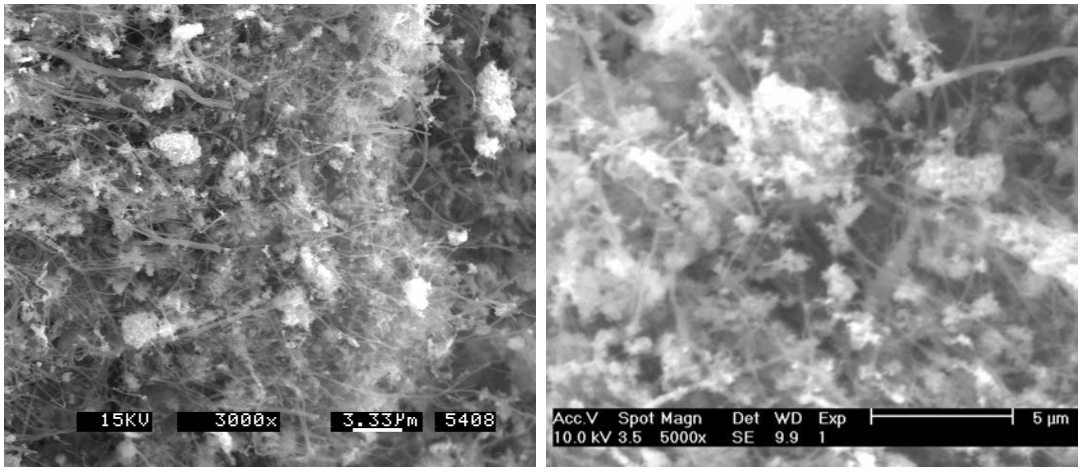

Figure 60: Copper coated CNFs ($SiCl_2$ aged for $\approx$ 3 days). left: Series 6 SEM: CISP, right: Series 9 SEM: PSU

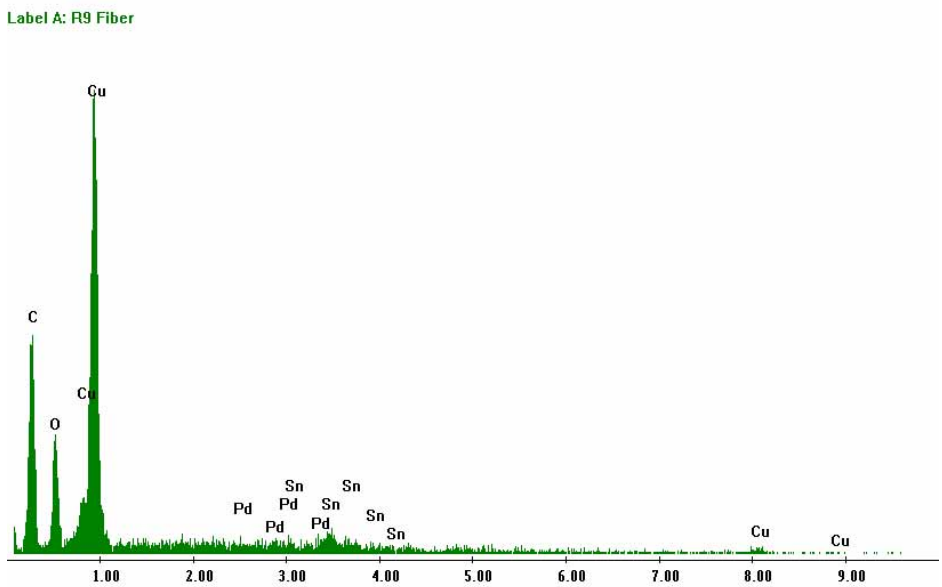

Figure 61: Spectrum of EDX analysis on a copper coated carbon nanofilament of Series 9, PSU

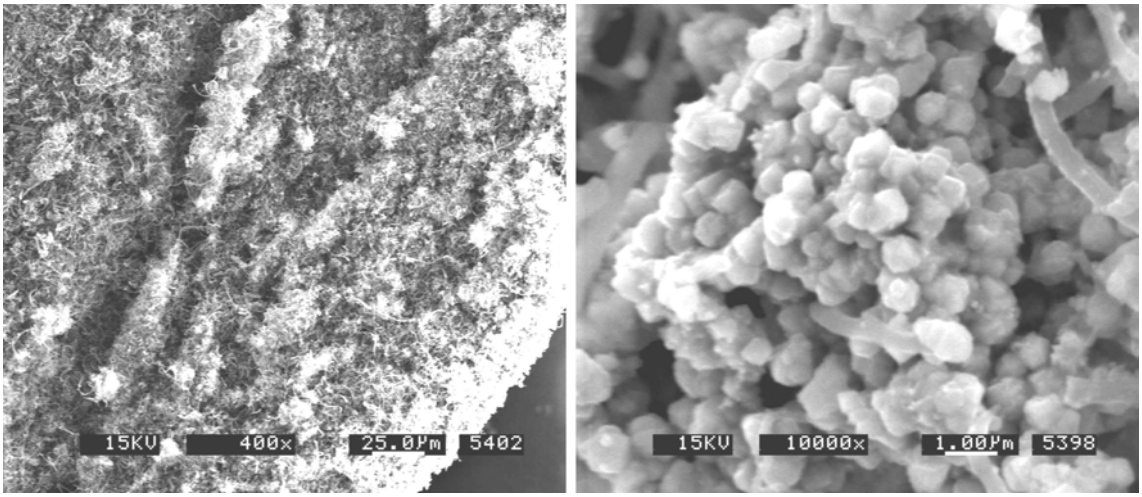

Figure 62: SEM images of CNF-HB foams show certain islands with lots of copper deposited, SEM: CISP

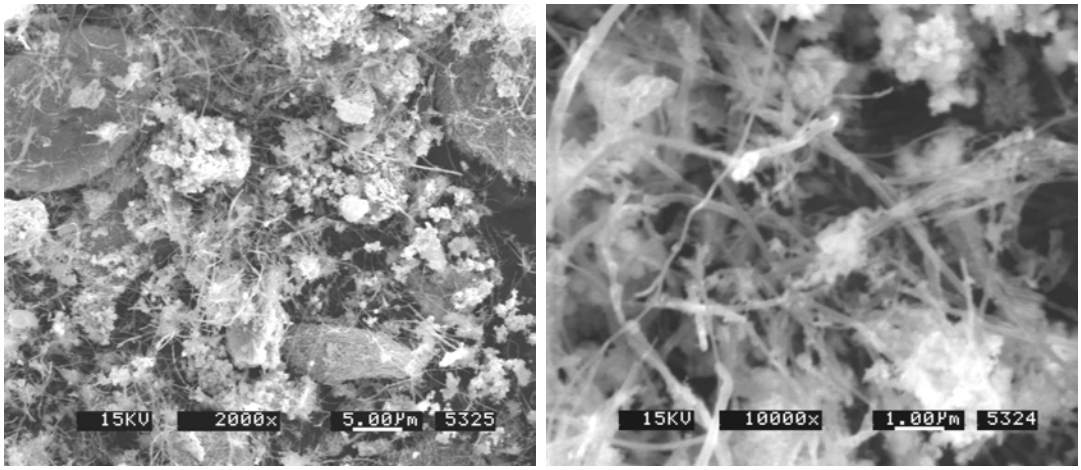

Figure 63: Copper coated carbon nanofilaments ($SiCl_2$ aged for > 3 days), SEM: CISP

Summary

Achieving a good coating efficiency on a substrate such as carbon nanofibers is a difficult process because of their very high surface-to-volume ratio. The nanofibers have been sensitized with Sn^{2+} and activated with $PdCl_2$ to facilitate the formation of catalytic Pd sites which aid the deposition process.

The presence of carbon-rich regions in the coated sample indicates that the deposition process has not yet been fully optimized.

A dense but not very uniform coating of copper on the carbon nanofibers has been achieved. The efficiency of the deposition process is still low. Better results are expected by increasing the copper concentration and by more rapidly heating the plating solution during deposition. As experimental results and literature [34] show, the concentration of formaldehyde plays an important role in the coating process.

4.6.3 Cold compacting, sintering in a conventional furnace and using microwaves

Additionally to the hot pressing approach (section 4.6.4), cold compacting of the powder to tablets and consequent sintering was performed. Generally this process gives samples with lower densities, but for a quick check of the changed parameters in the copper deposition process, cold compacting and sintering is an appropriate method.

A relatively new method for sintering powders is microwave sintering, described in section 2.5, which provides shorter heating times and rapid reactions. For investigating the two sintering methods on the Cu-CNF system, besides sintering in a conventional furnace, samples were prepared using microwaves as the heating method. When comparing these two different types of heating, one very important parameter for this study is the heating and holding time. The time at elevated temperatures is related to the reaction time for forming the carbide layer and therefor crucial for the properties of the resulting CNF-Cu composite material. The thickness of the carbide layer is of major importance in this system.

Conventional furnaces usually take a long timeperiod for their heating cycle. 5–10 °C/minute are common heating rates, where microwaves can heat the sample within several minutes to very high temperatures. Detailed information about

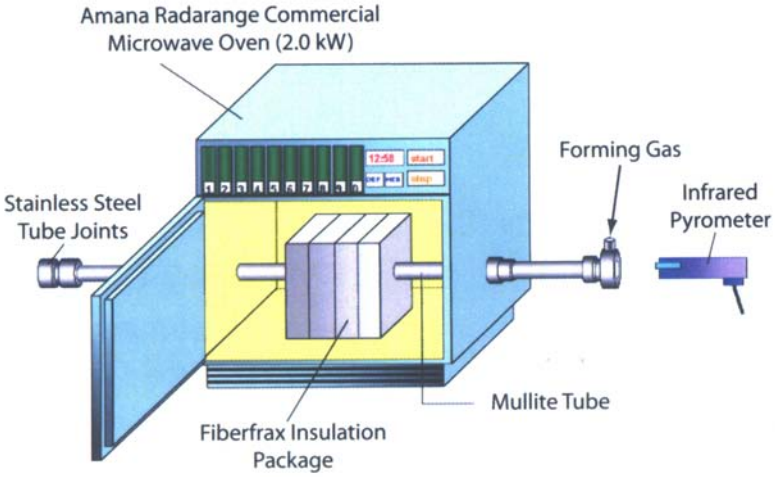

Figure 64: Microwave oven for sintering powders

the heating mechanism using microwaves is given in section 2.5. The used microwave oven is shown in figure 64.

Preparing the samples for sintering, the copper coated carbon nanofiber powders were compacted in a manual press to tablets of 1/2 inch diameter. The applied pressure was about 1.3 tons/200 mm^2.

Conventionally sintered samples

The sintering in the conventional furnace was done with a 5 °C/min heating rate up to 1034 °C (melting point of copper is 1034 °C) and after holding this temperature for 2 hours the samples were cooled to room temperature, again with 5 °C/min.

As expected, these samples have low density and high porosity due to the missing compression during the sintering process (figure 65). SEM images show several places, where dewetting of the coated CNFs took place and during sample polishing the nanofilaments were ripped out of the composite in some spots.

Microwave sintered samples

Heating powder metallurgical samples in a microwave oven is much faster than in a conventional oven. For MMCs this could be an advantage in respect to the reaction

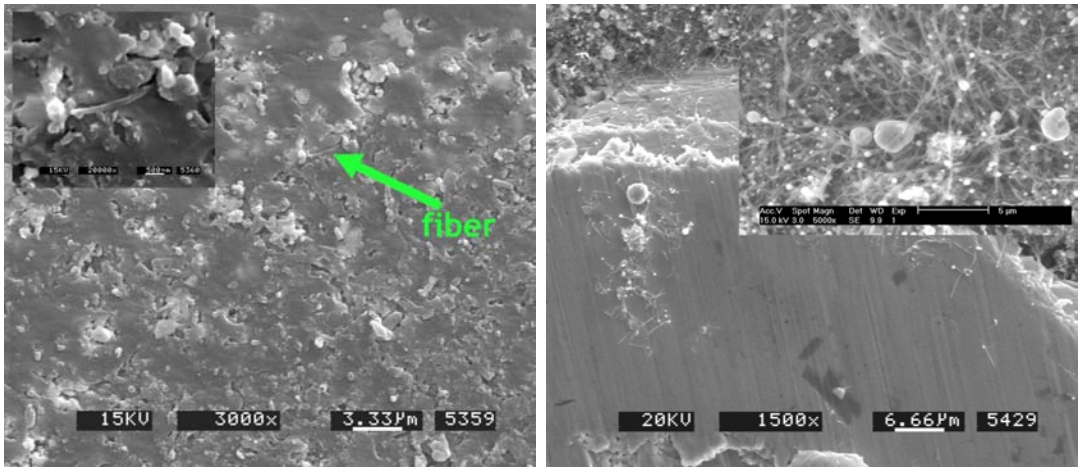

Figure 65: Conventional sintered samples exhibit high porosity, CNFs are ripped out of the composite and show dewetting, SEM: CISP

times of the carbide layer. Shorter heating times should correspond to the carbide thickness on the CNFs and CNTs.

Compared to hot pressed samples the microwave sintered samples did not reach high densities, because in the microwave setup used in this study no external (mechanical) pressure could be applied on the samples, but the samples are consolidated.

The CNFs are quite well distributed and large clusters are not observed frequently.

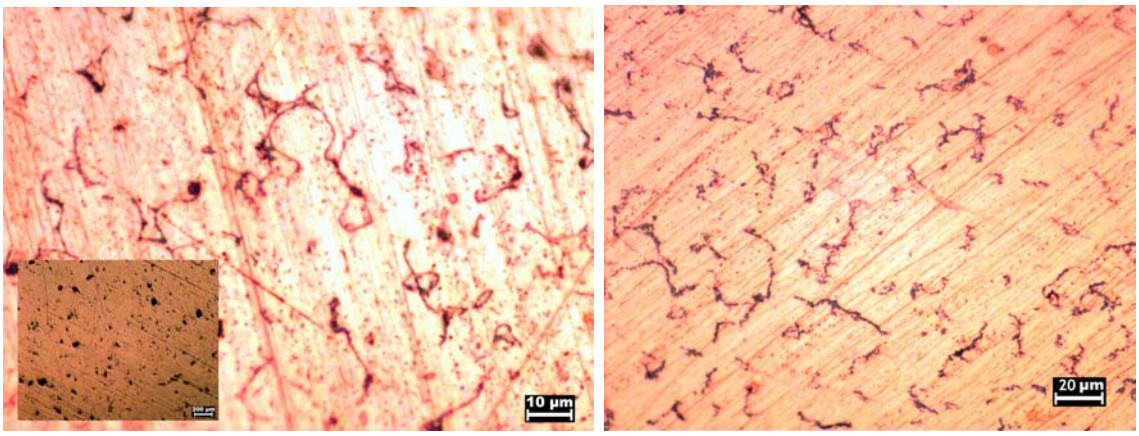

Figure 66: Microwave sintered samples with differently coated CNFs (left: R4MW5, right R9MW5), LM: CISP

Two samples are compared in figure 66. The cross section of the microwave sintered sample R4MW5 shows more CNF clusters then sample R9MW5 (Copper deposition is much denser in R9MW5), but R4MW5 exhibits better thermal diffusivity than

R9MW5 (see table XI). The reason for these results could be the difference in the matrices, R4MW5 contains 1wt.% Ti and R9MW5 has a pure copper matrix.

The fibrous structure of sample R9MW5 seen in figure 66 is believed to be chains of several CNFs.

	R4MW5 (Cu 1%Ti)	R9MW5 (Cu)
Thermal diffusivity	48.195 mm^2/s	23.395 mm^2/s

Table XI: Thermal diffusivity of MW-sintered samples R4MW5 amd R9MW5

4.6.4 Hot pressing

Using the hot pressing technique for producing composites has the advantage of less porosity in the final material. The results with this method using copper coated carbon nanofilaments from run 9 are very promising although there was not much copper in the composite and the final material is still quite porous. No carbide forming additives were used for this sample.

The thermal diffusivity measured for the hot pressed nanofilaments from copper coating run 9 is 71.23 mm^2/s which is a very promising result for a Cu-CNF MMC containing no carbide forming additives.

When comparing cold compacting – conventional sintering, cold compacting – microwave sintering and hot pressing, hot pressing seems to be the easiest to handle method for producing MMCs. Microwave sintering is a very interesting technique giving compact samples with competitive thermal properties and the possibility to shorten the heating and holding time. Both hot pressing and microwave sintering allow to produce samples with a homogeneous CNF distribution when using chemically copper coated CNFs as reinforcement.

5 Conclusion and outlook

Due to hardly any literature or publications on the copper – carbon nanofiber system and many unknown parameters in the various production approaches, as well as because nanofeatured composites lead into a tiny-scale world not completely understood yet, the work on this system is very challenging.

It was shown that the wetting behavior between carbon and copper alloys containing carbide forming elements is influenced by those additives causing the contact angle to decrease to small values, which means good to excellent wettability.

Three approaches for producing copper – carbon nanofiber MMCs were successfull and should be investivated in more detail.

Starting with the infiltration of a carbon preform a strong dependence on the used raw material was found. For repoducible results it is extremely important to get similar and well characterised raw materials. A clear sensitivity of the infiltration behavior on preform pre-treatments was not seen in this study. Adding carbide formers to the copper matrix is crucial for infiltrating the preform with the liquid metal. Externally applied pressure helps to increase the infiltration height. Using pure copper does not succeed. The maximal infiltration height found for the Titanium containing alloy TiCuSil [17] and for chromium containig alloys was 100–400 μm. In these samples partly carbidised carbon nanofibers could be determined. When introducing boron as the carbide former the maximal infiltration height increases to 800 μm and more, but in the boron containing samples no single nanofibers could be found any more. They seem to be consumed or flushed away by the metal during the infiltration process.

The second promising production route investigated is coating carbon nanofilaments with copper by chemical copper plating and subsequently sintering the precompacted coated CNFs (containing small amounts of carbide formers) using microwaves. The advantage of sintering with microwaves are the fast heating cycles of about
30–60 minutes from room temperature to 1000°C. The heating comes from the powder particles in the inside of the sample and not from the surrounding heating elements like in a conventional furnace. Additionally selective heating of different materials can be used depending on the position in the microwave field. Applying

external pressure during the sintering process was not possible in the setup used for this study.

Hot pressing of the coated CNFs leads to the third successfull approach. Like in the sintering technique, a homogeneous nanofiber distribution in the matrix was achieved by coating them with copper before hot pressing. The applied pressure avoids dewetting on the carbon surface and increases the final sample density. No fiber damage was observed.

For further investigations the serviceability of microwave sintering without external pressure should be clearified. Hot pressing is an established and successful method for producing MMCs. In the infiltration approach the principal feasibility was approved, but the microstructural infiltration behavior of the metal matrix has to be studied in more detail. The extreme sensibility of the infiltration behavior on the used preform material is a very challenging problem in this system.

6 Acknowledgements

This thesis was done in cooperation of the Vienna University of Technology, the Austrian Research Centers Seibersdorf and the Center of Innovative Sintered Products at the Pennsylvania State University.

For his encouragement and professional discussions as well as his personal mentoring I want to thank my advisor a.o. Univ. Prof. Christoph Eisenmenger-Sittner. The team of the Arbeitsgruppe Dünne Schichten was always open for interesting discussions and helpful with ideas how to interprete my results. Thanks to all of you.

A special thank goes to Dr. Erich Neubauer, my supervisor at the Austrian Research Centers Seibersdorf, who encouraged me to follow my own ideas and always found time for all my inquiries. Thank you to your team as well for all the hours you helped me to prepare, produce and analyse my samples.

Thanks to Prof. Ivi Smid I had the amazing chance to accomplish a big part of my thesis at the Center for Innovative Sintered Products at the Pennsylvania State University in the United States. This time was not only extremely informative but also very productive. All the support my collegues gave to me boosted my work. Kristina Cowan, Dan Cunningham, Matt Kropf, David Parkes and Joe Kearns, thank you for this great time and your assistance!

List of Figures

List of Tables

References

[1] N. Eustathopoulos *Dynamics of wetting in reactive metal/ceramic systems* Acta Metallurgica Vol.46, No.7 (1998) 2319-2327

[2] I. Smid, E. Neubauer: *Preparation and interface properties of carbon reinforced copper-MMC's* Conference paper: 16th International Converence on Composite Materials, Kyoto (2007)

[3] National Aeronautics and Space Administration, NASA *http://www.nasa.gov/centers/ames/research/technology-onepagers/heat_sinks.html* October 22, 2007

[4] D. Pickrell, S. Tillett: *Nanocomposite is hot for heat spreaders* The MDA Update Winter 04–05 issue 2 (2005) 6

[5] H. Weidmüller, T. Weissgärber et al.: *Carbon-Nanofiber Reinforced Cu Composites prepared by Powder Metallurgy for Thermal Management of Electronic Devices* Materials Science Forum Vols. 534–536 (2007) 853–856

[6] R.B. Barclay and W. Bonfield: Journal of Mat. Sci. 6 (1971) 1076

[7] B.W. Howlett et al.: *Paper No.14* Int. Conference on Carbon Fibres, Their Composites and Applications, Plastic Institute, London (1971)

[8] Naidich, Yu and Kolesnichenko G.A.: *Russian Metallurgy (Metally)* No.4 (1968) 141

[9] R. Voitovitch, A. Mortensen and F. Hodaj *Diffusion-limited reactive wetting: Study of spreading kinetics of Cu-Cr alloys on carbon substrates* Acta Metallurgica Vol.47, No.4 (1999) 1117-1128

[10] L.M. Ang, T.S.A. Hor, G.Q. Xu et al. *Decoration of activated carbon nanotubes with copper and nickel* Carbon 38 (2000) 363-372

[11] R. Chandrasekharan, T. Walker and I. Smid *Functionalisazion of CNTs as building blocks of metal-matrix composites* Engineering Science and Mechanics, The Pennsylvania State University

[12] C. Garcia-Cordovilla, E. Louis and J. Narciso *Pressure infiltration of packed ceramic particulates by liquid metals* Acta mater. Vol.47, No.18 (1999) 4461-4479

[13] T. Matsunaga, K. Ogata, T. Hatayama, K. Shinozaki, M. Yoshida *Effect of acoustc cavitation on ease of infiltration of molten aluminium alloys into carbon fiber bindles using ultrasonic infiltration method*, Composites: Part A 38 (2007) 771-778

[14] J.R. Lukes, H. Zhong: *Thermal Conductivity of Individual Single-Wall Carbon Nanotubes* Journal of Heat Transfer Vol. 129 (2007) 705-716

[15] D.A. Mortimer and M. Nicholas: *The wetting of carbon and carbides by copper alloys* Journal of Mat. Sci. 8 (1973) 640-648

[16] E. Neubauer, M. Kitzmantel, C. Eisenmenger-Sittner, I. Smid, P. Angerer: *Copper based composites reinforced with carbon nanofibers* Conference paper: PowderMet 2007 Conference, Denver (2007)

[17] Wesgo Ceramics GmbH: *Datasheet for Active Brazing Alloys (ABA)* Morgan Advanced Ceramics/Wesgo Metals Division, Erlangen (2007)

[18] T. Oku et al. *Effects of titanium impregnation on the thermal conductivity of carbon/copper composite materials* Journal of Nuclear Materials 257 (1998) 59-66

[19] N. Eustathopoulos, M.G. Nicholas and B. Drevet: *Wetting at high temperatures* Pergamon Materials Sciences Volume 3 (1999)

[20] V. Michaud and A. Mortensen: *Infiltration processing of fibre reinforced composites: governing phenomena* Composites: Part A 32 (2001) 981-996

[21] J. Wannasin and M.C. Flemings: *Threshold pressure for infiltration of ceramic compacts containing fine powders* Scripta Materialia 53 (2005) 657-661

[22] L.D. Landau, E.M. Lifshitz: *Fluid Mechanics* Pergamon Press NY (1987)

[23] A. Mortensen, L.J. Masur, J.A. Cornie and M.C. Flemings *Infiltration of fibrous preforms by a pure metal: part I. theory* Physical metallurgy and materials science. Vol.20, No.11 (1989) 2535-2547

[24] P.S. Turner: Journal Res. NBS 37 (1946) 239

[25] R.U. Vaidya and K.K. Chawla: *Thermal expansion of metal-matrix composites* Compos. Sci. Technol. 50 (1994) 13-22

[26] S. Elomari, R. Boukhili and D.J. Lloyd: *Thermal expansion studies of pre-strained Al_2O_3/Al metal matrix composite* Acta Mater 44 (5) (1996) 1873-1882

[27] R.A. Schapery: J. Composite Materials 2 (1968) 380

[28] C.C. Chamis: SAMPE Quaterly 15 (1984) 14

[29] E. Hammel, X. Tang, M. Trampert, T. Schmitt, K. Mauthner, A. Eder, P. Pötschke: *Carbon nanofibers for composite applications* Carbon 42 (2004) 1153-1158

[30] Aavid Thermalloy: *Metal Matrix Composite Materials. http://www.aavidthermalloy.com/technical/papers/matrix.shtml* January 4, 2008

[31] T.W. Ebbesen et al.: *Wetting, filling and decorating carbon nanotubes* J. Phys. Chem Solids vol 57 nos 6-8 (1996) 951-955

[32] Ch. Edtmaier, E. Wallnoefer: *Preparation and properties of carbon nanotube MMCs* Conference paper: PowderMet 2004 Conference, Vienna (2004)

[33] P. Bindra, JR. White *Electroless plating: Fundamentals and applications* American Electroplaters and Surface Finishers Society (1990) 307

[34] N. Kanani, E.G. Leuze *Electroplating and Electroless Plating of Copper & its alloys* Finishing Publications Ltd, Stevenage, UK (2003)

[35] M. Buryan: *Entwicklung von Auslegungsprinzipien für mikrowellen- und gasbeheizte Hybrid-Sinteröfen* Dissertation, Technische Universität Bergakademie, Freiberg (2004)

[36] D. Agarwal: *Microwave Materials Processing: Theory and Practice* Lecture materials, MRL at The Pennsylvania State University (2007)

[37] R. Peelamedu, R. Roy, D. Agrawal: *Anisothermal reaction synthesis of garnets, ferrites and spinels in microwave field* Mat. Res. Bulletin 36 (2001) 2723-2739

[38] R. Peelamedu, R. Roy, D. Agrawal: *Reaction kinetics and anisothermal effects in microwave fields: The system Y_2O_3-Fe_3O_4* J. Mat. Res 16 (10) (2001) 2770-2772

[39] B.P. Barnsely: *Microwave Processing of Materials* Metals and Materials 5 (11) (1989) 633

[40] J.H. Booske, R.F. Cooper, S.A. Freeman, K.I. Rybakov, V.E. Semenov: *Microwave ponderomotive forces in solid-state ionic plasmas* Phys. of Plasmas 5 (5) (1998) 1664

[41] M. Willert-Porada: *A microstructural approach to the origin of microwave effect in sintering of ceramics and composites* in: Microwaves: Theory and Applications in Materials Processing IV, Columbus: The American Ceramic Society (1998) 153

[42] Uni Würzburg *http://www.ep2.physik.uni-wuerzburg.de/ag_fricke/graphic/fibers/c_fibers_2.htm* June 16, 2007

[43] Future Carbon GmBH *http://www.futurecarbon.com* June 14, 2007

[44] Wikipedia *http://www.wikipedia.org* June 14, 2007

[45] P.J.F. Harris: *Fullerene-related structure of commercial glassy carbons* Philosophical magazine Vol. 84, No. 29 (2004) 3159-3167

[46] Electrovac AG: *http://www.electrovac.com* January 10, 2008

[47] S. Brunauer, P.H. Emmet, E. Teller: *Adsorption of gases in multimolecular layers* Journal of American Chem. Soc. vol 60 (1938) 309-319

[48] E.P. Barrett, L.G. Joyner, P.P. Halenda: *The determination of pore volume and area distributions in porous substances. I. Computations from nitrogen isotherms* Journal of American Chem. Soc. vol 73 (1951) 373-380

[49] B.C. Lippens, J.H. de Boer: *Studies on pore systems in catalysts V. The t-method* Journal of Catalysis, vol 4 issue 3 (1965) 319-323

[50] B.C. Lippens, J.H. de Boer: *Studies on pore systems in catalysts I. The adsorption of nitrogen; apparatus and calculation* Journal of Catalysis, vol 3 issue 1 (1964) 32-37

[51] B. Schwarz, C. Eisenmenger-Sittner, H. Steiner: *Construction of a high temperature drop sessile device* Vacuum, vol 82 issue 2 (2008) 186-188

[52] N. Froumin, N. Frage, M. Aizensthein, M.P. Dariel: *Ceramic-metal interaction and wetting phenomena in the B_4C/Cu system* Journal of the European Ceramic Society 23 (2003) 2821-2828

Overview on all experimental series performed:

Series MA	CNF-HB wetting for metals Im/Sb/Pb/Bi Vacuum 10^{-5} mbar, 5 min heating non-wetting behavior	TU
Series MB	CNF-HB uncoated, wetting for alloys CuABA/CuCr1Zr/CuMo/CuB: n/w TicusilABA: excellent wetting	TU
Series MC	CNF-HB coated w/ 100nm Ti/TiN CuCr1Zr/CuABA only CuABA shows wetting	TU
Series MD	Sigradur uncoated with alloys CuMo - n/w CuCr1Zr - KW approx. 70° CuCr - no result (literature: KW 40°) CuCrB2 - n/w, crater forming, good adhesion CuTiB - n/w in this experiment CuABA - KW approx. 10°	TU
Series ME	CNT-felt uncoated CuABA/CuCr1Zr only CuABA infiltrates, Cu evaporates	TU
Series MF	CNF-HB uncoated/coated 100nm Ti under weight, about 2kg, 1000°C III: Ti+Cu / IV: Ti+CuCuZr / V: Ti+CuABA no pressure VI: TiN+Cu / VIII: TiN+CuCrZr / X: CuABA no pressure Infiltration in certain very limited areas.	ARC
Series MG	powder metallurgical approach, uncoated CNF 30 vol	ARC
Series MH	inductive hot pressed, high vacuum, H_2, 2 kg weight IN30 – IN35	ARC
Series MI	hot pressed HP1225 in one copper matrix, H_2 20 Mpa, 1000-1200°C	ARC
Series MJ	CNT-felt uncoated pressureless spontanuous infiltration CuABA and Ticusil show wetting behavior	TU
Series MK	Comparing Wesgo ABA alloys on FC preforms IN37 – IN42	ARC
Series ML	HP FC Preforms in plain and alloyed copper containing B or Cr	ARC
Series MM	pressureless FC Preform wetting/infiltration, N_2 Wesgo ABA in Conventional Furnace	CISP

Series Chem	Chemical coating of Carbon nanofilaments Run 1 – Run 11 (details follow)	CISP
CS	Conventional sintering of series Chem mechanically precompacted with about 5 tons on 1/2 inch diameter	CISP
MW	Microwave sintering of series Chem precompacted, no pressure applied during sintering	CISP
HP	Hot pressing of series Chem	ARC

Series	Samplename	Results	Setup	Atmosphere	Info
MA	CNF-In	MP: 156°C n/w	CNF topped w/ In (10mg)	Vacuum 10^{-5}mbar	5 min
MA	CNF-Sn	n/w (MP: 232°C)	CNF/Sn	Vacuum 10^{-5}mbar	5 min
MA	CNF-Bi	n/w (MP: 271°C)	CNF/Bi	Vacuum 10^{-5}mbar	5 min
MA	CNF-Pb	n/w (MP: 327°C)	CNF/Pb	Vacuum 10^{-5}mbar	5 min
MB	CNF-CuCr1Zr_1	did not melt	1	Vac 1,6 10^{-5} mbar	5 min
MB	CNF-CuCr1Zr_2	no result	1	Vac1,3 10^{-5} mbar	8 min
MB	CNF-CuCr1Zr_3	no result	1	Vacuum 10^{-5}mbar	
MB	CNF-CuCr1Zr_4	n/w	small pieces of preform topped with the alloy	Vacuum 10^{-5}mbar	3 min
MB	CNF-CuCr1Zr_5	did not melt well	2	Vac 1,3 10^{-5} mbar	5 min
MB	CNF-CuCr1Zr_6	nice melting pearl	2	Vac. 3 10^{-6} mbar	4 min
MB	CNF-CuMo HP1177/155	melting pearl falls off.	2	Vac. 7 10^{-7} mbar	3 min
MB	CNF-CuB HP1177/157	melting pearl falls off.	2	Vac. 5 10^{-5} mbar	4 min
MB	CNF-ABA	not infiltrated, black color at contact area black	2	Vac. 2 10^{-5} mbar	4 min
MB	CNF-CuCr1Zr_7	no result, alloy wets the sample holder.	2 modified	Vac. 3 10^{-5} mbar	1 min
MC	CNF-Ti100-ABA_1 (120nm Ti)	ABA deliquesces on the 120nm Ti-layer, eventually infiltrated.	2	Vac. 4 10^{-5} mbar	4 min
MC	CNF-Ti100 CuCr1Zr_2	100nm Ti. n/w! Pearl sticks on the foam black color on contact area	2	Vac 1,5 10^{-5} mbar	4 min
MC	CNF-Ti100-ABA_2	wetting like ...ABA_1	2	Vacuum 10^{-5}mbar	
MC	CNF-TiN100-ABA_1	no result	2	Vacuum 10^{-5}mbar	3 min
MC	CNF-TiN100-ABA_2	rapid wetting	2	Vacuum 10^{-5}mbar	2 min
MD	VC-CuMo_b1 HP1177/155	n/w melting pearl inflates and shrinks again! Possible air inclusions.	4 HTSDD	Vacuum 10^{-5}mbar	3 min
MD	VC-CuCr_b1/b2 HP1177/156	no result	4 HTSDD	Vacuum 10^{-5}mbar	3 min
MD	VC-CuCr_b3 HP1177/156	no result, alloy popped away n/w	4 vacc. dep	Vac. 2 10^{-5} mbar	2 min
MD	VC-CuB HP1177/157	KW ~ 170°, pearl sticks, breaks piece from the substrate (crater formation: literature)	4 HTSDD	Vacuum 10^{-5}mbar	3 min
MD	VC-CuCrB2_b1 HP1177/159	n/w, pearl sticks well	4 HTSDD	Vacuum 10^{-5}mbar	3 min
MD	VC-CuCrB2_b2 HP1177/159	n/w, pearl sticks well, forming crater	4 vacc. dep..	Vac. 2 10^{-5} mbar	3 min
MD	VC-CuTiB_b1 HP1177/161	pearle, n/w problems with the heating.	4 HTSDD	Vacuum 10^{-5}mbar	3 min
MD	VC-CuCr1Zr_b2	KW ~ 60°	4 HTSDD	Vacuum 10^{-5}mbar	2 min
MD	VC-CuCr1Zr_b3	KW ~ 95° heating problems	4 HTSDD	Vacuum 10^{-5}mbar	3-4 min
MD	VC-CuCrZr_b2	KW ~ 68°	4 HTSDD	Vacuum 10^{-5}mbar	3 min

Series	Samplename	Results	Setup	Atmosphere	Info
ME	CP-CuCr1Zr	did not infiltrate	1	Vacuum 10^{-5}mbar	2-3 min
ME	CP-ABA_1				
ME	CP-ABA_2				
ME	CP-ABA_3				
ME	CP-ABA_4				
ME	CP-ABA_5	Iniltrating., Cu evaporated	1		2-3 min
MF	CNF-HB Gew-III	Ti100+Cu	ARC weight		
MF	CNF-HB Gew-IV	Ti100+CuCrZr	ARC weight		
MF	CNF-HB Gew-V	Ti100+ABA no external weight	ARC		
MF	CNF-HB Gew-VI	TiN100+Cu	ARC weight		
MF	CNF-HB Gew-VIII	TiN100+CuCrZr	ARC weight		
MF	CNF-HB Gew-X	CuABA no external weight	ARC		
MG	CNF hotpressed	Cu/Cr/Mo/Ti (12 samples)	ARC 12fold die HP		
MH	IN30	Cu, FC-CNT-OH, Mo coating	ARC weight	H2	
MH	IN31	Cu, FC-CNT-ann, Mo coating	ARC weight	H2	
MH	IN32	Cu, FC-CNT paper, B coating	ARC weight	H2	
MH	IN33	Cu, FC-CNT paper, Mo coating	ARC weight	H2	
MH	IN34	Cu, FC-CNF-HB, B coating	ARC weight	H2	
MH	IN35	Cu, FC-CNF-HB, Mo coating	ARC weight	H2	
MI	HP1225 #1	Cu, FC-CNT-ann, Mo coating 20 MPa 1000-1200°	ARC circ10.		
MI	HP1225 #2	Cu, FC-CNT-OH, Mo coating 20 MPa 1000-1200°	ARC circ10.		
MI	HP1225 #3	Cu, FC-CNT paper, B coating 20 MPa 1000-1200°	ARC circ10.		
MI	HP1225 #4	Cu, FC-CNT paper, Mo coating 20 MPa 1000-1200°	ARC circ10.		
MI	HP1225 #5	Cu, FC-CNF-HB, B coating 20 MPa 1000-1200°	ARC circ10.		
MI	HP1225 #6	Cu, FC-CNF-HB, Mo coating 20 MPa 1000-1200°	ARC circ10.		
MJ	CTF-CuABA	excellent and rapid wetting	1	Vacuum 10^{-6} mbar	
MJ	CTF-TiCuSil_1	excellent and rapid wetting	1	Vacuum 10^{-6}mbar	
MJ	CTF-OH TiCuSil_1	excellent and rapid wetting	1	Vacuum 10^{-6}mbar	
MJ	CTF-OH CuSil_1	excellent and rapid wetting	1	Vacuum 10^{-6}mbar	
MJ	CTF-OH SilverABA_1	excellent and rapid wetting	1	Vacuum 10^{-6}mbar	
MK	IN 37		Ind. HP		
MK	IN 38		Ind. HP		
MK	IN 39		Ind. HP		
MK	IN 40		Ind. HP		
MK	IN 41		Ind. HP		
MK	IN 42		Ind. HP		
ML	IN50	Cu	Ind. HP		
ML	IN51	CuCrZr	Ind. HP		
ML	IN52	CuCrZr	Ind. HP		
ML	IN53	CuCrZr	Ind. HP		
ML	IN54	CuCrZr	Ind. HP		
ML	IN55	CuCrZr	Ind. HP		
ML	IN56	Cu	Ind. HP		

Series	Samplename	Results	Setup	Atmosphere	Info
ML	IN57	Cu	Ind. HP		
ML	IN58	CuCrZr	Ind. HP		
ML	IN59	CuCrZr	Ind. HP		
ML	IN60	Cu	Ind. HP		
ML	IN61	Cu	Ind. HP		
ML	IN62	Cu-B1/#157	Ind. HP		
ML	IN63	Cu-B2/#158	Ind. HP		
ML	IN64	Cu-Cr1	Ind. HP		
ML	IN65	Cu-Cr2	Ind. HP		
ML	IN66	CuCr3	Ind. HP		
ML	IN67	CuCr3	Ind. HP		
MM	CNF HB PSU1/1	CuCr 1400°C	PSU	N2	hold 30 min
MM	CNF HB PSU1/2	TiCuSil 1400°C	PSU	N2	hold 30 min
MM	CNF HB PSU1/3	InCuSil 1400°C	PSU	N2	hold 30 min
MM	CNF HB PSU1/4	CuSil 1400°C	PSU	N2	hold 30 min
MM	CNF HB PSU1/5	CuSin 1400°C	PSU	N2	hold 30 min

Series Chem, copper plating treatments runs 1–12:

The copper plating experiments are explained in section 4.6 in more detail. Carbon nanofilaments produced by Electrovac AG and CNF preforms produced by Future Carbon GmbH were investigated for the chemical coating behavior.

Run 1	**Description**	**Temp. / Ultrasound**	**Duration**
Cleaning	70% HNO_3	Room temperature (RT)	15 min
Filter and Rinse	Vacuum, H_2O	-	-
Sensitization	0.1M $SnCl_2$ aged for 4 days	25–39°C, Ultrasound	15 min
Filter	Vacuum	-	-
Activation	0,00056M $PdCl_2$	RT, Ultrasound	15 min
Filter	Vacuum	-	-
Copper deposition	1.9 g $CuSO_4$ * 5 H_2O 5 g Potassium Sodium Tartrate * 4 H_2O 30 ml Triethylamine 12.58 g NaOH 10 ml Formaldehyde 400 ml H_2O Adjusting the pH-value to 12.5	45°C, Ultrasound	10 min
Filter and Rinse	Vacuum, H_2O	-	-

Weight increase by copper in run 1: 0.45288 g.

Run 2	**Description**	**Temp. / Ultrasound**	**Duration**
Cleaning	70% HNO_3	RT	10 min
Filter and Rinse	Vacuum, H_2O	-	-
Sensitization	0.1M $SnCl_2$ aged for 19 days	25–30°C, Ultrasound	15 min*
Filter	Vacuum	-	-
Activation	0,0014M $PdCl_2$	28°C, Ultrasound	15 min*
Filter	Vacuum	-	-
Copper deposition	1.95 g $CuSO_4$ * 5 H_2O 5 g Potassium Sodium Tartrate * 4 H_2O 30 ml Triethylamine 5 g NaOH 10 ml Formaldehyde 400 ml H_2O Adjusting the pH-value to 12.5	45°C, Ultrasound	10 min
Filter and Rinse	Vacuum, H_2O	-	-

*For this run another filter paper was used that caused clogging and changing the paper several times during the filtering process. This expanded the filtering time and the time in the sensitizer and activating solution.
Weight increase for this run by deposited copper is $\Delta_{weight} = 1.5773$ g (31.3392%)

Run 3	Description	Temp. / Ultrasound	Duration
Cleaning	70% HNO_3	RT	15 min
Filter and Rinse	Vacuum, H_2O	dried at 100°C	24 hrs -
Sensitization	0.1M $SnCl_2$ aged for 4 days	20–40°C, Ultrasound	15 min
Filter	Vacuum	-	-
Activation	0,0014M PdCl2	RT, Ultrasound	15 min
Filter	Vacuum	-	-
Copper deposition	1.9 g $CuSO_4$ * 5 H_2O	45°C, Ultrasound	60 min
	5 g Potassium Sodium Tartrate * 4 H_2O		
	30 ml Triethylamine		
	0.8 g NaOH		
	400 ml H_2O		
	Formaldehyde to adjust 12.5 pH		
Filter and Rinse	Vacuum, H_2O	-	-

Weight increase for this run by deposited copper is 32.4%.

Run 4	Description	Temp. / Ultrasound	Duration
Cleaning	70% HNO_3	RT	15 min
Filter and Rinse	Vacuum, H_2O	dried at 100°C	24 hrs -
Sensitization	0.1M $SnCl_2$ aged for 35 days	20–40°C, Ultrasound	15 min
Filter	Vacuum	-	-
Activation	0,0014M PdCl2	20–40°C, Ultrasound	15 min
Filter	Vacuum	-	-
Copper deposition	1.9 g $CuSO_4$ * 5 H_2O	35–45°C, Ultrasound	30 min
	5 g Potassium Sodium Tartrate * 4 H_2O		
	30 ml Triethylamine		
	0.8 g NaOH		
	400 ml H_2O		
	12.5 pH, no Formaldehyde		
Filter and Rinse	Vacuum, H_2O	-	-

In this run no Formaldehyde was added, resulting in a much less dense copper deposition.
Weight increase for this run by deposited copper is 11.2%.

Run 5	Description	Temp. / Ultrasound	Duration
Cleaning	70% HNO_3	RT	15 min
Filter and Rinse	Vacuum, H_2O	dried at 100°C	24 hrs -
Sensitization	0.1M $SnCl_2$ aged for 35 days	20–40°C, Ultrasound	15 min
Filter	Vacuum	-	-
Activation	0,0014M PdCl2	20–40°C, Ultrasound	15 min
Filter	Vacuum	-	-
Copper deposition	1.9 g $CuSO_4$ * 5 H_2O	60°C, Ultrasound	30 min
	5 g Potassium Sodium Tartrate * 4 H_2O		
	30 ml Triethylamine		
	0.8 g NaOH		
	400 ml H_2O		
	12.5 pH, no Formaldehyde		
Filter and Rinse	Vacuum, H_2O	-	-

No Formaldehyde again, but increased temperature for the plating bath increases the deposition slightly compared to run 4.
Weight increase for run 5 by deposited copper is 13.3%.

Run 6	Description	Temp. / Ultrasound	Duration
Cleaning	70% HNO_3	RT	15 min
Filter and Rinse	Vacuum, H_2O	dried at 100°C	24 hrs -
Sensitization	0.1M $SnCl_2$ aged for 4 days	25°C, Ultrasound	15 min
Filter	Vacuum	-	-
Activation	0,0014M PdCl2	20–40°C, Ultrasound	15 min
Filter	Vacuum	-	-
Copper deposition	1.9 g $CuSO_4$ * 5 H_2O	40–60°C, Ultrasound	30 min
	5 g Potassium Sodium Tartrate * 4 H_2O		
	30 ml Triethylamine		
	5 ml NaOH		
	400 ml H_2O		
	12.5 pH, 40 ml Formaldehyde		
Filter and Rinse	Vacuum, H_2O	-	-

Using Formaldehyde to adjust the pH-value.
Increasing weight of the fibers in run 6 by the deposited copper is 58%.

Run 7	Description	Temp. / Ultrasound	Duration
Cleaning	70% HNO_3	RT	15 min
Filter and Rinse	Vacuum, H_2O	dried at 100°C	24 hrs -
Sensitization	0.1M $SnCl_2$ aged for 46 days	25°C, Ultrasound	15 min
Filter	Vacuum	-	-
Activation	0,0014M PdCl2	20–40°C, Ultrasound	15 min
Copper deposition	1.9 g $CuSO_4$ * 5 H_2O aged for 1 day	60°C, Ultrasound	30 min
	5 g Potassium Sodium Tartrate * 4 H_2O		
	30 ml Triethylamine		
	0.8 g NaOH		
	400 ml H_2O		
	12.5 pH, adjusting with Formaldehyde		

Fibers were copper-colored, not much copper deposited on the nanofilaments.

Run 8	Description	Temp. / Ultrasound	Duration
Sensitization	0.1M $SnCl_2$ aged for 3 days	20–40°C, Ultrasound	180 min
Filter	Vacuum	-	-
Activation	0,0014M PdCl2	20–40°C, Ultrasound	360 min
Filter	Vacuum	-	-
Copper deposition	1.9 g $CuSO_4$ * 5 H_2O	60°C, Ultrasound	30 min
	5 g Potassium Sodium Tartrate * 4 H_2O		
	30 ml Triethylamine		
	10 ml NaOH		
	400 ml H_2O		
	12.5 pH, adjusting with Formaldehyde		

In Run 8 CNF-HB preforms were coated. The foams were submersed during the ultrasonic treatment for better infiltration results.

Run 9	Description	Temp. / Ultrasound	Duration
Cleaning	70% HNO_3	RT	15 min
Filter and Rinse	Vacuum, H_2O	dried at 100°C	24 hrs -
Sensitization	0.1M $SnCl_2$ aged for 4 days	25°C, Ultrasound	15 min
Filter	Vacuum	-	-
Activation	0,0014M PdCl2	25°C, Ultrasound	15 min
Copper deposition	5.7 g $CuSO_4$ * 5 H_2O	50–60°C, Ultrasound	20 min
	15 g Potassium Sodium Tartrate * 4 H_2O		
	90 ml Triethylamine		
	10 ml NaOH		
	400 ml H_2O		
	12.5 pH, adjusting with Formaldehyde		

Coating 0.8609 g nanofilaments, they gained slightly more than 2 g by copper deposition.

Run 10	Description	Temp. / Ultrasound	Duration
Cleaning	70% HNO_3	RT	15 min
Filter and Rinse	Vacuum, H_2O	dried at 100°C	24 hrs -
Sensitization	0.1M $SnCl_2$ aged for 4 days	25°C, Ultrasound	15 min
Filter	Vacuum	-	-
Activation	0,0014M PdCl2	25°C, Ultrasound	15 min
Copper deposition	2.5 g $CuSO_4$ * 5 H_2O	50–60°C, Ultrasound	20 min
	7.3 g Potassium Sodium Tartrate * 4 H_2O		
	45 ml Triethylamine		
	10 ml NaOH		
	400 ml H_2O		
	12.5 pH, adjusting with Formaldehyde		

Coating 0.615 g nanofilaments. Not as good results as Run 9.

Run 11	Description	Temp. / Ultrasound	Duration
Cleaning	70% HNO_3	RT	15 min
Filter and Rinse	Vacuum, H_2O	dried at 100°C	24 hrs -
Sensitization	0.1M $SnCl_2$ aged for 4 days	25°C, Ultrasound	15 min
Filter	Vacuum	-	-
Activation	0,0014M PdCl2	25°C, Ultrasound	15 min
Copper deposition	1.9 g $CuSO_4$ * 5 H_2O	50–60°C, Ultrasound	20 min
	5 g Potassium Sodium Tartrate * 4 H_2O		
	30 ml Triethylamine		
	0.9 g NaOH		
	400 ml H_2O		
	12.5 pH, adjusting with Formaldehyde		

Coating 0.317 g nanofilaments. Not as good results as Run 9. Upscaling showed better results than the coating with smaller amounts of CNF.

Run 12	Description	Temp. / Ultrasound	Duration
Sensitization	0.1M $SnCl_2$ aged for 4 days	25°C, Ultrasound	20 min
Filter	Vacuum	-	-
Activation	0,0014M PdCl2	25°C, Ultrasound	20 min
Filter	Vacuum	-	-
Copper deposition	5.9 g $CuSO_4$ * 5 H_2O	60°C, Ultrasound	30 min
	15 g Potassium Sodium Tartrate * 4 H_2O		
	90 ml Triethylamine		
	0.9 g NaOH		
	400 ml H_2O		
	12.5 pH, adjusting with Formaldehyde		

In Run 12 CNF-HB preforms were coated using a higher amount of copper in the plating solution.

	R1 Fibers	R2 Fibers	R3 Fibers	Foam	R4 Fibers	Foam	R5 Fibers	Foam	R6 Fibers	R7 Fibers	R8 A/B/C Foam	R9 Fibers	R10 Fibers	R11 Fibers	R12 Foam
after coating				CNF-HB		CNF-HB					CNF-HB/CNT-OH				CNF-HB
Photos	yes	yes													
LM	yes	no		yes	yes										
SEM	yes SE	yes SE			yes SE	yes HB(3/4)			yes SE	yes SE	HB A/B/C SE	yes SE+BS	yes SE+BS	yes SE+BS	
EDX	no	yes				yes HB(3/4)						spot Fiber	spot Fiber		
CS1	**CNF+Cu+Ti**			**foam**											
Photos	yes														
LM	no														
SEM	no			embedded											
Diffusivity	yes														
CS2		**CNF+Cu+Ti**	**CNF+Cu+Ti**		**CNF+Cu+Ti**		**CNF coated**								
Photos		no													
LM															
SEM			yes SE												
Diffusivity			yes		yes										
CS3									**CNF+Cu**						
Photos															
LM															
SEM					SE BS EDX										
Diffusivity															
MW1			**CNF+Cu+Ti**												
Photos															
LM			yes												
SEM															
Diffusivity															
MW2		**CNF+Cu+Ti**			**CNF+Cu+Ti**										
Photos															
LM															
SEM															
Diffusivity															
MW3		**CNF+Cu+Ti**			**CNF+Cu+Ti**							**CNF+Cu+Ti**			
Photos															
LM															
SEM															
Diffusivity															
HIP				**yes (B acid)**		**yes (B acid)** **yes (plain)**		**HB**			**yes/yes/yes**				
MW4 (1200°)		**CNF+Cu+Ti**			**CNF+Cu+Ti**							**CNF+Cu**			
Photos															
LM															
SEM															
Diffusivity															
MW5 (925°)		**CNF+Cu+Ti**	**CNF+Cu+Ti**		**CNF+Cu+Ti**							**CNF+Cu**			
Photos															
LM					yes							yes			
SEM															
Diffusivity					yes							yes			